Simple Models of Legged Locomotion based on Compliant Limb Behavior

---

Grundmodelle pedaler Lokomotion basierend auf nachgiebigem Beinverhalten

Dissertation
zur Erlangung des akademischen Grades

doctor philosophiae (Dr. phil.)

Gutachter

1. Prof. Dr. R. Blickhan

2. Prof. Dr. H. Herr

3. Prof. Dr. H. Witte

Tag des Kolloquiums: 22. 06. 2005

Zusammenfassung

In der vorliegenden Dissertation werden einfache Modelle zur Beinlokomotion unter der gemeinsamen Hypothese entwickelt, dass die beiden grundlegenden und als verschieden angesehenen Gangarten *Gehen* und *Rennen* auf ein allgemeines Konzept zurückgeführt werden können, welches allein auf *nachgiebigem Beinverhalten* beruht.

Hierzu werden im **Kapitel 1** zunächst die bestehenden einfachen mechanischen Modelle von Gehen und Rennen, respektive das *inverse Pendel* und das *Masse-Feder-Modell*, vorgestellt und sowohl ihre inhaltlichen Möglichkeiten als auch ihre innewohnenden Beschränkungen in der Beschreibung biologischer Beinlokomotion aufgezeigt. Hierbei tritt ein Unterschied der Qualität beider Modelle deutlich in den Vordergrund. Während das Masse-Feder-Modell die charakteristische Schwerpunktsdynamik der Standphase des Rennens wiedergibt und somit als 'Grundmodell' dieser Gangart angesehen wird, gilt Gleiches nicht für das inverse Pendel-Modell und die Schwerpunktsdynamik beim Gehen. Im Gegenteil: Anstelle einer Bogenbewegung, die den Schwerpunkt wie bei einem inversen Pendel über die Landehöhe hebt, zeigen biomechanische Experimente, dass beim Gehen der Schwerpunkt deutlich näher an der Landehöhe geführt wird, was tatsächlich ein nachgiebiges Beinverhalten auch für diese Gangart nahe legt. Entsprechend dieser Vermutung wird in den nachfolgenden Kapiteln die Bedeutung des allgemeinen Konzepts nachgiebigen Beinverhaltens für die Fortbewegung biologischer Systeme anhand von einfachen mechanischen und neuromechanischen Modellen untersucht. Den Ausgangspunkt bildet hierbei das als Grundmodell des Rennens akzeptierte Masse-Feder-Modell, welches nachgiebiges Beinverhalten in seiner einfachsten Form repräsentiert.

Im **Kapitel 2** wird zunächst auf eine Einschränkung dieses Modells eingegangen. Entgegen seiner scheinbaren Einfachheit beschreibt es ein *nichtlineares System*, dessen Bewegungsgleichungen nicht integrierbar sind, was aufgrund der allgemeinen Bedeutung dieses Modells innerhalb der Lokomotionsforschung und der Laufrobotik wiederholt zu Bemühungen um eine geeignete Näherungslösung geführt hat. Trotz dieser Anstrengungen ist es bisher nicht gelungen, eine Näherung zu finden, die mathematische Einfachheit mit geeigneter Genauigkeit innerhalb des physiologisch sinnvollen Parameterbereichs verbindet. Ersteres würde einen analytischen Zugang zum Einfluss der Parameter auf das Verhalten des Masse-Feder-Modells ermöglichen.

Letzteres ist notwendig, um daraus resultierende Hypothesen zur Beinlokomotion anhand von Laufexperimenten überprüfen zu können.

Ausgehend von der Annahme kleiner Winkelamplituden und kleiner Federkompressionen wird in diesem Kapitel eine Näherungslösung hergeleitet, die nur aus elementaren mathematischen Funktionen besteht. Anschließend wird im Rahmen der aus numerischen Berechnungen bekannten Selbststabilität des Rennens sowohl die Genauigkeit der Näherungslösung als auch ihr Potential, analytisch Parameterabhängigkeiten aufzuzeigen, für Modellparameter untersucht, die für menschliches Rennen relevant sind.

Der Vergleich mit den numerischen Berechnungen zeigt, dass die Näherungslösung **(i)** für Federkompressionen von bis zu 20% (Beinanstellwinkel $\geq 60°$, Winkelamplitude $\leq 60°$) die Schwerpunktsbewegung mit einer Genauigkeit von 1% für die Federkompression und 0.6° für die Winkelbewegung beschreibt und **(ii)** trotz ihrer vergleichbaren Einfachheit stabiles Rennen innerhalb des physiologisch sinnvollen Parameterraums exakt vorhersagt. **(iii)** Des Weiteren wird für einen Spezialfall die Parameterabhängigkeit für selbststabiles Laufen explizit berechnet. Hierbei zeigt sich, dass die identifizierte Abhängigkeit eine aus den numerischen Berechnungen empirisch vorgeschlagene Relation beinhaltet und darüber hinaus erweitert.

Aufgrund dieser Ergebnisse wird die gefundene Näherungslösung als analytisches Werkzeug für die weitergehende Erforschung der Beinlokomotion biologischer Systeme und für Anwendungen im Bereich der Laufrobotik vorgeschlagen.

Im **Kapitel 3** wird das traditionell nur dem Rennen zugeordnete Masse-Feder-Modell auf den Gangartenwechsel angewandt. Obgleich Zweibeiner in ihrer Anatomie große Unterschiede aufweisen, kann die Geschwindigkeit v_{trans}, bei der sie bevorzugt vom Gehen zum Rennen (und umgekehrt) wechseln, durch den einfachen Zusammenhang $v_{trans} \approx \sqrt{0.5\,g\ell_0}$ dargestellt werden, in dem allein die Gravitationsbeschleunigung g und die Beinlänge ℓ_0 als Einflussgrößen auftreten.

Diese erstaunlich einfache Abhängigkeit nur von mechanischen Parametern legt eine gleichermaßen mechanische Ursache des Gangartwechsels nahe. Tatsächlich zeigt eine einfache Betrachtung am inversen Pendel-Modell, bei der die auftretende Zentrifugalkraft mit der ihr entgegenwirkenden Schwerkraft gleichgesetzt wird, eine obere Geschwindigkeitsschranke $v_{max} = \sqrt{g\ell_0}$ des Gehens auf, die zu identischen Einflussgrößen führt. Allerdings kann das Pendel-Modell den zahlenmäßigen Unterschied um den Faktor $\sqrt{2}$ nicht erklären. Diese Diskrepanz hat zu der Annahme geführt, dass anstelle einer mechanischen, eine physiologische Ursache den Gangartenwechsel auslöst. Zum Beispiel wurden metabolische Kosten, maximal mögliche Beinwinkel oder die wahrgenommene Anstrengungsrate vorgeschlagen. Es konnte jedoch bis heute keine befriedigende Erklärung des Unterschieds gefunden werden.

In diesem Kapitel wird zu einer rein mechanischen Betrachtung des Gangartwechsels zurückgekehrt und die Annahme verfolgt, dass dieser, anstelle von einer oberen Grenzgeschwindigkeit des Gehens, durch eine untere Grenzgeschwindigkeit des Rennens bestimmt ist. Im Speziellen wird untersucht, ab welcher Geschwindigkeit Ren-

nen eine nahezu horizontale Bewegung des Schwerpunkts innerhalb der Standphase zulässt, so dass ein 'glatter', mechanisch komfortabler Übergang zwischen beiden Gangarten sichergestellt werden kann. Letzterer wird insbesondere bei der Vielzahl am Boden lebender Vögel beobachtet.

Unter Verwendung eines vereinfachten Masse-Feder-Modells kann analytisch gezeigt werden, **(i)** dass ein glatter Wechsel zwischen Gehen und Rennen eine Mindestrenngeschwindigkeit $v_{min} \simeq \sqrt{0.4\,g\ell_0}$ benötigt, die erstaunlich gut mit der experimentell beobachteten Geschwindigkeit des Gangartwechsels übereinstimmt. **(ii)** Darüber hinaus folgt aus der Analyse, dass für niedrigere Geschwindigkeiten $v < v_{min}$ die Gangart Rennen zu übertriebenen vertikalen Auslenkungen führt, welche sowohl auf erhöhte metabolische Kosten der Fortbewegung als auch auf einen verringerten mechanischen Komfort hindeuten. **(iii)** Der Vergleich dieser Vorhersagen mit den Ergebnissen einer Laufbandstudie zum menschlichen Gehen und Rennen bestätigt diese mechanische Einschränkung des Rennens bei niedrigen Geschwindigkeiten und deutet darauf hin, dass Zweibeiner das Gehen unterhalb der Wechselgeschwindigkeit bevorzugen könnten, da es ausreichenden mechanischen Komfort sicherstellt.

Es wird vorgeschlagen, dass die Vorhersagbarkeit des Gangartwechsels nicht auf die von der inversen Pendelbewegung abgeleitete, obere Grenzgeschwindigkeit v_{max} des Gehens beschränkt ist, sondern gleichermaßen aus einer unteren Grenzgeschwindigkeit v_{min} des Rennens folgt, die unter der Annahme eines glatten, mechanisch komfortablen Wechsels der Gangarten vom nachgiebigen Masse-Feder-Modell abgeleitet werden kann und zugleich die numerische Diskrepanz zwischen berechnetem und beobachtetem Übergang auflöst.

Im **Kapitel 4** wird untersucht, inwiefern ein nachgiebiges Beinverhalten tatsächlich die Schwerpunktsdynamik beim Gehen beschreibt. Hierzu wird das einfache Masse-Feder-Modell des Rennens durch eine zweite, idealisierte Beinfeder ergänzt und nach selbststabilen, periodischen Laufmustern gesucht (analog zu Seyfarth A, Geyer H, Günther M, Blickhan R, 2002, A movement criterion for running. *J. Biomech.* **35**: 649–655).

Die Analyse zeigt, dass **(i)** das *zweibeinige Masse-Feder-Modell* ähnlich dem einbeinigen Modell des Rennens selbststabile und robuste Beinlokomotion beschreiben kann, wenn die Parameter Beinanstellwinkel, Federsteifigkeit und Systemenergie geeignet gewählt sind, und **(ii)** die resultierenden Schwerpunktsdynamiken die für das Gehen von Tieren und Menschen bekannten Muster beinhalten. **(iii)** Darüber hinaus stimmen die für stabiles Gehen vorhergesagten Modellparameter mit ihren aus Laufbandexperimenten gewonnenen Abschätzungen für eine moderate Gehgeschwindigkeit von etwa 1.5m/s überein. **(iv)** Ober- und unterhalb dieser Geschwindigkeit treten Abweichungen auf. Für niedrigere Geschwindigkeiten können diese erklärt werden durch die Beschränkung auf feste Landeanstellwinkel in der Schwungphase des Modells. Für höhere Geschwindigkeiten offenbaren sie jedoch eine Grenze der Beschreibung von Gehen allein durch federartige Beine und deuten hier auf ein komplexeres, nachgiebiges Beinverhalten hin.

Aufgrund der Fähigkeit, die charakteristische Schwerpunktsdynamik des Gehens zu reproduzieren, wird das zweibeinige Masse-Feder-Modell als *Grundmodell* dieser Gangart vorgeschlagen, welches die Forschung auf dem Gebiet biologischer Kontrollstrategien der Beinlokomotion durch seine parametrische Einfachheit effektiv begleiten könnte.

Im **Kapitel 5** wird die Betrachtung biologischer Beinlokomotion auf der Ebene mechanischer Grundmodelle verlassen und der Fragestellung nachgegangen, inwiefern ein globales, nachgiebiges Verhalten durch das neuromechanische Zusammenspiel innerhalb eines biologischen Beins sichergestellt werden kann.

Obwohl passive Strukturen des Muskelskelettapparats, wie z.B. Sehnen, oft für dieses Verhalten als Ursache angenommen werden, zeigen Experimente, dass diese nur einen Teil der Schrittenergie speichern und wieder freigeben können (z.B. beim Menschen nur bis zu 50%). Entsprechend müssen die unvermeidlichen Verluste durch aktive Muskelarbeit der Beinstrecker kompensiert werden, was eine geeignete, motorische Kontrolle dieser Muskeln erfordert. Anhand eines einfachen, neuromechanischen Beinmodells des menschlichen Hüpfens auf der Stelle (das eindimensionale Analogon zum Rennen) wird untersucht, inwieweit sensorische Informationen der Muskelrezeptoren (Muskelspindeln und Golgi-Sehnen-Organe) durch einfache Rückkopplungsschleifen in diese Kontrolle eingebunden sein könnten.

Die Analyse zeigt, dass **(i)** die positive Rückkopplung der Muskelfaserlänge oder der Muskelkraft zu periodischen Hüpfmustern führen kann und **(ii)** hierbei die positive Kraftrückkopplung das Hüpfmuster innerhalb eines großen Bereichs von Hüpfhöhen stabilisiert (maximale Hüpfhöhe mit 16cm etwa doppelt so hoch wie bei positiver Längenrückkopplung). **(iii)** Für moderate Hüpfhöhen von bis zu 9cm erzeugt die positive Kraftrückkopplung elastisches Beinverhalten in der Standphase mit Beinsteifigkeiten von 9kN/m bis 27kN/m (Hüpffrequenz: 1.4-3Hz). **(iv)** Darüber hinaus zeigt die Erweiterung des Modells auf planare Bewegungen, dass eine positive Kraftrückkopplung auch Rennen stabilisieren kann.

Es wird vorgeschlagen, dass in der Standphase von Hüpfen und Rennen die reflexgenerierte, motorische Kontrolle basierend auf *positiver Kraftrückkopplung* eine effiziente und zuverlässige Alternative zu zentralen Kontrollmechanismen des Nervensystems darstellen könnte, um ein nachgiebiges Verhalten auf der globalen Beinebene sicherzustellen.

Im letzten Teil der Dissertation, im **Kapitel 6**, werden die Ergebnisse der vorangegangenen Kapitel schließlich in einem Gesamtbild zur Beinlokomotion zusammengefasst. Hierbei werden die beiden fundamentalen Gangarten Gehen und Rennen innerhalb des zweibeinigen Masse-Feder-Modells *vereinigt* und die Bedeutung dieses, auf nachgiebigem Beinverhalten basierenden Zusammenschlusses sowohl für die biomechanische und motorische Grundlagenforschung als auch für Anwendungen in der Robotik, Rehabilitation und Prothetik erörtert.

Abstract

In this dissertation, simple models of legged locomotion are developed mainly following the hypothesis that rather than reflecting two distinct phenomena, the fundamental gait patterns of *walking and running* can be described within a single conceptual framework that is based on *compliant limb behavior*.

In **Chapter 1**, the most prominent mechanical paradigms of walking and running, namely the *stiff-legged inverted pendulum* and the *compliant spring-mass model*, are introduced by demonstrating their importance for investigating legged locomotion. However, it is also discussed that both models must be ranked differently when assessing their value as basic *gait templates* that encode parsimoniously the strikingly uniform whole body dynamics observed during animal and human locomotion. Whereas the spring-mass model can describe the characteristic motion of the center of mass in running, the inverted pendulum fails to reproduce the corresponding pattern in walking. By contrast, walking experiments show that, instead of vaulting over rigid legs as suggested by the inverted pendulum motion, the center of mass experiences much less vertical excursion requiring substantial stance-leg compressions. Inspired by this observation, in the following chapters, the general significance of limb compliance for biological legged locomotion is explored utilizing simple mechanical and neuromechanical models. Here, the spring-mass model for running is used as starting point since it not only represents a known gait template, but also embodies limb compliance in its simplest form.

In **Chapter 2**, a limitation of the spring-mass model is addressed. Although with a Hooke's law spring attached to a point mass the planar spring-mass model may appear trivial, it describes a nonlinear system whose equations of motion are nonintegrable. In light of the model's growing importance for basic research on legged locomotion and for applications in robotics, the lack of a closed form solution of its system dynamics has prompted scientists to seek suitable approximations. However, as of today, no approximation could be found that combines mathematical tractability with sufficient accuracy in the physiologically relevant parameter domain. The former would allow to extract parametric dependencies of the model's behavior by analytical means, the latter is required to verify resulting hypotheses on legged locomotion, in experiments.

Assuming a small angular sweep and a small spring compression, in this chapter, an approximate solution in elementary functions is derived. Within the scope of gait stability, the quality and the predictive power of this solution are investigated for model parameters relevant to human locomotion.

The comparison with numerical calculations shows that **(i)**, for spring compressions of up to 20% (angle of attack $\geq 60°$, angular sweep $\leq 60°$), the approximate solution describes the stance dynamics of the center of mass within a 1% tolerance of spring compression and $0.6°$ tolerance of angular motion, and **(ii)**, despite its relative simplicity, the approximate solution accurately predicts stable locomotion well extending into the physiologically reasonable parameter domain. **(iii)** Furthermore, in a particular case, an explicit parametric dependency required for gait stability can be revealed extending an earlier, empirically found relationship.

It is suggested that this approximation of the planar spring-mass dynamics may serve as an analytical tool for further research on legged locomotion and for applications in robotics.

In **Chapter 3**, the spring-mass model for running is applied to the walk-run transition. Although bipedal animals and humans are characterized by different morphologies, the velocity v_{trans} at which they prefer to switch from walking to running (and from running to walking), can be described by the simple relationship $v_{trans} \approx \sqrt{0.5\,g\ell_0}$ where g is the gravitational acceleration and ℓ_0 represents the leg length.

The dependence of the transition speed only on mechanical parameters suggests a mechanical explanation for the gait transition. And indeed, assuming an inverted-pendulum-like motion of the center of mass, a maximum walking speed $v_{max} = \sqrt{g\ell_0}$ can be obtained from the equilibrium of the counteracting centrifugal and gravitational forces, which leads to a similar functional relationship. Yet the inverted pendulum model cannot explain the numerical difference of factor $\sqrt{2}$. This discrepancy has led to the assumption that rather than a mechanical, there might be a physiological constraint inducing the gait transition. For instance, metabolic costs, or a maximum inter-thigh angle, or the rate of perceived exertion are suggested as the possible trigger. However, a conclusive explanation for the difference in number still remains elusive.

In this chapter, it is returned to a mechanical interpretation of the walk-run transition by assuming that, instead of an upper speed limit in walking, the gait transition could be induced by a lower speed limit in running. More precisely, it is investigated at which speed running with a virtual horizontal center-of-mass motion during stance becomes possible, so that a 'smooth', mechanically comfortable transition between both gaits can be ensured. The latter is observed especially for the multitude of ground dwelling birds.

By employing a simplified version of the spring-mass model, it is found analytically **(i)** that the smooth transition requires a minimum running speed $v_{min} \simeq \sqrt{0.4\,g\ell_0}$, which surprisingly well matches the experimentally observed speed of the preferred

gait transition. **(ii)** Moreover, the model predicts that, for lower speeds $v < v_{min}$, running leads to exaggerated vertical motions indicating an unfavorable growth of the cost of transport, as well as a reduced mechanical comfort. **(iii)** The comparison of the model predictions with the results of a treadmill study on human locomotion confirms this mechanical limitation of running, and indicates that, below the preferred transition speed, bipeds may choose walking since it can guarantee sufficient mechanical comfort.

It is suggested that the predictability of the walk-run transition is not constrained to the maximum walking speed v_{max} derived from the inverted pendulum model, but equally results from a lower speed limit v_{min} of running, which can be derived from the compliant spring-mass model assuming a smooth, mechanical comfortable gait transition, and which resolves the numerical discrepancy between predicted and observed transition speed.

In **Chapter 4**, it is addressed to what extent a compliant leg behavior can indeed account for the characteristic whole body dynamics observed in animal and human walking. Therefore, the simple spring-mass model for running is extended by a second, idealized leg spring, and self-stable periodic locomotion patterns are sought (analogue to Seyfarth, Geyer, Günther, Blickhan, 2002, A movement criterion for running. *J. Biomech.* **35**: 649-655).

The analysis reveals that **(i)**, similar to the simple running model, the *bipedal spring-mass model* can describe self-stable and robust periodic locomotion if the parameters angle of attack, spring stiffness, and system energy are properly chosen, and **(ii)** the resulting steady-state dynamics include those typical for animal and human walking. **(iii)** Furthermore, an agreement between the model parameters predicted for stable walking and their experimental estimates is found for moderate walking speeds of about 1.5m/s. **(iv)** Above and below this speed differences are observed, which, for slower speeds ($v < 1.5$m/s), can be explained by the restrictions imposed by the methodological approach of investigating stability using fixed leg angles during swing. For higher speeds ($v > 1.5$m/s), however, the discrepancy reveals an intrinsic limitation of describing the stance phase dynamics solely based on elastic legs indicating a more complex, compliant leg behavior to become indispensable at these speeds.

Reproducing the characteristic motion of the center of mass in walking, the bipedal spring-mass model is suggested as a *template* for this gait, which, due to its parametric simplicity, might effectively guide future research on biological control strategies for legged locomotion.

In **Chapter 5**, the focus shifts from exploring legged locomotion based on simple gait templates, to the higher-dimensional problem of how the remarkable uniform, spring-like leg response of animals and humans can be ensured by the neuromechanical interplay within the musculo-skeletal system.

Although passive structures, such as tendons or ligaments, are frequently suggested

as the likely origin for the spring-like leg response, experiments show that they can only partially store and restore the stride energy (e.g. in humans only up to 50%), which requires active extensor-muscle contributions to compensate for the inevitable losses. Consequently, the muscles must adequately be stimulated by the nervous system. With a simple neuromechanical model of human hopping (the one-dimensional paradigm for running), it is investigated whether afferent information from muscle receptors (muscle spindles, Golgi tendon organs) can contribute to the required neural control, using single-loop feedbacks.

It is found that **(i)** the positive feedbacks of muscle fiber length and muscle force can result in periodic bouncing, and **(ii)** positive force feedback stabilizes bouncing patterns within a large range of stride energies (maximum hopping height 16cm, almost twofold higher than by using length feedback). **(iii)** Employing this reflex scheme, for moderate hopping heights (up to 9cm), an overall elastic leg behavior is predicted with a leg stiffness ranging from 9kN/m to 27kN/m (hopping frequency: 1.4-3Hz). **(iv)** Moreover, by extending the model to planar motions, it is shown that positive force feedback can also stabilize running.

It is suggested that, during the stance phase of bouncing tasks, the reflex generated motor control based on *positive force feedback* might be an efficient and reliable alternative to central motor commands, to guarantee a compliant limb behavior on the global leg level.

In the final part of this dissertation, in **Chapter 6**, the results of the preceding chapters are summarized to a more coherent picture of legged locomotion. Here, the two fundamental gait patterns of walking and running are *combined* within a single, the bipedal spring-mass model; and the implications of this functional, compliance-based unification are discussed with respect to basic research in biomechanics and motor control, as well as to applications in robotics, rehabilitation, and prosthetics.

Contents

Preface

On an international scale, investigating biological locomotor systems is a rapidly advancing field of a much more general and interdisciplinary approach to animal and human behavior requiring the combined expertise in research areas as diverse as artificial intelligence, medicine, physics, robotics, and systems theory. Such a development appears natural and necessary since, with animals and humans, we are facing very complex biological systems often denying access by classical methods fostered within a single discipline, and a joint effort seems to promise the most success.

Receiving a graduate student scholarship of the German Academic Exchange Service (DAAD) I was granted the opportunity to partake in this interdisciplinary approach during my doctoral work by visiting two of the most recognized research laboratories investigating legged locomotion, the Leg Laboratory of the Artificial Intelligence Laboratory of the Massachusetts Institute of Technology, Cambridge, USA, famous for its achievements in the fields of legged robots and prosthetics, and the ParaCare Research Laboratory of the University Hospital Balgrist of the University of Zurich, Switzerland, where one of the first orthotic devices was and continues to be developed to help spinal cord injured patients regaining their locomotor ability. I would like to take this opportunity to express my gratitude to the German Academic Exchange Service and to Prof. H. Herr (MIT Leg Laboratory) and Prof. V. Dietz (ParaCare Research Laboratory) who, by their support, invitation and collaboration, made such an international research project possible.

I would also like to express my indebtedness to my head supervisor Prof. R. Blickhan and to Dr. A. Seyfarth of the Jena University. Prof. R. Blickhan as Chair of Motion Sciences of the Institute of Sport Science accepted to supervise my thesis work although a substantial part was undertaken abroad. I am thankful to him for this decision and his inspiring advice and suggestions which I received even when our communication was reduced to email contacts and phone calls by geographic constraints. As holder of an Emmy-Noether scholarship of the German Research

Foundation (DFG), Dr. A. Seyfarth visited both the MIT Leg Laboratory and the ParaCare Research Laboratory at about the same time as I did, although his time schedule always led him first to the research facilities we visited, which more than once noticeably lowered the administrative hurdles I had to take when arriving. I am grateful to him for this organizational help, his ideas and suggestions he communicated about my work during our joint time abroad, and his continuing support within the framework of the Emmy-Noether scholarship he still receives to establish and maintain a young scientists group (Locomotion Laboratory at the Jena University).

At the outset of my doctoral term, I intended to analyze whether the remarkable uniform, global spring-like leg response of the running gait of animals and humans can be embedded within an articulated leg in a largely decentralized and autonomous manner using the reflex-based interplay of musculo-skeletal mechanics and neural control. Embarking on this program, however, it soon became obvious that many questions concerning legged locomotion on the more general, global leg level were unresolved, and we were fortunate enough to have some scientific tools at hand, which made it possible to elucidate part of them. In consequence, I decided to continue investigating legged locomotion using simple mechanical models first and postponed the higher-dimensional and more complex problem of their morphological embodiment within the biological system. Such an approach is strongly advised in the interdisciplinary field of biomechanics and motor control since although we possess the computational power to develop more complex models, these models seem best to advance our knowledge of the neuromechanical organization in the presence of underlying functional templates.

During my doctoral work, I have received much advice and valuable help from many including my supervisors, numerous colleagues, anonymous reviewers, and friends. As such, the ideas presented in this thesis are influenced by provoking discussions and stimulating criticism and I cannot claim them to be based solely on my own thoughts. What I can say is that, with this dissertation, I have worked out the consequences of these ideas to their present state.

Finally, I must thank my family for their loving support throughout this time.

Hartmut Geyer

Jena

April 11th, 2005

Chapter 1

General introduction

1.1 Legged locomotion

A formal definition may state that *legged locomotion* is the motion of the bodies locus among a path in space using legs as means of transportation. Although very simple in description, our understanding of the fundamental principles underlying legged locomotion is far from adequate. For instance, we hardly know what construction and control principles yield a prosthetic limb which conveys a patient the feeling of a natural limb, why a particular therapeutic approach in rehabilitation helps one spinal cord injured patient regaining his locomotor ability and not the other, or how we should devise robotic platforms to realize dynamic, fast and stable legged machines.

On the other hand, in our daily experience we are surrounded by remarkable examples of legged locomotion. The astonishing elegance and efficiency with which legged animals and humans traverse natural terrain outclasses any present day man-made competitor. And consequently, beyond sheer fascination, such a 'technological' superiority heavily attracts the interest from many scientists. However, concerned with animals and humans, we are also facing an overwhelming diversity. Biological legged systems range from small (e.g. ants) to large animals (elephants) and from bipeds to millipedes. Even between systems of comparable size and with equal number of legs, we still observe different morphologies (e.g. limb design and actuation in large ground dwelling birds vs. humans). Hence, it seems that nature in her resourcefulness has invented a great variety of prototypes confronting scientists with the difficult question of how to extract the underlying principles.

Here, two contrasting approaches are employed. In the *first method* as much features of the biological system under consideration as known from or potentially

identified in experiments are implemented. By successive elimination of single features it is then tried to identify the crucial components. Whereas this approach allows to produce sophisticated models in terms of complexity, it suffers from the vast number of parameters or degrees of freedom this simulated complexity requires. Lacking experimentally valid data for most of the parameters, the starting point of the elimination process can be any from close to the biological prototype to almost entirely arbitrary. On the contrary, in the *second method* only those features are implemented that seem indispensable. Whereas, due to its parametric simplicity, this approach allows to investigate more thoroughly the model behavior and, hence, parametric insights are more likely to be disclosed, it suffers from the choice of the indispensable components. Lacking essential features can lead to substantially wrong conclusions.
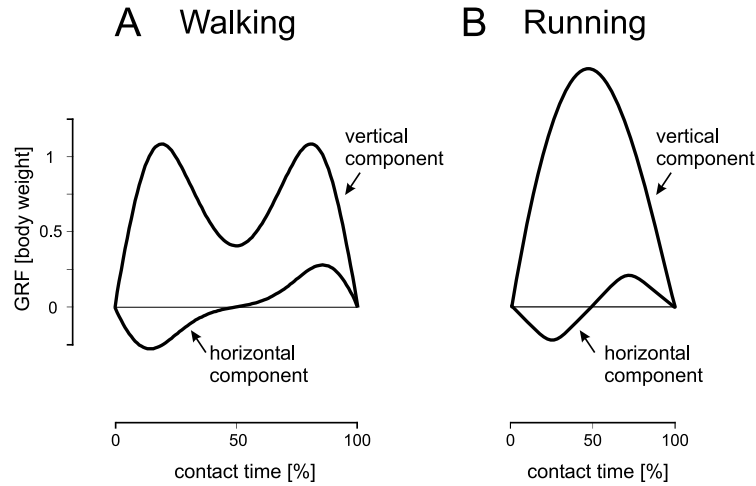
Figure 1.1. Characteristic ground reaction force (GRF) patterns observed during the stance phase in walking (**A**) and running (**B**).

Which method is appropriate when addressing legged locomotion of biological systems? Certainly, both have their advantages and disadvantages, but it seems that high-dimensional models are better suited to reveal *how* fundamental mechanisms are *implemented* in the actual system once they are *identified* by simple functional models. This notion may reflect the personal preference of the author, however, nature itself provides a surprising insight when considering legged locomotion on a purely mechanical level. Despite the diversity in size, number of legs, and limb design and actuation, classifying the integral force the legs exert on the ground (ground reaction force, GRF), only two functional gait patterns prevail with remarkably simple force shapes. For comparably slow speeds, biological systems

prefer the *walking gait* recognized by its characteristic double-peak of the vertical GRF (Fig. 1.1A). And with increasing speed, they switch to *bouncing gaits* (running, trotting, and hopping), which have in common that the vertical force pattern reduces to a single-peak structure (Fig. 1.1B).

1.2 Two mechanical paradigms of the fundamental gaits

Understanding this striking uniformity is a likely candidate to unveil some essentials of legged locomotion. A first step towards this aim is to find suitable model representations covering the salient features inherent in these two basic patterns. In an early study, SAUNDERS *et al.* (1953) observed that walking seems to resemble a 'compass gait' where the center of mass (COM) vaults over rigid stance legs suggesting an *inverted pendulum* as an appropriate plant for the walking gait (Fig. 1.2A).
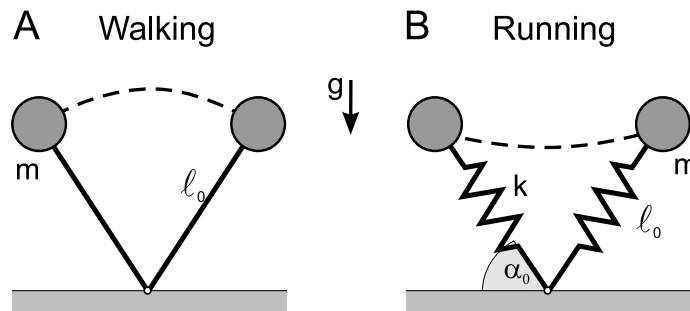
Figure 1.2. Mechanical paradigms of the stance phase in walking and running. The body is reduced to a point mass m at the COM. For the inverted pendulum model of walking (**A**) the COM is supported by a massless rigid stick of length ℓ_0, for the spring-mass model of running (**B**) it is supported by a massless spring (rest length ℓ_0, spring stiffness k). The angle α_0 denotes the leg orientation at touch-down, g the gravitational acceleration.

Later, this model enjoyed increasing attention when experiments showed that it can in part explain the transfer of potential and kinetic energy during walking (CAVAGNA *et al.*, 1977), and that it correctly predicts the speed at which animals and humans prefer to switch from walking to running to be solely a function of gravitational acceleration and leg length (e.g. ALEXANDER and JAYES, 1983; KRAM *et al.*, 1997). Since the pioneering work of MCGEER (1990), the inverted pendulum is also exploited in robotics. For instance, it could be demonstrated that, when starting on a shallow down-slope, 'passive dynamic walkers' mimicking the inverted pendulum can exhibit stable periodic forward locomotion without active control or energy supply (MCGEER, 1990; COLEMAN and RUINA, 1998). But, although the inverted

pendulum renders the simplest walking model conceivable, it generates GRF patterns notably inconsistent with experimental observations (FULL and KODITSCHEK, 1999; PANDY, 2003). Correspondingly, investigations on human walking revealed that, instead of vaulting over rigid legs, the COM experiences much less vertical excursion necessitating significant stance-limb compression (LEE and FARLEY, 1998; GARD *et al.*, 2004).

Such a stance-limb compression, however, is traditionally assigned to bouncing gaits as a characteristic feature. Here, part of the stride energy is stored and released in passive compliant structures such as tendons, ligaments, and perhaps even bone (in some animals up to 70% of the stride energy can be stored in these structures, ALEXANDER and VERNON, 1975; BIEWENER, 1998). In consequence, an elastic leg behavior is observed (CAVAGNA *et al.*, 1964, 1977), which led to the introduction of the planar *spring-mass model* (BLICKHAN, 1989; McMAHON and CHENG, 1990). Of similar simplicity as the inverted pendulum model (Fig. 1.2B), the spring-mass model realizes a simple mechanical paradigm of the stance phase in running or hopping. More importantly, it also well describes the characteristic GRF pattern. In consequence, not only biomechanical studies investigating hopping (FARLEY *et al.*, 1991; SEYFARTH *et al.*, 2001) or running (HE *et al.*, 1991; BLICKHAN and FULL, 1993; FARLEY *et al.*, 1993), but also fast legged robots driven by model based control algorithms (RAIBERT, 1986; SARANLI and KODITSCHEK, 2003) rely on this plant.

1.3 Stable spring-mass running

By constructing hopping robots, RAIBERT (1986) was among the first who showed that a statically instable legged system can exhibit *dynamically stable* locomotion. To achieve stable hopping, only as few as three quantities needed to be addressed by servo control within a state machine: hopping height, forward speed, and body attitude (pitch). Although the 'Raibert-Controller' based on the idea of a simple spring-mass system as a virtual control model (STENTZ, 1983), the identification of the correct servo parameters was still limited to *trial and error*. As the spring-mass model represents a non-integrable system (WHITTACKER, 1904), parametric insights remained obscured. Nevertheless, aside from the animal-like ease and elegance these robots conveyed, they also demonstrated that dynamic stability might be one important clue to the understanding of legged locomotion. In consequence, the exploration of dynamic stability using the spring-mass model started to enjoy increasing attention. Lacking a closed form solution of the model's equations of

motion, two parallel developments commenced.

On the one hand, research activities concentrated on identifying a suitable *approximate solution* for the stance phase dynamics. To achieve this, the common approach was to simply neglect the acting gravitational force in the equations of motion reducing the system to a central force problem. Although a closed form representation could be derived, the resulting solution involved elliptic integrals (SCHMITT and HOLMES, 2000; GHIGLIAZZA *et al.*, 2003) hampering the desired parametric insight. Moreover, it could be demonstrated that neglecting gravity produces quantitatively erroneous parameter relations (SCHWIND and KODITSCHEK, 2000; GEYER, 2001). To correct for this discrepancy, SCHWIND and KODITSCHEK (2000) suggested an iterative algorithm similar to Picard iterations that successively reintegrates the gravitational force. Although with each iteration the resulting approximate solution more closely fitted the original system, its mathematical tractability significantly decreased.

On the other hand, dynamic stability of the spring-mass model was investigated using *numerical parameter identifications.* Here, simulations using the spring-mass model without gravity yielded first insights. By modeling the horizontal plane motion of the alternating tripod gait of six-legged insects with spring-legs for each tripod, SCHMITT and HOLMES (2000) could show that lateral perturbations diminish within this alternating contact regime. Later, we demonstrated that this *self-stabilization* also holds for sagittal plane running with alternating flight and contact phases using a ballistic motion of the COM during flight and the planar spring-mass model during stance (GEYER *et al.*, 2002; SEYFARTH *et al.*, 2002). The term 'self-stabilization' here refers to the observation that, after disturbances of the periodic locomotion pattern (e.g. by ground irregularities), the COM returns to the limit-cycle trajectory without any feedback control processing sensory information on the actual disturbance (compare also RINGROSE, 1997; BLICKHAN *et al.*, 2003). Comparing the parameter combinations required for the self-stabilizing behavior in spring-mass running with experimental data on human running, we also found that biological systems seem well to adapt to this parameter region (Fig. 1.3) suggesting the exploration of self-stability as important concept for the identification of general principles in legged locomotion.

Correspondingly, in a follow-up research, we expanded upon this concept and could demonstrate that the parameter region leading to self-stable spring-mass running largely enhances if a feedforwardly controlled retraction motion of the swing-leg is introduced during the flight phase (SEYFARTH and GEYER, 2002; SEYFARTH *et al.*,
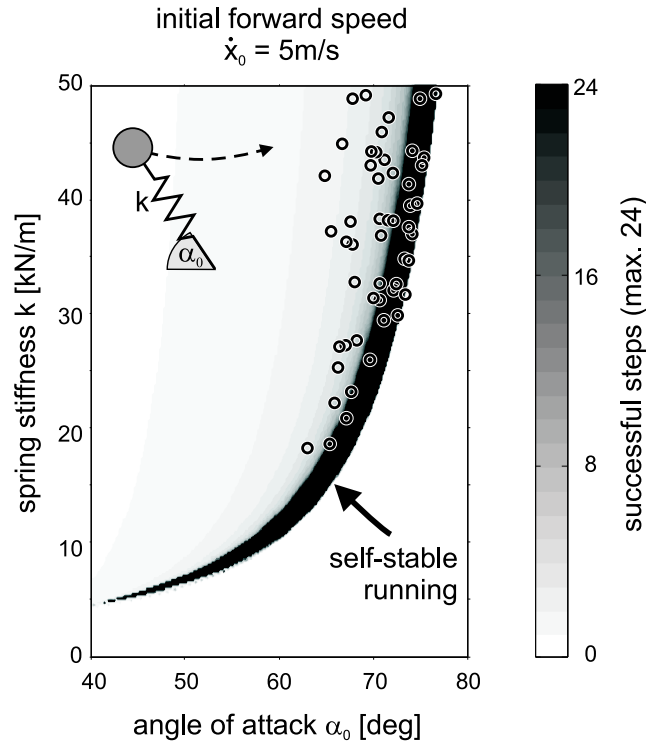
Figure 1.3. Comparison of model parameters required for self-stable spring-mass running (region indicated by the arrow) with experimental results (open circles, adapted from SEYFARTH *et al.*, 2002).

2003). This research was inspired by the observation that running animals and humans retract their swing-legs prior to touch-down (MUYBRIDGE, 1955; GRAY, 1968) instead of having a fixed leg orientation during flight, which has been used in the preceding investigations on spring-mass running. Additionally, simulation results on a more complex biomechanical model for quadrupedal locomotion indicated that a leg retraction strategy could indeed improve running stability (HERR, 1998; HERR and MCMAHON, 2000, 2001).

Recently, the results from the analysis of the spring-mass model find an increasing interest in robotics. The design and control of the fastest legged running machines is based on this gait paradigm and speeds of up to 15 body lengths per second (2.3m/s) are achieved (KIM *et al.*, 2004) – a record that can compete with wheeled toy vehicles of about the same size. Taking advantage of their limbs, these six-legged machines outperform wheeled systems in unstructured terrain already (ALTENDORFER *et al.*, 2001).

1.4 Thesis outline

The scientific advances discussed in the previous sections indicate that the spring-mass model serves as a remarkable simple yet sufficiently complex model to address fundamental control strategies of legged locomotion in running. However, due to the lack of a mathematically tractable approximate solution of the stance phase dynamics, the success mainly depends on numerical simulation studies rather than thorough understanding of the parametric relationships. In the light of the model's simplicity, this might be deemed of minor concern. Yet if more complex representations of the basic spring-mass model are addressed (e.g. three dimensional spring-mass running or more elaborate leg recirculation strategies during flight), the situation rapidly changes and tractable analytical descriptions become indispensable.

Motivated by the lack of an analytical access to the planar spring-mass dynamics, in *Chapter 2* an approximate solution is derived that combines mathematical simplicity with surprising accuracy. The approach taken is similar to that of an earlier work (GEYER, 2001) where an approximation was identified which, due to neglecting the effects of gravity, produced quantitatively erroneous results. In contrast, by assuming a small angular sweep and a small spring compression during stance, the solution derived in Chapter 2 inherently incorporates the effects of gravity. Its predictive power and quality with respect to self-stability in spring-mass running is demonstrated for model parameters relevant to human locomotion.

In contrast to the running pattern, for walking, such an analytical access has not yet been identified. Although dynamic stability has also been investigated on a mathematical basis for the inverted pendulum model (e.g. GARCIA *et al.*, 1998), this model cannot describe the biologically observed GRF pattern and corresponding model results are limited to some qualitative predictions. Hence, the identification of a sufficiently simple mechanical model is required that encodes parsimoniously the fundamental characteristics of the whole body dynamics in walking.

The identification of such a gait template for walking is addressed in *Chapters 3 and 4*. Motivated by experimental observations of significant stance limb compressions (LEE and FARLEY, 1998; GARD *et al.*, 2004, compare section 1.2), in these chapters, the traditional approach of understanding walking as a stiff legged gait is abandoned in favor of the hypothesis that walking can rather be understood assuming compliant leg behavior during stance. Hereto, in Chapter 3, it is first addressed whether the characteristic walk-run transition speed of animals and humans, which is generally derived using the inverted pendulum model for walking, can alternatively be explained from a running perspective using a simplified version of the compliant

spring-mass model. One step further, in Chapter 4, the spring-mass model so well-known for the running gait is put forth as an equally adequate gait template for walking hereby unifying both fundamental gait patterns within a single theoretical framework.

Chapter 5 leaves the realm of simple mechanical models. If the two fundamental gaits of walking and running can be described by a spring-like leg behavior, this behavior should somehow be embodied in the actual musculo-skeletal system. Although in some animals passive elastic structures are suggested as origin, a different situation applies to humans where active muscle tissue with non-negligible viscous properties contributes to the leg force generation to a large extent. Hence, the observed 'functional' spring-leg representation requires proper neural stimulation of the load bearing extensor muscles. And, by investigating a simple neuro-muscle-skeleton model with only one extensor muscle, it is addressed whether this internal leg control can largely be decentralized using autonomous muscle reflex loops.

Finally, in *Chapter 6* the separate findings of this thesis work are summarized to a more coherent picture of legged locomotion and general conclusions suggested by the results are drawn.

Chapter 2

Spring-mass running: simple approximate solution and application to gait stability

2.1 Introduction

The planar spring-mass model for bouncing gaits (BLICKHAN, 1989; MCMAHON and CHENG, 1990) has drawn increasing attention since, while advocating a largely reductionist description, it retains key features discriminating legged from wheeled systems: phase switches between flight (swing) and stance phase, a leg orientation, and a repulsive leg behavior in stance. In consequence, not only biomechanical studies investigating hopping (FARLEY et al., 1991; SEYFARTH et al., 2001) or running (HE et al., 1991; FARLEY et al., 1993), but also fast legged robots driven by model based control algorithms (RAIBERT, 1986; SARANLI and KODITSCHEK, 2003) rely on this plant. Yet still, even for the simple spring-mass model, parametric insights remain obscured as the dynamics of the stance phase are non-integrable (WHITTACKER, 1904). Lacking a closed form solution, research is either bound to extensive numerical investigations or needs to establish suitable approximations.

For instance, by mapping the model's parameter space, simulation studies suggest that the spring-mass system for running can display a 'self-stable' behavior (SEYFARTH et al., 2002; GHIGLIAZZA et al., 2003). Here, self-stability refers to the observation of asymptotically stable gait trajectories automatically recovering after disturbances without having to resort to sensory information about the actual disturbances. As the spring-mass model is energy preserving, i.e. non-dissipative, this behavior seems counterintuitive. However, it also constitutes a piecewise holo-

nomic system experiencing phase-dependent dynamics (different stance and flight phase dynamics), and several recent investigations demonstrate that such systems can exhibit asymptotic stability (COLEMAN *et al.*, 1997; RUINA, 1998; COLEMAN and HOLMES, 1999).

Analytical investigations assessing this issue for the spring-mass model in particular, for reasons of accessibility, mostly neglect gravity when approximating the stance-phase dynamics (e.g. GHIGLIAZZA *et al.*, 2003). As this can hardly be done in general locomotion (SCHWIND and KODITSCHEK, 2000) or when addressing physiologically motivated parameters (GEYER, 2001), in SCHWIND and KODITSCHEK (2000) an iterative algorithm reincorporating the effect of gravity is introduced. Although the quality of the approximate solution improves with each iteration, its decreasing mathematical tractability hampers the intended deeper parametric insight into the functional relations.

In this chapter, a comparably simple approximate solution for the dynamics of the planar spring-mass model is derived including gravitational effects. Within the scope of stability in spring-mass running, the predictive power and the quality of this solution are investigated. The former by considering a special case, the latter by comparing a return-map analysis based on the approximation with numerical results throughout the range of the parameters spring stiffness, angle of attack, and system energy. In both situations, model parameters relevant to human locomotion are addressed.

2.2 Spring-mass running

2.2.1 Model

Planar spring-mass running is characterized by alternating flight and contact phases. As described previously (SEYFARTH *et al.*, 2002), during flight the center of mass trajectory is influenced by the gravitational force. Here, a virtual leg of length l_0 and a constant angle of attack α_0 are assumed (Fig. 2.1). When the leg strikes the ground, the dynamic behavior of spring-mass running is further influenced by the force exerted by the leg spring (stiffness k, rest length l_0) attached to the center of mass. The transition from stance to flight occurs if the spring reaches its rest length again during lengthening.
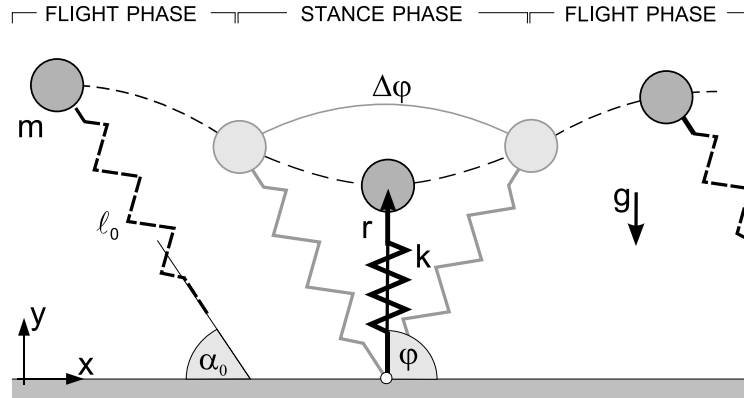
Figure 2.1. Spring-mass model for running. Parameters: m - point mass, ℓ_0 - rest length, α_0 - leg angle of attack during flight, g - gravitational acceleration, k - spring stiffness, r - radial and φ - angular position of the point mass, $\Delta\varphi$ - angle swept during stance.

2.2.2 Apex return map

To investigate periodicity for this running model, it suffices to consider the apex height y_i of two subsequent flight phases. This holds since (i) at apex the vertical velocity $\dot{y}_i$ equals zero, (ii) the forward velocity $\dot{x}_i$ can be expressed in terms of the apex height due to the constant system energy E_s, and (iii) the forward position x_i has no influence on the further system dynamics.

Consequently, the stability of spring-mass running can be analyzed with a one-dimensional return map $y_{i+1}(y_i)$ of the apex height of two subsequent flight phases (single step analysis). In terms of the apex return map, a periodic movement trajectory in spring-mass running is represented by a fixed point $y_{i+1}(y_i) = y_i$. Moreover, as a sufficient condition, a slope $dy_{i+1}(y_i)/dy_i$ within a range of $(-1, 1)$ in the neighborhood of the fixed point indicates the stability of the movement pattern (higher than period 1 stability, which corresponds to symmetric contacts with time reflection symmetry about midstance, is not considered). The size of the neighborhood defines the basin of attraction of the stable trajectory.

2.3 Approximate solution

2.3.1 Model approximations

The analytical solution for the center of mass motion during flight is well known (ballistic flight trajectory), but a different situation applies to the stance phase. Using polar coordinates (r, φ), the Lagrange function of the contact phase is given

by (see Fig. 2.1 for notation)

$$L = \frac{m}{2}\left(\dot{r}^2 + r^2\dot{\varphi}^2\right) - \frac{k}{2}\left(\ell_0 - r\right)^2 - mgr\sin\varphi \,. \tag{2.1}$$

From the Lagrange function, the derived center of mass dynamics is characterized by a set of coupled nonlinear differential equations. As of today, the analytical solution for the contact phase remains open. For such situations, a common approach is to ask for simplifications, which could provide an approximate solution. In the case of (2.1), for sufficiently small angles $\Delta\varphi$ swept during stance, the sine term on the right side can assumed to be

$$\sin\varphi \approx 1 \tag{2.2}$$

and the equations of motion simplify to

$$m\ddot{r} = k(\ell_0 - r) + mr\dot{\varphi}^2 - mg \tag{2.3}$$

and

$$\frac{d}{dt}\left(mr^2\dot{\varphi}\right) = 0 \tag{2.4}$$

transforming the spring-mass model into an integrable central force system, where the mechanical energy E and the angular momentum $P = mr^2\dot{\varphi}$ are conserved.

To derive the apex return map $y_{i+1}(y_i)$, it suffices to identify the system state at the phase transitions (flight-to-stance and stance-to-flight), regardless of the actual motion during stance. Due to both, the radial symmetry of the model (spring assumes rest length ℓ_0 at each phase transition) and the conservation of angular momentum (2.4), the system state at take-off (TO) relates to the state at touch-down (TD) with

$$\begin{aligned}
r_{TO} &= r_{TD} \\
\dot{r}_{TO} &= -\dot{r}_{TD} \\
\varphi_{TO} &= \varphi_{TD} + \Delta\varphi \\
\dot{\varphi}_{TO} &= \dot{\varphi}_{TD}
\end{aligned} \quad, \tag{2.5}$$

where only the angle $\Delta\varphi$ swept during stance can not simply be expressed by the state at touch-down. Hence, we will calculate this angle from the dynamics of the central force system (2.3) and (2.4) in the following sections. Particularly, we will first derive the radial motion $r(t)$ and then integrate $\dot{\varphi} = \frac{P}{mr^2}$. In both cases, we will use the further assumption of small relative spring amplitudes

$$|\rho| \ll 1 \,, \tag{2.6}$$

with $\rho = \frac{r - \ell_0}{\ell_0} \leq 0$ to attain an approximate solution of the central force system and, consequently, of the planar spring-mass dynamics in elementary functions.

2.3.2 Radial motion during stance

Using the conservation of angular momentum P, the constant mechanical energy of the contact phase is given by

$$E = \frac{m}{2}\dot{r}^2 + \frac{P^2}{2mr^2} + \frac{k}{2}(\ell_0 - r)^2 + mgr . \tag{2.7}$$

Applying the substitutions $\varepsilon = \frac{2E}{m\ell_0^2}$, $\omega = \frac{P}{m\ell_0^2}$, and $\omega_0 = \sqrt{\frac{k}{m}}$, the equation rewrites to

$$\varepsilon = \dot{\rho}^2 + \frac{\omega^2}{(1 + \rho)^2} + \omega_0^2 \rho^2 + \frac{2g}{\ell_0}(1 + \rho) , \tag{2.8}$$

where ρ represents the relative spring amplitude introduced in the previous section. The term $\frac{1}{(1+\rho)^2}$ can be represented as a Taylor expansion around the initial relative amplitude $\rho = 0$

$$\left. \frac{1}{(1 + \rho)^2} \right|_{\rho=0} = 1 - 2\rho + 3\rho^2 - O(\rho^3) . \tag{2.9}$$

The restriction (2.6) to small values of ρ allows to truncate the expansion after the square term. Hence, the differential equation (2.8) transforms into

$$t = \int \frac{d\rho}{\sqrt{\lambda \rho^2 + \mu \rho + \nu}} , \tag{2.10}$$

where the factors are given by $\lambda = -(3\omega^2 + \omega_0^2)$, $\mu = 2(\omega^2 - g/\ell_0)$, and $\nu = (\varepsilon - \omega^2 - 2g/\ell_0)$. The integral in (2.10) is given by

$$\int \frac{d\rho}{\sqrt{\lambda \rho^2 + \mu \rho + \nu}} = -\frac{1}{\sqrt{-\lambda}} \arcsin\left(\frac{2\lambda \rho + \mu}{\sqrt{\mu^2 - 4\lambda\nu}} \right) , \tag{2.11}$$

provided that both the factor λ and the expression $4\lambda\nu - \mu^2$ are negative. The first condition is fulfilled by the definition of λ. The second one holds if ν is positive. Since ν is constant, it suffices to check this condition at the instant of touch-down. From here it follows that $\nu = \dot{r}_0^2/\ell_0^2$. Using (2.11), equation (2.10) can be resolved and yields the general radial motion

$$r(t) = \ell_0\left(1 + a + b\sin\hat{\omega}_0 t\right) \tag{2.12}$$

with

$$a = \frac{\omega^2 - g/\ell_0}{\omega_0^2 + 3\omega^2} \, ,$$

$$b = \frac{\sqrt{(\omega^2 - g/\ell_0)^2 + (\omega_0^2 + 3\omega^2)(\varepsilon - \omega^2 - 2g/\ell_0)}}{\omega_0^2 + 3\omega^2} \, ,$$

$$\hat{\omega}_0 = \sqrt{\omega_0^2 + 3\omega^2} \, .$$
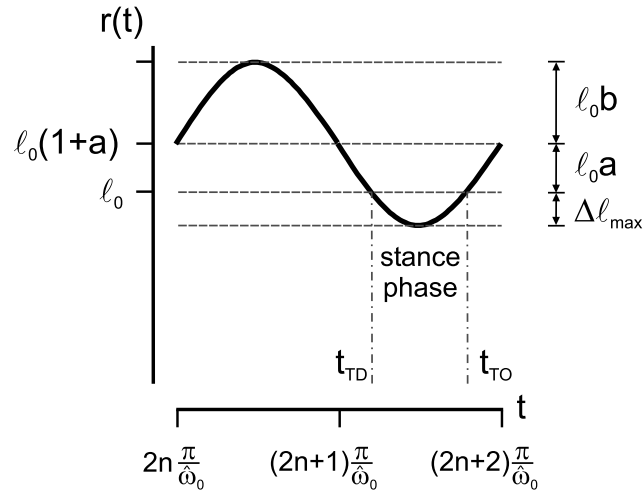
Figure 2.2. General solution for the radial motion $r(t)$ during stance describing a sinusoidal oscillation around $r = \ell_0(1+a)$ with amplitude $\ell_0 b$ and frequency $\hat{\omega}_0$. The solution only holds for $r(t) \leq \ell_0$. Note that a can also be negative shifting ℓ_0 above $\ell_0(1 + a)$. $\Delta\ell_{max}$ - maximum leg compression.

The radial motion $r(t)$ describes a harmonic oscillation around the length $\ell_0(1 + a)$ with an amplitude $\ell_0 b$ and an angular frequency $\hat{\omega}_0$ (Fig. 2.2). However, the solution $r(t)$ only holds for the contact phase of spring-mass running where $r \leq \ell_0$. Using the condition $r = \ell_0$, (2.12) can be resolved to identify the instances of touchdown and take-off (Fig. 2.2)

$$t_{TD} = \frac{1}{\hat{\omega}_0} \left\{ \left(2n + \frac{3}{2} \right) \pi - \left[\frac{\pi}{2} + \arcsin\left(-\frac{a}{b} \right) \right] \right\} \tag{2.13}$$

and

$$t_{TO} = \frac{1}{\hat{\omega}_0} \left\{ \left(2n + \frac{3}{2} \right) \pi + \left[\frac{\pi}{2} + \arcsin\left(-\frac{a}{b} \right) \right] \right\} \tag{2.14}$$

where n is an arbitrary integer.

The maximum spring compression $\Delta\ell_{max}$ during stance is given by the difference of the amplitude $\ell_0 b$ of $r(t)$ and the shift $\ell_0 a$ of the touch-down position $r(t_{TD}) = \ell_0$

14

(Fig. 2.2). Thus, restriction (2.6) to small values of ρ is adequately formulated by

$$b - a \ll 1 . \tag{2.15}$$

2.3.3   Angle swept during stance

With the radial motion $r(t)$, the angle swept during stance can be derived from the equation $P = mr^2\dot{\varphi}$ describing the constant angular momentum. Using the substitutions ω and ρ, the angular velocity is given by

$$\dot{\varphi} = \frac{\omega}{(1 + \rho)^2} . \tag{2.16}$$

To integrate (2.16), again, we use the Taylor expansion (2.9), but cancel this expansion after the linear term already. The Taylor expansion of $\frac{1}{(1+\rho)^2}$ to the second order in ρ for both the r- and φ-trajectory would lead to a more accurate approximate solution of the central force dynamics (2.3) and (2.4). However, approximating the actual spring-mass dynamics (2.1), the central force approach (2.2) is error-prone itself. Carrying out the expansion to the first order only for $\dot{\varphi}$ allows in part to compensate for the error introduced by this general approach (see appendix).

   With $\dot{\varphi} = \omega(1 - 2\rho)$ and substituting ρ by r, we obtain the angle $\Delta\varphi$ swept during stance

$$\Delta\varphi = \int_{t_{TD}}^{t_{TO}} \omega \left[(1 - 2a) - 2b \sin \hat{\omega}_0 t \right] \, dt . \tag{2.17}$$

Considering (2.13) and (2.14) as integration limits, and using the identities $\cos(\arcsin x) = \sqrt{1 - x^2}$ and $\pi + 2\arcsin\left(-\frac{a}{b}\right) = 2\arccos\left(\frac{a}{b}\right)$, the angle swept during stance resolves to

$$\Delta\varphi = 2\frac{\omega}{\hat{\omega}_0} \left[(1 - 2a) \arccos \frac{a}{b} \; + \; 2\sqrt{b^2 - a^2} \right] . \tag{2.18}$$

As both the mechanical energy and the angular momentum are conserved, the parameters ω, $\hat{\omega}_0$, a and b can be related to the system state at touch-down by solving (2.4) and (2.8) at this instant. Therefore, $\Delta\varphi$ is uniquely determined by the system state at touch-down (ℓ_0, $\dot{r}_{TD}$, φ_{TD}, $\dot{\varphi}_{TD}$) and the parameters of the spring-mass system (k, m, g). Although not explicitly appearing when re-substituting in (2.18), the landing angle $\varphi_{TD} = \pi - \alpha_0$ influences $\Delta\varphi$ by determining the distribution of the landing velocity to the radial and angular component.

2.3.4 Approximate solution

By defining the instant of touch-down as $t = 0$, the radial (2.12) and angular motions during stance (2.17) rewrite to

$$r(t) = \ell_0 + \ell_0 \left[a \left(1 - \cos \hat{\omega}_0 t \right) - \sqrt{b^2 - a^2} \, \sin \hat{\omega}_0 t \right] \tag{2.19}$$

$$\varphi(t) = \varphi_{TD} + (1 - 2a)\omega t + \frac{2\omega}{\hat{\omega}_0} \left[a \sin \hat{\omega}_0 t + \sqrt{b^2 - a^2} \, \left(1 - \cos \hat{\omega}_0 t \right) \right] \tag{2.20}$$

with t ranging from 0 to $t_c = [\pi + 2 \arcsin(-a/b)]/\hat{\omega}_0$. By substituting a and b (2.12) as well as expressing ε, ω, and ω_0 with the system state at touch-down, the center of mass trajectory during stance resolves to

$$r(t) = \ell_0 - \frac{|\dot{r}_{TD}|}{\hat{\omega}_0} \sin \hat{\omega}_0 t + \frac{\dot{\varphi}_{TD}^2 \ell_0 - g}{\hat{\omega}_0^2} \left(1 - \cos \hat{\omega}_0 t \right) \tag{2.21}$$

$$\begin{aligned} \varphi(t) \;=\; & \pi - \alpha_0 + \left(1 - 2 \frac{\dot{\varphi}_{TD}^2 - g/\ell_0}{\hat{\omega}_0^2} \right) \dot{\varphi}_{TD} t \\ & + \frac{2\dot{\varphi}_{TD}}{\hat{\omega}_0} \left[\frac{\dot{\varphi}_{TD}^2 - g/\ell_0}{\hat{\omega}_0^2} \sin \hat{\omega}_0 t + \frac{|\dot{r}_{TD}|}{\hat{\omega}_0 \ell_0} \left(1 - \cos \hat{\omega}_0 t \right) \right] \end{aligned} \tag{2.22}$$

The radial motion corresponds to the motion of a one-dimensional spring-mass system under the influence of gravity except for the increased oscillation frequency $\hat{\omega}_0 = \sqrt{k/m + 3\dot{\varphi}_{TD}^2}$. The angular motion has a linear characteristic, which is modulated by trigonometric functions. The time in contact resolves to

$$t_c = \frac{1}{\hat{\omega}_0} \left[\pi + 2 \arctan \left(\frac{g - \ell_0 \dot{\varphi}_{TD}^2}{|\dot{r}_{TD}| \hat{\omega}_0} \right) \right] \tag{2.23}$$

2.4 Stability of spring-mass running

2.4.1 Analytical apex return map

In the following section we use the derived analytical solution for the contact to calculate the dependency of two subsequent apex heights. Based on this apex return map, for a special case, we derive an explicit parametric dependency required for stable spring-mass running and, within the scope of gait stability, compare parameter predictions with previous numerical results.

With the angle swept during stance (2.18), we know how the system state at take-off relates to the initial state of the contact phase at touch-down (2.5). But, to apply the correct initial values, the mapping between the apex height y_i and the

touch-down state in polar coordinates is required

$$
y_i \mapsto
\begin{bmatrix}
\dot{x} = \sqrt{\frac{2}{m}(E_s - mgy_i)} \\
y = \ell_0 \sin \alpha_0 \\
\dot{y} = -\sqrt{2g(y_i - y)}
\end{bmatrix}_{TD}
\mapsto
\begin{bmatrix}
r = \ell_0 \\
\dot{r} = \dot{x} \cos \varphi + \dot{y} \sin \varphi \\
\varphi = \pi - \alpha_0 \\
\dot{\varphi} = \frac{1}{\ell_0}(\dot{y} \cos \varphi - \dot{x} \sin \varphi)
\end{bmatrix}_{TD}
\tag{2.24}
$$

where E_s is the system energy prior to touch-down (for details see sections 2.2.2 and 2.4.2). To obtain the apex return map $y_{i+1}(y_i)$, the system state at the following apex $i+1$ has to be derived, i.e. the mapping between the state at take-off and the apex $i+1$ is further required

$$
\begin{bmatrix}
\dot{x} = \dot{r} \cos \varphi - \ell_0 \dot{\varphi} \sin \varphi \\
y = \ell_0 \sin \varphi \\
\dot{y} = \dot{r} \sin \varphi + \ell_0 \dot{\varphi} \cos \varphi
\end{bmatrix}_{TO}
\mapsto
\begin{array}{l}
\dot{x}_{i+1} = \dot{x}_{TO} \\
y_{i+1} = y_{TO} + \frac{1}{2g} \dot{y}_{TO}
\end{array}.
\tag{2.25}
$$

Using both mappings, the apex return map function of approximated spring-mass running can be constructed and yields after simplification

$$
\begin{aligned}
y_{i+1}(y_i) \;=\;& \frac{1}{mg} \Big[\cos(\Delta\varphi - 2\alpha_0) \sqrt{mg(y_i - \ell_0 \sin \alpha_0)} \\
& + \sin(\Delta\varphi - 2\alpha_0) \sqrt{E_s - mgy_i} \Big]^2 + \ell_0 \sin(\alpha_0 - \Delta\varphi).
\end{aligned}
\tag{2.26}
$$

Next to the preceding apex height (y_i), y_{i+1} is a function of the system energy (E_s), the landing leg configuration (ℓ_0, α_0), and the dynamic response of the spring-mass system (k, m, g). However, the apex return map can only exist where y_{i+1} exceeds the landing height $y_{i+1} \geq \ell_0 \sin \alpha_0$. Otherwise, the leg would extend into the ground (stumbling).

2.4.2 System energy correction

For spring-mass running, the stability analysis can be performed based on a one-dimensional apex return map since the system energy E_s remains constant (see section 2.2.2). When using the approximation for the stance phase, in particular due to assumption (2.2), this conservation of energy is violated if the vertical position at take-off differs from that at touch-down ($y_{TD} \neq y_{TO}$, i.e. asymmetric contact phase):

In a central force system approach, the kinetic energy $\frac{m}{2}(\dot{r}^2 + r^2\dot{\varphi}^2)$ is equal at touch-down and take-off (2.5), regardless of the angle swept during stance. At the transitions between flight and stance phase the direction of the gravitational force

'switches' between vertical and leg orientation. The corresponding shifts in energy at touch-down and take-off compensate each other for symmetric stance phases ($y_{TD} = y_{TO}$). In contrast, for asymmetric contact phases, a net change in system energy $\Delta E = mg\left(y_{TO} - y_{TD}\right)$ occurs. To restore the conservative nature of the model ($E_s = const$), this change is corrected in (2.25) by readjusting the horizontal velocity to

$$\dot{x}_{i+1} = \sqrt{\frac{2}{m}\left(E_s - mgy_{i+1}\right)}. \tag{2.27}$$

When reapplying the apex return map (2.26) for the new apex height y_{i+1}, this is automatically taken into account by reusing the system energy E_s.

2.4.3 Stability analysis: the special case $a = 0$

From (2.26) we obtain that the fixed point condition $y_{i+1}(y_i) = y_i$ is fulfilled if (2.18) describes symmetric contacts with $\Delta\varphi = 2\alpha_0 - \pi$. In general, solving (2.18) appears to be difficult since this equation involves nonlinearities. However, in order to demonstrate the existence and stability of fixed points of the apex return map, it suffices to present one example. In the following, we will confine our investigation to the special case $a = 0$, i.e. when the angular velocity at touch-down is identical to the pendulum frequency $\omega = \dot{\varphi}_{TD} = -\sqrt{g/\ell_0}$ (although $\omega = +\sqrt{g/\ell_0}$ equally satisfies $a = 0$, we are concerned with forward locomotion only). In this particular situation, (2.18) considerably simplifies to

$$\Delta\varphi(\tilde{k}, \alpha_0, \tilde{E}_s) = -\frac{2}{\sqrt{\tilde{k} + 3}}\left(\frac{\pi}{2} + 2\sqrt{\frac{2\tilde{E}_s - 1 - 2\sin\alpha_0}{\tilde{k} + 3}}\right) \tag{2.28}$$

where $\tilde{k} = \frac{k\ell_0}{mg}$ represents the dimensionless spring stiffness and $\tilde{E}_s = \frac{E_s}{mg\ell_0}$ is the dimensionless system energy.[1]

Apart from its mathematical simplicity, this special case addresses a characteristic running speed in animals and humans. Considering that, for rather steep angles of attack, the horizontal velocity $\dot{x}$ relates to the angular velocity with $\dot{x} \approx \ell_0\dot{\varphi}_{TD}$, the case $a = 0$ describes running with a Froude number $Fr = \frac{\dot{x}^2}{g\ell_0} = 1$, which is close to the preferred trotting speed in horses (ALEXANDER, 1989; WICKLER et al., 2001) or to a typical jogging speed in humans (ALEXANDER, 1989).

---

[1]The appearance of $\tilde{k}$ and $\tilde{E}_s$ is not restricted to the special case $a = 0$. Rather, these substitutes can be identified as independent parameter groups when applying a dimensional analysis of the governing equations in spring-mass running. Specifically, the dimensionless stiffness $\tilde{k}$ is a well known parameter group frequently used in comparative studies on animal and human locomotion (e.g. BLICKHAN, 1989; BLICKHAN and FULL, 1993).

Existence of fixed points

Before continuing with (2.28), we need to check whether apex states y_i restricted by the touch-down condition $\omega = -\sqrt{g/\ell_0}$ can be found. By using the apex-to-touch-down map (2.24), we find the formal expression

$$\omega = \sqrt{\frac{2g}{\ell_0}} \left(\cos\alpha_0 \sqrt{y_i/\ell_0 - \sin\alpha_0} - \sin\alpha_0 \sqrt{\tilde{E}_s - y_i/\ell_0} \right). \tag{2.29}$$

Resolving for $\omega = -\sqrt{g/\ell_0}$ leads to the corresponding apex height

$$
\begin{aligned}
y_i &= \ell_0 \sin\alpha_0 &+ \frac{\ell_0}{2} \left(\cos\alpha_0 - \sin\alpha_0 \sqrt{2\tilde{E}_s - 1 - 2\sin\alpha_0} \right)^2 \\
&= \ell_0 \tilde{E}_s &- \frac{\ell_0}{2} \left(\sin\alpha_0 + \cos\alpha_0 \sqrt{2\tilde{E}_s - 1 - 2\sin\alpha_0} \right)^2 .
\end{aligned}
\tag{2.30}
$$

However, substituting (2.30) back into (2.29) yields

$$
\begin{aligned}
-1 &= \cos\alpha_0 \, | \cos\alpha_0 - \sin\alpha_0 \sqrt{2\tilde{E}_s - 1 - 2\sin\alpha_0} | \\
&\quad - \sin\alpha_0 \, | \sin\alpha_0 + \cos\alpha_0 \sqrt{2\tilde{E}_s - 1 - 2\sin\alpha_0} |
\end{aligned}
\tag{2.31}
$$

and it follows that the solution (2.30) only holds if $\cos\alpha_0 \leq \sin\alpha_0 \sqrt{2\tilde{E}_s - 1 - 2\sin\alpha_0}$, i.e. the system energy fulfils $\tilde{E}_s \geq \tilde{E}_s^{min}$ with

$$\tilde{E}_s^{min} = \frac{1}{2\sin^2\alpha_0} + \sin\alpha_0 . \tag{2.32}$$

For a system energy $\tilde{E}_s = \tilde{E}_s^{min}$, the apex height is identical to the landing height $y_i = \ell_0 \sin\alpha_0$. Above this level $\tilde{E}_s > \tilde{E}_s^{min}$, the apex height increases, but never approaches the upper boundary $y_i = \ell_0 \tilde{E}_s$.

Having established the flight phase limitations for the existence of apex states y_i characterized by $a = 0$, we can proceed with (2.28). Solving for $\Delta\varphi = 2\alpha_0 - \pi$ involves a quadratic equation for $\sqrt{\tilde{k} + 3}$, which has only one physically reasonable solution yielding an expression for the required spring stiffness

$$\tilde{k}(\alpha_0, \tilde{E}_s) = \frac{\left[\pi + \sqrt{\pi^2 + 32\left(\frac{\pi}{2} - \alpha_0\right)\sqrt{2\tilde{E}_s - 1 - 2\sin\alpha_0}} \right]^2}{16\left(\frac{\pi}{2} - \alpha_0\right)^2} - 3 . \tag{2.33}$$

At given angle of attack ($\alpha_0 \in [0, \frac{\pi}{2}]$ in forward locomotion), the stiffness is lowest

for the minimum system energy

$$\tilde{k}^{min}(\alpha_0) = \tilde{k}^{min}(\alpha_0, \tilde{E}_s^{min}) = \frac{\left[\pi + \sqrt{\pi^2 + 32\left(\frac{\pi}{2} - \alpha_0\right)\frac{\cos\alpha_0}{\sin\alpha_0}}\right]^2}{16\left(\frac{\pi}{2} - \alpha_0\right)^2} - 3 \, , \qquad (2.34)$$

with increasing system energy $\tilde{E}_s > \tilde{E}_s^{min}$, a larger spring stiffness is required to ensure symmetric contacts (Fig. 2.3).
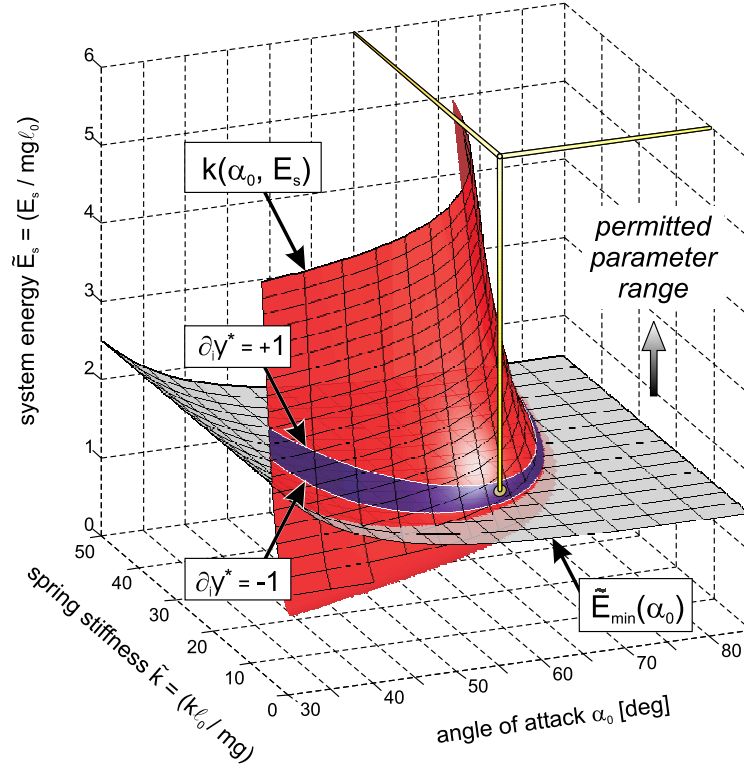
Figure 2.3. Parameter interdependence for fixed point solutions with $a = 0$. The fixed points can only exist if a minimum energy $\tilde{E}_{min}(\alpha_0)$ is exceeded (permitted parameter range). Above this level, the required parameter combinations of angle of attack α_0, system energy $\tilde{E}_s$, and spring stiffness $\tilde{k}$ are defined by relation (2.33) describing a sub set $\tilde{k}(\alpha_0, \tilde{E}_s)$ within the parameter space. The dark area within this sub set characterizes stable fixed point solutions (see section 2.4.3). The open lines indicate the parameter combination that is used as apex return map example in Fig. 2.4.

With (2.32) and (2.33) we have identified the parameter dependence required for periodic locomotion constrained by $\omega = -\sqrt{g/\ell_0}$. Although the resulting steady-state solutions (2.30) demonstrate the existence of fixed points of the apex return map, it remains to investigate to what extent the derived parameter relations represent stable gait patterns.

Stability of fixed points

Stable fixed point solutions y_i are characterized by

$$-1 \quad < \quad \tfrac{\partial}{\partial y_i}\left[y_{i+1}(y_i)\right]_{y_{i+1}=y_i} = \partial_i y^* \quad < \quad 1 \,. \tag{2.35}$$

To prove stability, we need to identify at least one parameter set $(\alpha_0, \tilde{E}_s)$ leading to solutions y_i satisfying (2.35). Starting with (2.26), we obtain

$$\partial_i y^* = 1 + \left[\ell_0 \cos\alpha_0 + 2\sqrt{(\ell_0 \tilde{E}_s - y_i)(y_i - \ell_0 \sin\alpha_0)}\right]\partial_i \Delta\varphi^* \tag{2.36}$$

by using $\Delta\varphi = 2\alpha_0 - \pi$ for symmetric contacts. As the bracketed expression always remains positive, (2.35) transforms into a condition for the angle swept during stance $\partial_i\Delta\varphi^* \in \left(-\frac{2}{\ell_0\cos\alpha_0 + 2\sqrt{(\ell_0\tilde{E}_s - y_i)(y_i - \ell_0\sin\alpha_0)}}, 0\right)$ indicating that disturbed apex conditions towards higher (lower) apices must be compensated for by a larger (smaller) amount of angular sweep in contact ($\Delta\varphi^*$ is negative). However, to remain stable, the rate of this 'negative' correlation must not exceed $-\frac{2}{\ell_0\cos\alpha_0 + 2\sqrt{(\ell_0\tilde{E}_s - y_i)(y_i - \ell_0\sin\alpha_0)}}$. From (2.18) it follows that

$$
\begin{aligned}
\partial_i\Delta\varphi^* \;=\; & \left(\tfrac{1}{\omega} - \tfrac{3\omega}{\hat{\omega}_0^2}\right)(2\alpha_0 - \pi)\;\partial_i\omega^* \\
& -2\tfrac{\omega}{\hat{\omega}_0}\left[2\arccos\left(\tfrac{a}{b}\right)\;\partial_i a^* - \frac{\left(\tfrac{a}{b} - 2\tfrac{a^2}{b} + 2b\right)\partial_i b^* - \partial_i a^*}{\sqrt{b^2 - a^2}}\right],
\end{aligned}
\tag{2.37}
$$

which, by expressing $\partial_i a^*$ and $\partial_i b^*$ with $\partial_i\omega^*$, and resolving $\partial_i\omega^*$, can be further deduced to

$$
\begin{aligned}
\partial_i\Delta\varphi^* \;=\; & \left\{\left(\tfrac{1}{\omega} - \tfrac{3\omega}{\hat{\omega}_0^2}\right)(2\alpha_0 - \pi) - 2\tfrac{\omega^2}{\hat{\omega}_0^3}\left[(4 - 12a)\arccos\left(\tfrac{a}{b}\right)\right.\right. \\
& \left.\left. -\frac{\left(\tfrac{a}{b} - 2\tfrac{a^2}{b} + 2b\right)\left(2\tfrac{a}{b} - \tfrac{1}{b} - 3\tfrac{a^2}{b} - 3b\right) - 2 + 6a}{\sqrt{b^2 - a^2}}\right]\right\} \\
& \times \frac{\sqrt{2g}}{2\ell_0}\left(\frac{\cos\alpha_0}{\sqrt{y_i^* - \ell_0\sin\alpha_0}} + \frac{\sin\alpha_0}{\sqrt{\ell_0\tilde{E}_s - y_i^*}}\right).
\end{aligned}
\tag{2.38}
$$

Note that (2.38) is valid for any fixed point solution with symmetric contacts $\Delta\varphi^* = 2\alpha_0 - \pi$ since $a = 0$ has not yet been utilized. Finally, applying $a = 0$ and $\omega = -\sqrt{g/\ell_0}$ yields

$$
\begin{aligned}
\partial_i\Delta\varphi^* \;=\; & \frac{1}{\tilde{k}+3}\left[\tilde{k}\left(\tfrac{\pi}{2} - \alpha_0\right) - \frac{2\pi}{\sqrt{\tilde{k}+3}} - \frac{6\sqrt{2\tilde{E}_s - 1 - 2\sin\alpha_0}}{\tilde{k}+3}\right. \\
& \left. -\frac{4}{\sqrt{2\tilde{E}_s - 1 - 2\sin\alpha_0}}\right] \times \sqrt{\tfrac{2}{\ell_0}}\left(\frac{\cos\alpha_0}{\sqrt{y_i^* - \ell_0\sin\alpha_0}} + \frac{\sin\alpha_0}{\sqrt{\ell_0\tilde{E}_s - y_i^*}}\right).
\end{aligned}
\tag{2.39}
$$

By substituting (2.39) back into (2.36) and using (2.30) as well as (2.33), we obtain an expression $\partial_i y^* = \partial_i y^*(\alpha_0, \tilde{E}_s)$ identifying the parameter dependence of the derivative of the apex height return map $y_{i+1}(y_i)$ at the fixed points y_i^* in the special case $a = 0$.

Based on this result, in Fig. 2.3, parameter combinations leading to stable fixed points are indicated in the $\tilde{k}(\alpha_0, \tilde{E}_s)$–region as dark area, which is limited by two curves denoting the lower ($\partial_i y^* = -1$) and upper constraint ($\partial_i y^* = +1$) for stable solutions (2.35). Although this area narrows and almost diminishes below the minimum system energy $\tilde{E}_{min}(\alpha_0)$ for steep angles of attack, parameter combinations above this critical level remain existent. For example, an angle of attack $\alpha_0 = 85°$ (not shown in Fig. 2.3) necessitates a minimum system energy $\tilde{E}_{min} = 1.500$, and the lower stability constraint corresponds to a system energy ($\tilde{E}_s^- = 1.497$) below this minimum. Nevertheless, the system energy related to the upper constraint ($\tilde{E}_s^+ = 1.506$) still exceeds the critical level, and, for instance, for a system energy $\tilde{E}_{min} < \tilde{E}_s = 1.503 < \tilde{E}_s^+$, one easily checks that, besides the steep angle condition (2.2), with $b - a < 0.06$ the resulting apex return map (2.26) fulfils (2.15) required for the validity of the approximate solution.

As a result of the steep angle $\alpha_0 = 85°$, the return map $y_{i+1}(y_i)$ almost matches the diagonal $y_{i+1} = y_i$, if viewed on the large scale of all possible apex heights, hampering a compact overview of its qualitative behavior. However, to provide such an overview, in Fig. 2.4, an explicit return map example is shown for the moderate angle of attack $\alpha_0 = 60°$. Here, the system energy $\tilde{E}_s = 1.61$ and, as a result of (2.33), the spring stiffness $\tilde{k} = 10.8$ (indicated by the open lines in Fig. 2.3) are chosen such that the fixed point $y^* = 0.872\ell_0$ (open circle) calculated from (2.30) is stable with $\partial_i y^* = 0$. Starting from disturbed apex heights, the system stabilizes within a few steps (as indicated by the arrow traces in the small panel of Fig. 2.4). Here, the basin of attraction contains all apex heights from the landing height $y_\ell = \ell_0 \sin \alpha_0$ to the second, unstable fixed point (closed circle). As the analysis performed in this section is restricted to local predictions, both the basin and the second fixed point are merely observations from plotting (2.26). However, from Fig. 2.3 it is obtained that, if the system energy is not adequately selected, the fixed point given by (2.30) is unstable. Without proof we observed the following behavior: For a system energy leading to $\partial_i y^* < -1$, (2.30) still traces the lower fixed point being unstable. For $\partial_i y^* = 1$, both fixed points collapse to a single one, and, if $\partial_i y^* > 1$, (2.30) describes the upper, unstable fixed point.
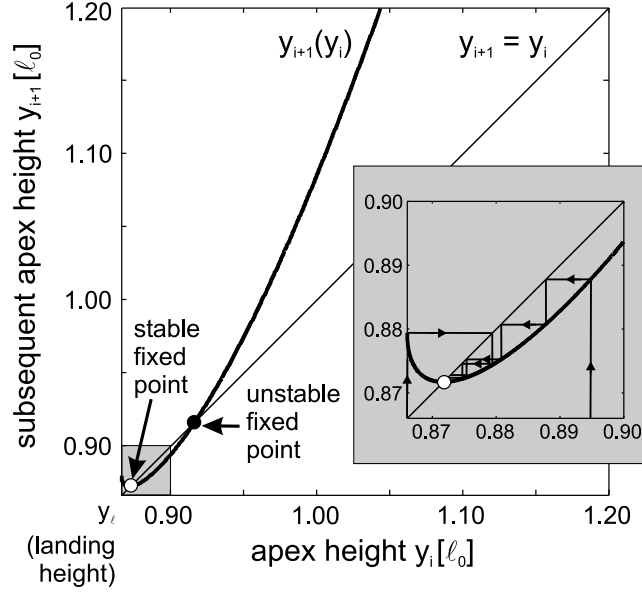
Figure 2.4. Stability of spring-mass running. The return map function $y_{i+1}(y_i)$ is shown for the parameter set $\alpha_0 = 60°$, $\tilde{E}_s = 1.61$, and $\tilde{k} = 10.8$, which belongs to the calculated region of parameter combinations producing stable fixed point solutions. As predicted, the return map has a stable fixed point $y_{i+1} = y_i$ attracting neighboring apex states within a few steps (arrow traces in the magnified region). Furthermore, the return map is characterized by an additional, unstable fixed point representing the upper limit of the basin of attraction of the stable one (the lower limit is given by the landing height $y_\ell = \ell_0 \sin \alpha_0$).

k-α_0-relationships for stable running

In the last two sections, we have identified the parameter combinations ($\tilde{k}$, α_0, and $\tilde{E}_s$) required to achieve self-stable running patterns characterized by $a = 0$ (dark area in Fig. 2.3). Specifically, for steep angles of attack $\alpha_0 \to \frac{\pi}{2}$, stable trajectories are obtained when the system energy $\tilde{E}_s$ is close to the minimum system energy $\tilde{E}_s^{min}$ (2.32), i.e. the parametric dependency approaches the minimum stiffness-angle-relation $\tilde{k}^{min}(\alpha_0)$ (2.34). In the numerical study (Seyfarth et al., 2002), we empirically found a different estimate for the stiffness-angle-relationship $k(\alpha_0) \approx \frac{1600N}{\ell_0(1-\sin\alpha_0)}$, and the question arises in how far both relationships relate to each other.

Considering that, for $\alpha_0 \to \frac{\pi}{2}$, the minimum system energy $\tilde{E}_s^{min}$ approaches a value of 1.5, in the numerical study this corresponds to a system energy of $E_s = mg\ell_0\tilde{E}_s \approx 1200$J ($m = 80$kg, $g = 9.81$m/s^2, and $\ell_0 = 1$m). As the initial apex height was fixed to $y_0 = \ell_0$ therein, this is equivalent to an initial speed of $\dot{x}_0 = \sqrt{\frac{2}{m}(E_s - mg\ell_0)}$ of about 3.3m/s, which is slightly less than the initial speed

the empirical k-α_0-relationship is derived from ($\dot{x}_0 = 5$m/s, Fig. 2A in SEYFARTH *et al.* (2002)). However, the general shape of the stable domain does not change much for initial running velocities below $\dot{x}_0 = 5$m/s (the domain only narrows, Fig. 2B,C in SEYFARTH *et al.* (2002)) and, hence, from an energetic point of view both relationships should be comparable.

A similar argument holds for the restriction to the special case $a = 0$. As in SEYFARTH *et al.* (2002) running stability is scrutinized for all possible parameter combinations, certainly more than the steady-state solutions belonging to this special case are identified. Actually, the stable domain forms a single volume in the k-α_0-$\dot{x}_0$ space (GEYER, 2001; SEYFARTH *et al.*, 2002), which, due to the restriction to the special case $a = 0$, cannot be obtained from (2.33). Here, only a surface element of this volume can be derived (dark area in Fig. 2.3). However, for $\dot{x}_0 \leq 5$m/s the stable parameter domain is rather narrow (for steep angles of attack the angular range is limited to $2°$) and, although we do not expect exactly the same result, both the empirical relationship and (2.34) should qualitatively be equivalent for $\alpha_0 \to \frac{\pi}{2}$.

Using that for $\alpha_0 \to \frac{\pi}{2}$, $\frac{1}{1-\sin\alpha_0} \to \frac{2}{(\frac{\pi}{2}-\alpha_0)^2}$, and taking the body mass used in the numerical study ($m = 80$kg) into account, the empirical k-α_0-relationship can be written as $\tilde{k}_{\alpha_0 \to \frac{\pi}{2}} \approx \frac{4}{(\frac{\pi}{2}-\alpha_0)^2}$. In the same limit (2.34) reads $\tilde{k}^{min}_{\alpha_0 \to \frac{\pi}{2}} = \frac{\pi^2/4}{(\frac{\pi}{2}-\alpha_0)^2}$, which indeed confirms that the qualitative behavior of (2.34) is consistent with the empirically found stiffness-angle relation. In addition to this mere comparison, (2.33) emphasizes the change of the stiffness-angle relation with increasing system energy, introducing a quality observed but not formulated in the numerical study.

2.4.4 Quality of approximate solution

Considering the steep angle assumption (2.2), the valid range of the approximate solution is always bound to a spring stiffness exceeding physiologically reasonable values. For instance, taking the example $\alpha_0 = 85°$ and $\tilde{E}_s = 1.503$ of the last section, the dimensionless stiffness $\tilde{k}(\alpha_0, \tilde{E}_s)$ is $\tilde{k} = 326$. Scaled into absolute values, for a human with a body mass of $m = 80kg$ and a leg length of $\ell_0 = 1m$, the required stiffness $k = \frac{mg}{\ell_0}\tilde{k}$ approaches $260kN/m$. Compared to experiments, where typical stiffness values are in the range of $k = 10 - 50kN/m$ (e.g. ARAMPATZIS *et al.*, 1999), the predicted stiffness is far above the biological range, which, however, is no contradiction since humans do use flatter angles of attack in running (speed dependent, e.g. $\alpha_0 = 60 - 70°$, FARLEY and GONZALEZ (1996)).

At this point, the question arises of how applicable the approximate solution is to biological data, or, more technically spoken, how restrictive are the assumptions

made? To gain a quantitative judgement, the quality of the approximation shall be demonstrated by the following example: Still considering a human subject with $m = 80kg$ and $\ell_0 = 1m$, the running speed is set to be $\dot{x}_0 = 5m/s$ at the apex $y_0 = \ell_0$, and a leg stiffness $k = 11kN/m$ and an angle of attack $\alpha_0 = 60°$ are assumed. The contact phase of the resulting steady-state motion is characterized by a maximum spring compression of 20%, which corresponds to a relative spring amplitude $\rho = -0.2$. At this configuration, the accuracy (i.e. the maximum error) of the analytically predicted center of mass trajectory (2.21 and 2.22) is better than 1% in spring compression and 0.6° for the angle swept during stance ($|\Delta\varphi| = 60°$) compared to the numerical counterpart.

This indicates that, even for configurations with reasonable angles of attack, the approximate solution well describes the dynamics of the stance phase. However, it cannot be concluded with such a single example whether the quality of the solution satisfies the demands of a specific application. To illustrate its predictive power in the context of self-stability, in Fig. 2.5 the parameter combinations leading to self-stable movement trajectories (Fig. 2.5A-C) are compared to numerical results (Fig. 2.5D-F, after SEYFARTH *et al.* (2002)) throughout the parameter space. Although, for the stability of steady-state trajectories, it would suffice to compare the analytically predicted with the numerically calculated apex return maps for each single parameter combination, in Fig. 2.5 the investigation of the number of successful steps is adopted from SEYFARTH *et al.* (2002). This not only allows a direct comparison to the numerical and experimental results presented in SEYFARTH *et al.* (2002), but, starting from disturbed apex conditions, also scrutinizes the performance of the approximate apex return map (2.26) if consecutively applied, hereby addressing the influence of the arbitrary energy correction following each stance phase (section 2.4.2) on the quality of the approximate solution. For angles of attack $\alpha_0 \geq 60°$, the predicted region matches the simulation results surprisingly well. This holds not only for the general shape, but also for the subtle details (e.g. the sharp edges in the stability region close to the level of $\dot{x}_0 = 5m/s$ in Fig. 2.5B and C, E and F, respectively). Again, a quantitative comparison shall be provided: For $\alpha_0 = 60°$, the range of spring stiffness resulting in stable running narrows from $2kN/m$ ($10.5 - 12.5kN/m$, Fig. 2.5D) to $1.6kN/m$ ($10.6 - 12.2kN/m$, Fig. 2.5A). Complementary, for a given spring stiffness of $k = 11kN/m$, the angle of attack range narrows from 2.7° ($58.0 - 60.7°$) to 1.7° ($58.6 - 60.3°$).

ANALYTICAL APPROXIMATION   successful steps (max. 24)

NUMERICAL SIMULATION   successful steps (max. 24)
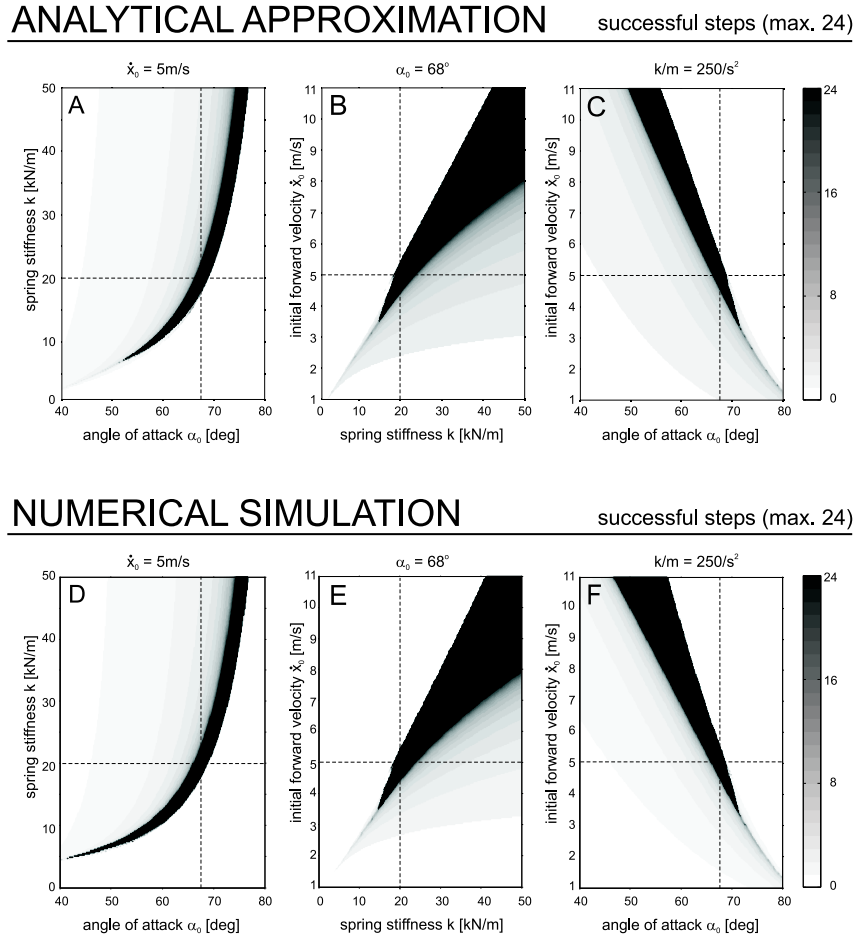
Figure 2.5. Comparison of the stability region for spring-mass running predicted by the analytical approximation (A-C) with the results from a previous simulation study (SEYFARTH *et al.*, 2002) (D-F). Starting from the initial condition $y_0 = \ell_0$ and $\dot{x}_0$, the number of successful steps is predicted by iteratively applying the return map function (2.26) (A-C), or obtained through numerical integration of the spring-mass system (D-F). The movement is interrupted if (i) the vertical or horizontal take-off velocity becomes negative, or (ii) the number of successful steps exceeds 24 (scale on the right). In each subplot (A-C, or D-F, respectively), one of three parameters $(k, \alpha_0, \dot{x}_0)$ is held constant. *Additional parameters:* m=80kg, g=9.81m/s^2, ℓ_0=1m, and $E_s = \frac{m}{2}\dot{x}_0^2 + mg\ell_0$.

2.5   Discussion

In this chapter, we addressed the stability of spring-mass running within a theoretical framework. We derived an analytical solution for the stance phase dynamics assuming steep spring angles and small spring compressions, and investigated the return map of the apex height. The analysis confirms the previously identified self-stabilization of spring-mass running. Moreover, the stability prediction surprisingly

well matches the numerical results throughout the parameter space (leg stiffness k, angle of attack $\alpha \geq 60°$, and system energy E_s or, adequately, initial forward speed $\dot{x}_0$), suggesting that, within this range, the approximate solution sufficiently describes the dynamics of the center of mass during the stance phase of spring-mass running. The solution is not restricted to the parameter setups used in this study, but also holds in dynamically similar situations (BLICKHAN, 1989).

2.5.1 Closed form representations of the stance phase dynamics

As mentioned in the introduction (section 2.1), the stance phase dynamics of the spring-mass model are non-integrable (WHITTACKER, 1904) and, thus, approximate solutions are in demand when seeking parametric insights into the properties of the system. A common approach to this issue is to simply ignore the gravitational force. The resulting central force problem allows a closed form solution in the formal mathematical sense, which, however, involves elliptic integrals (SCHMITT and HOLMES, 2000) and, therefore, lacks a representation in elementary functions hampering the desired parametric insight. At this point, one either proceeds by resuming to numerical studies (e.g. GHIGLIAZZA *et al.*, 2003), or further simplifications are introduced. For instance, in SCHWIND and KODITSCHEK (2000) the mean value theorem is applied to circumvent elliptic integrals yielding a good approximation of the modified system dynamics in stance, especially, when the spring compression is close to its maximum.

However, in these studies it is also demonstrated that the effects of gravity can hardly be neglected in general locomotion (SCHWIND and KODITSCHEK, 2000) or when using physiologically motivated model parameters (GEYER, 2001). The resulting approximate solutions clearly deviate from numerical calculations for the spring-mass model incorporating gravity (e.g. in SCHWIND and KODITSCHEK (2000) mean errors as high as 20% for the radial velocity at take-off are observed). Although these solutions may be used for qualitative assessments (GHIGLIAZZA *et al.*, 2003), any quantitative result seems highly questionable. Bearing in mind that the spring-mass model is employed to devise general control schemes for running machines (RAIBERT, 1986; SARANLI and KODITSCHEK, 2003) and to investigate animal and human locomotion (HE *et al.*, 1991; FARLEY *et al.*, 1991, 1993; SEYFARTH *et al.*, 2001), this leaves a rather unsatisfactory state.

To surmount the discrepancy, in SCHWIND and KODITSCHEK (2000) a general approach similar to Picard iterations is introduced that iteratively fits the solution without gravity in stance to the complete system. The algorithm does not depend

on the particular spring law, and changes of angular momentum as observed in the complete spring-mass system are taken into account. Again, this approach best approximates the solution for the instant of maximum spring compression, although it seems that, with an increasing number of iterations, the result for the subsequent apex condition also improves (in SCHWIND and KODITSCHEK (2000) the 'bottom-to-apex map' from maximum spring compression to apex position is investigated). The authors report a reduction of the largest mean errors from 20% for the zeroth iterate (solution without gravity) to 7% for the first iterate and to 3.5% for the second iterate. Yet with increasing number of iterates, the algebraic tractability of the approximate solution decreases. However, it should be noted that, although most of the model parameters in SCHWIND and KODITSCHEK (2000) are human-like, a body mass of $m = 1kg$ is used, and the correct assessment of accuracy in the physiological parameter domain requires re-investigation for this approximation.

Similar to existing approaches, the approximate solution derived in this study is based on a simplification of the stance-phase dynamics to a central force problem rendering the planar spring-mass model integrable. But instead of ignoring gravity, the gravitational force vector is realigned from the vertical to the spring axis. This approach is motivated by the assumption of steep spring angles during stance. By introducing the further assumption of small spring amplitudes, a Taylor series expansion allows to rewrite the resulting differential equation for the radial motion into an integral equation of familiar type ($\int \frac{dx}{ax^2+bx+c}$). Although the dynamics of the central force system could have been obtained by consequently solving elliptic integrals, this approach avoids the difficult quadratures that typically remain even when gravity is ignored (e.g. SCHMITT and HOLMES, 2000; GHIGLIAZZA et al., 2003). Hence, the radial and angular motions can be extracted in terms of elementary functions. But, more importantly, the approximation error introduced by using the Taylor series expansions in part compensates for the error made by converting the planar spring-mass model into a central force system (see appendix). In consequence, the exemplified approach combines a comparatively simple solution with surprising accuracy well extending into the physiologically motivated parameter domain (compare Fig. 2.5). Although a Hooke's law spring has been considered in this study, the applied ideas might be transferable to other spring potentials as well.

However, it should not be overlooked that, for any approximation based on the central force system approach during stance, the conservation of system energy is inherently violated for asymmetric contact phases (take-off height unequal to touch-down height). A pragmatic solution to this is to simply restore the preset system

energy at take-off, for instance, by artificially manipulating the vertical and/or horizontal take-off velocity (SARANLI *et al.*, 1998; GHIGLIAZZA *et al.*, 2003). We resolved this discrepancy in the same manner (by forcing E_s to be constant, the horizontal velocity is automatically adapted in the next flight phase), but would like to emphasize that, in a formal mathematical sense, there is not yet any justification of such a method guaranteeing the exact same qualitative behavior of approximate solution and complete spring-mass model. The only confidence we can reach is that (i) steady-state solutions are characterized by symmetric contact phases, where the conservation of system energy equally holds for central force approximations, and (ii) in a small neighborhood of such an equilibrium state the change in system energy seems negligible compared to the system energy itself.

Without doubt, if flat spring angles are considered, the quality of the solution decreases, and further approximation refinements are required incorporating the effects of the accurate alignment of the gravitational force during stance. For instance, it could be tested whether the derived approximate solution would provide a better zeroth iterate for the algorithm suggested in SCHWIND and KODITSCHEK (2000). As gravity has been taken into account except for the exact alignment with the vertical axis, the iterative solution might converge faster to a result within a certain, small error tolerance compared to numerical calculations. On the other hand, since the misalignment of gravity only causes rather small changes for steep spring angles, classical perturbation theory might be applicable, possibly yielding better results for a larger angular range.

2.5.2 Self-stability and control of spring-mass running

Before investigated in sagittal plane running, the self-stabilizing property of the spring-mass system could be demonstrated when modeling the alternating tripod of six-legged insects in the horizontal plane (SCHMITT and HOLMES, 2000). As gravity is not interfering in this case, the authors benefitted from the mean value approximation of SCHWIND and KODITSCHEK (2000) (compare last section) replacing the numerical computation of the angle swept during stance with an analytical expression.

In a simulation study, it could later be shown that, by simply resetting the spring orientation (angle of attack) during the flight phase, the spring-mass model can also exhibit self-stable behavior in sagittal plane running in the presence of gravity (SEYFARTH *et al.*, 2002). By mapping the model behavior throughout the parameter space (spring stiffness, angle of attack, and initial running velocity), the

required parameter combinations for self-stable spring-mass running were compared with data from human running. It was found that biological systems seem well to adapt to the predicted parameter domain. Subsequently, in GHIGLIAZZA *et al.* (2003) this model was investigated within a more theoretical framework. Apart from the angle swept during stance, which was still calculated by numerical integration, the authors derived an explicit expression for the return map of spring-mass running by neglecting gravity during stance. By not aiming at quantitative comparisons with specific animals or machines, they could (i) clarify some of the general observations made in SEYFARTH *et al.* (2002) (e.g. minimum running speed), and (ii) illustrate key behaviors of the derived return map (e.g. bifurcation and period doubling).

In contrast to other approaches, the stability analysis performed in this study is based on the apex return map derived from an approximate solution of the stance phase dynamics including gravity. For a special case ($a = 0$), we could show the existence of stable fixed point solutions in spring-mass running without having to recourse numerical integrations. We hereby confirmed the qualitative behavior of an empirically found parametric dependency for stable running between spring stiffness and angle of attack, and extended it it by the system energy. Furthermore, by comparing the predicted parameter combinations for stable running with numerical results, we observed a quantitative agreement far beyond the valid range of the approximate solution, suggesting that, whether in biomechanics or robotics, if the stability of bouncing gaits is of concern, the presented solution may well serve as an analysis tool.

For instance, it could be investigated to what extent the stability of movement trajectories can be manipulated when incorporating leg swing policies other than the fixed leg orientation (SEYFARTH *et al.*, 2002; GHIGLIAZZA *et al.*, 2003) during flight. In a recent investigation (ALTENDORFER *et al.*, 2003), a necessary condition for asymptotic stability could be derived when incorporating specific leg recirculation schemes relevant for the robot RHex (SARANLI *et al.*, 2001). Based on the factorization of return maps, in this special application, the condition was formulated as an exact algebraic expression without having to resort to the actual stance-phase dynamics.

However, no information about the system's behavior could be obtained from this condition when applied to a retracting swing leg policy. Here, recent simulation studies (SEYFARTH and GEYER, 2002; SEYFARTH *et al.*, 2003) suggest that the stability of running can largely be enhanced. In particular, it could be demonstrated that a simple feedforward kinematic leg-angle program $\alpha(t - t_{apex})$ during flight can

enforce the movement trajectory of spring-mass running to a 'dead beat' (Saranli *et al.*, 1998) behavior: independent of the actual apex height y_i, the next apex height y_{i+1} resumes to a preset steady-state height $y_{control}$, guaranteeing 'maximum' stability $y_{i+1}(y_i) = y_{control}$. Of course, this can only be achieved if a critical apex height $y_{min} = \ell_0 \sin \alpha_{apex}$ is exceeded. Different initial apex heights can also be considered as alternating ground levels with respect to one absolute apex height and, thus, the kinematic leg program allows to choose a high level of running safety ($y_{control}$ far above y_{min}, bouncy gait as observed in kangaroos). As the model is conservative, such a 'secure', bouncy movement would exhaust the energy available for forward locomotion, which might not be required in flat, predictable terrain. Accordingly, by selecting an apex height $y_{control}$ close to the minimum height y_{min}, the kinematic leg program allows to maximize the energy efficiency (the share of system energy spent for forward locomotion). Such a flexibility, strongly reminiscent of animal behavior, could largely enhance the repertoire of movement patterns available to legged machines.

Despite these progresses, whether the observed self-stabilizing behavior has been ascribed to 'angular momentum trading' (Schmitt and Holmes, 2000) or 'enforced energy distribution among the systems degrees of freedom' (Geyer *et al.*, 2002), we still lack a comprehensive understanding of the key features responsible for its emergence. What properties of the system dynamics during stance allow a proper interaction with the gravitational force field during flight yielding self-stability in the regime of intermittent contacts? And, further on, in how far can we manipulate these properties? Intensifying theoretical approaches seems desirable at this point since they might not only support suggested control strategies, but could also disclose further and maybe not obvious alternatives.

2.5.3 Conclusion

Considering this lack of knowledge and comparing the ease and maneuverability distinguishing animal and human locomotion with the skills of legged machines, the investigation of gait stabilization in biological systems seems to be a substantial research direction. Here, the planar spring-mass model served as an efficient analysis tool in the past. Benefitting from its parametric simplicity, its stabilizing behavior could well be investigated by purely numerical means (dependence on three parameter groups only). Yet the situation rapidly changes if more complex models of locomotion are addressed, for instance, when incorporating leg recirculation strategies during flight and/or investigating the stability of locomotion in three dimensions.

At this point, numerical approaches become more difficult and tractable analytical descriptions more important. In the simplest case, approximate solutions could substitute the numerical calculation of the stance phase dynamics significantly reducing the computational effort. In the best case, they could provide the parametric insight themselves (e.g. as exemplified by equation 2.33). In that sense, the relevance of the presented approximate solution may be seen in its simplicity and predictive power within the physiological parameter domain, which allows to experimentally validate further control strategies of biological systems likely to be disclosed in more complex models of legged locomotion than the simple planar spring-mass system.

2.6 Appendix: Mixed accuracy approximation of $\frac{1}{(1+\rho)^2}$

The central force approximation of the stance phase dynamics captures an important feature of the planar spring-mass model: the presence of the centrifugal force $\mathbf{F}_c = mr\dot{\varphi}^2\mathbf{e}_r$ accelerating the compression-decompression cycle of the spring. In consequence, the oscillation frequency $\hat{\omega}_0$ of the planar system is increased when compared to the frequency $\omega_0 = \sqrt{k/m}$ of the corresponding one-dimensional system (vertical spring-mass model). To account for such an increase, the Taylor expansion of $\frac{1}{(1+\rho)^2}$ must be performed to at least second order in ρ (9). Otherwise, $\hat{\omega}_0$ would equal ω_0 and the radial motion (12) or (21) would represent the motion of a vertical spring-mass system hardly resembling the planar dynamics.

On the other hand, the central force approximation also introduces a substantial drawback: the conservation of initial angular momentum $P_{TD} = m\ell_0^2\dot{\varphi}_{TD}$ throughout stance. Although the net change in angular momentum is zero for symmetric (time-reflection symmetry about midstance $t_{mid} = t_c/2$) contacts of the planar spring-mass system, the mean angular momentum

$$\bar{P} = \frac{1}{t_c}\int_0^{t_c} P(t)dt \tag{2.40}$$

changes ($\bar{P} \neq P_{TD}$). Expressing $P(t)$ by the initial value and the rate of change $P(t) = P_{TD} + \int_0^t \dot{P}(t')dt'$, and using $\dot{P}(t') = -mgr(t')\cos\varphi(t') = -mgx(t')$ for the planar spring-mass system, we obtain

$$
\begin{aligned}
\bar{P} &= P_{TD} - \tfrac{mg}{t_c}\int_0^{t_c}\int_0^t x(t')dt'dt \\
&= P_{TD} - \tfrac{mg}{t_c}\Big[\int_0^{t_{mid}}\int_0^t x(t')dt'dt \\
&\quad + \int_{t_{mid}}^{t_c}\int_0^{t_{mid}} x(t')dt' + \int_{t_{mid}}^{t_c}\int_{t_{mid}}^t x(t')dt'dt\Big].
\end{aligned}
\tag{2.41}
$$

Using that, for symmetric contacts, at midstance the horizontal position x switches from negative to positive values, (2.41) can be written as

$$
\begin{aligned}
\bar{P} \quad = \quad & P_{TD} + \frac{mg}{t_c} \left[\int_0^{t_{mid}} \int_0^t |x(t')| dt' dt + \int_{t_{mid}}^{t_c} \int_0^{t_{mid}} |x(t')| dt' dt \right. \\
& \left. - \int_{t_{mid}}^{t_c} \int_{t_{mid}}^t |x(t')| dt' dt \right].
\end{aligned} \tag{2.42}
$$

The time reflection symmetry about midstance yields $\int_{t_{mid}}^{t_c} = \int_0^{t_{mid}}$, and (2.42) simplifies to

$$
\bar{P} = P_{TD} + \frac{mg}{t_c} \int_{t_{mid}}^{t_c} \int_0^{t_{mid}} |x(t')| dt' dt = P_{TD} + \frac{mg}{2} \int_0^{t_{mid}} |x(t')| dt'. \tag{2.43}
$$

The mean angular momentum is increased compared to the initial value, which, however, means that the amount of mean angular momentum decreases $|\bar{P}| < |P_{TD}|$ since the initial value P_{TD} is negative (according to the definition of the coordinate system in Fig. 2.1 the angular velocity $\dot{\varphi}$ is defined negative for forward motion).

The miscalculation of angular momentum in the central force approach ($P \equiv P_{TD}$) has a more profound effect on the angular motion ($P \sim \dot{\varphi}$) than on the radial ($P \sim r^2$). Considering that, due to the alignment of the gravitational force with the radial axis ($-mg \sin \varphi \rightarrow -mg$ in (3)), the spring compression is increased, this leads to a clear overestimation of the angular velocity.

Here, an approximation of the central force system dynamics with an error decreasing this inherent overestimation may result in a better performance when compared to the actual spring-mass dynamics. Considering $\frac{1}{(1+\rho)^2}$, the Taylor expansion to the n-th order about $\rho = 0$ is given by

$$
\left. \frac{1}{(1+\rho)^2} \right|_{\rho=0} = \sum_{i=0}^n (-1)^i (i+1) \rho^i. \tag{2.44}
$$

Since $\rho \leq 0$ during contact, this simplifies to

$$
\begin{aligned}
\left. \frac{1}{(1+\rho)^2} \right|_{\rho=-0} \quad = \quad & \sum_{i=0}^n (i+1)|\rho|^i \\
= \quad & 1 + 2|\rho| + 3|\rho|^2 + \ldots + (n+1)|\rho|^n
\end{aligned} \tag{2.45}
$$

showing that the approximation of angular velocity $\dot{\varphi} = \frac{\omega}{(1+\rho)^2}$ increases with each expansion term. Hence, it might be advantageous to cancel this expansion earlier than second order. In fact, it turns out it is. Comparing different order (zeroth to second) approximations of $\frac{1}{(1+\rho)^2}$ for $\dot{\varphi}$ with numerical computations of the actual spring-mass dynamics, the first order approximation performs best.

Chapter 3

From running to walking: the smooth gait transition model

In the previous chapter, we derived a comparably simple approximate solution for the planar spring-mass model, which allowed us to verify the self-stabilizing behavior of spring-mass running observed in numerical simulation studies. Moreover, we could identify a parametric dependency required for stable locomotion as an explicit expression hereby extending an empirically suggested relationship. Naturally, the question arises whether this method in gaining parametric insights into legged locomotion would similarly be applicable to the walking gait. However, the feasibility of the approach heavily depends on the prior identification of a sufficiently simple mechanical template capturing the salient features of the whole body dynamics during stance (ground reaction forces). And the simplest walking model known, the stiff-legged inverted pendulum model, produces ground reaction force patterns inconsistent with the experimental findings (see general introduction).

Motivated by experimental observations revealing significant stance-limb compressions not only in running but also in walking (LEE and FARLEY, 1998; GARD *et al.*, 2004), in the subsequent two chapters, we pursue the idea that in contrast to the traditional distinction between stiff and compliant legs in walking and running, for *both* gaits the observed whole body dynamics might essentially be determined by compliant leg behavior. Following the idea, in this chapter we at first ask whether the predictability of the walk-run transition speed, which is generally derived from limits of the inverted pendulum motion, can similarly be obtained from a running constraint.

3.1 Introduction

The inverted pendulum model idealizes the body to be a point mass m that is supported by a massless rigid leg of length ℓ_0. The vaulting motion then introduces the centrifugal force $\frac{mv^2}{\ell_0}$ acting upon the COM, which, at a critical speed $v_{max} = \sqrt{g\ell_0}$, equals the counteracting gravitational force mg (g: gravitational acceleration) suggesting an upper speed limit of the walking gait. Any excess velocity threatens the system to get airborne indicating that legged systems are obliged to leave the walking pattern when approaching this limit. To compare different species and gravitational environments, this relationship is conveniently stated in terms of the dimensionless Froude number $Fr = \frac{v^2}{g\ell_0}$ (ALEXANDER and JAYES, 1983) with $Fr_{max} = 1$ corresponding to the critical speed v_{max}.

Experiments investigating the walk-run transition support this mechanical interpretation inasmuch as the transition speed v_{trans} indeed seems to follow a functional dependency given by the square root of leg length ℓ_0 and gravitational acceleration g. This not only holds for species as different as birds and humans (HAYES and ALEXANDER, 1983; THORSTENSSON and ROBERTHSON, 1987; GATESY and BIEWENER, 1991; HRELJAC, 1995a), but also applies to the same individual experiencing reduced gravity environments (KRAM et al., 1997). Yet although these experiments demonstrate a qualitative agreement, they equally disclose a quantitative discrepancy. Instead of at the maximum Froude number Fr_{max} derived from the inverted pendulum model, bipeds prefer to change their gait at a Froude number of approximately 0.5. Hence, the attentional focus on the origin of the gait transition has shifted from a global mechanical interpretation to more local and physiological constraints in recent years, and factors as diverse as metabolic costs (e.g. MARGARIA, 1938; CAVAGNA et al., 1977; MCMAHON, 1985; ALEXANDER, 1989; MINETTI and ALEXANDER, 1997), kinematic constraints (MINETTI et al., 1994; HRELJAC, 1995a), rate of perceived exertion (NOBLE et al., 1973; HRELJAC, 1993) and force attenuation limits (e.g. BIEWENER and TAYLOR, 1986; FARLEY and TAYLOR, 1991) are discussed for potential triggers. Nevertheless, a conclusive explanation for the difference in number still remains elusive (for an overview: RAYNOR et al., 2002; SAIBENE and MINETTI, 2003).

In this chapter, we return to a global mechanical interpretation by exploiting the fact that although bipeds prefer to switch their gait at about the same Froude number, they seem to employ two different kinematic strategies. Whereas humans and flying birds preferably change from walking to running or hopping with an abrupt change in the kinematics rendering the transition distinct (HAYES and ALEXANDER,

35

1983; THORSTENSSON and ROBERTHSON, 1987; MINETTI *et al.*, 1994; HRELJAC, 1995b; VERSTAPPEN and AERTS, 2000), especially the multitude of ground-dwelling birds ranging from 50g quails to 90kg ostriches exhibits an alternative gait transition where running emerges as a more gradual shift from walking without a clear difference in the kinematics and with an initial lack of an aerial phase (GATESY and BIEWENER, 1991; VERSTAPPEN and AERTS, 2000; RUBENSON *et al.*, 2004). Although running without aerial phases seems contradictory, based on the characteristic motion of the COM and its respective mechanical paradigms, the latter indeed represents a walk-run transition (MCMAHON, 1985; GATESY and BIEWENER, 1991).

Such a gradual shift implies that, at transition, the kinematic differences of both gaits ideally disappear, which, in a more abstract picture, means that the COM neither lifts above (walking) nor falls below (running) the landing height during stance, but rather remains close to a horizontal line (Fig. 3.1). We cannot, however, explore the smooth transition using the inverted pendulum model. Due to the idealization of a rigid leg, it always yields a vaulting motion of the COM never approaching a horizontal line. But the walk-run transition concerns both walking and running, and the mechanical template for running, the spring-mass model, allows to investigate more or less bouncy motions.
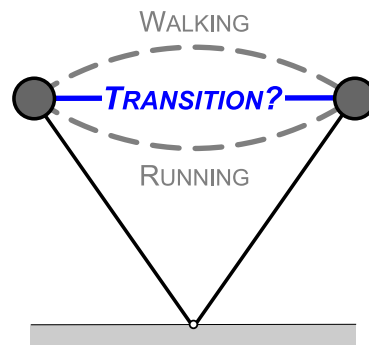
Figure 3.1. Schematic characterization of the COM kinematics in the stance phase of walking and running with the gait transition as intermediate solution not belonging to either gait.

Consequently, we follow the hypothesis that the smooth walk-run transition is governed by the necessity to minimize the difference in the kinematics using a simplified version of the spring-mass model, and ask whether there is a lower speed limit for contact phases with nearly horizontal COM kinematics. Furthermore, we investigate what implications the result may have for running at slower speeds and,

by means of an experimental study on treadmill walking and running, scrutinize in how far these implications apply to human locomotion.

3.2 Minimum walk-run transition speed

3.2.1 Simplified stance kinematics and dynamics

During stance, the average running speed v is given by

$$v = \frac{x_c}{t_c} \tag{3.1}$$

where x_c is the distance the COM travels in the horizontal direction and t_c is the contact time. As an idealization characterizing the walk-run transition, the COM is assumed to describe a horizontal trajectory at the landing height level (Fig. 3.2A). Thus, x_c simplifies to

$$x_c = 2\,\ell_0 \cos \alpha_0 \tag{3.2}$$

where ℓ_0 represents the landing leg length and α_0 is the angle of attack.
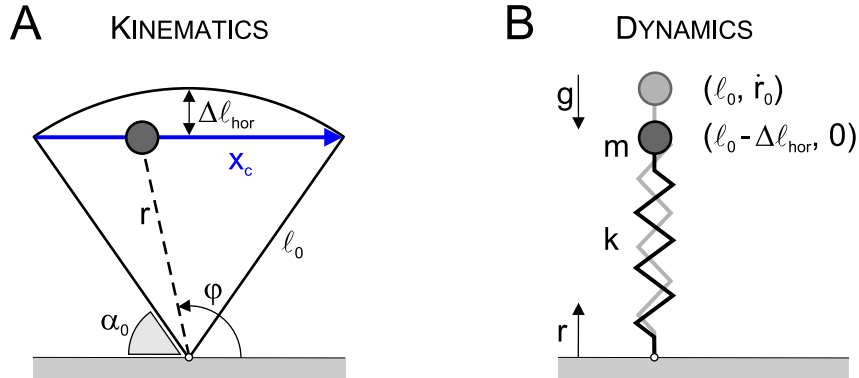
Figure 3.2. Simplified model of the COM kinematics and dynamics in running at the smooth walk-run transition. (**A**) The kinematics are reduced to a straight line at the landing height level. (**B**) The dynamics are approximated by the dynamics of a one-dimensional spring-mass system in the radial direction r of the COM. See text for abbreviations.

To estimate t_c, we consider the radial stance phase dynamics. But instead of investigating the radial motion of the planar spring-mass system, we use the approximation of a one-dimensional spring-mass model under the influence of gravity

$$m\ddot{r} = k\,(\ell_0 - r) - mg \tag{3.3}$$

where k is the spring stiffness, and, due to the constrained kinematics, assume a maximum spring compression $\Delta r_{max} = \Delta \ell_{hor}$ with

$$\Delta \ell_{hor} = \ell_0 \left(1 - \sin \alpha_0 \right) \tag{3.4}$$

at midstance (Fig. 3.2B). Solving (3.3) for the initial condition $r(0) = \ell_0$ and $\dot{r}(0) = \dot{r}_0$ with $\dot{r}_0 \leq 0$ yields

$$r(t) = \ell_0 + \frac{\dot{r}_0}{\omega_0} \sin \omega_0 t + \frac{g}{\omega_0^2} \left(\cos \omega_0 t - 1 \right) \tag{3.5}$$

where $\omega_0 = \sqrt{k/m}$ is the natural frequency of the spring. The midstance time $t_{1/2}$ can be calculated by differentiating (3.5) and then solving $\dot{r}(t_{1/2}) = 0$ yielding

$$t_{1/2} = \frac{1}{\omega_0} \left[\pi + \tan^{-1} \left(\frac{\omega_0 \dot{r}_0}{g} \right) \right]. \tag{3.6}$$

Substituting (3.6) back into (3.5) leads to

$$\Delta r_{max} = \frac{g}{\omega_0^2} \left(1 + \sqrt{1 + \frac{\omega_0^2 \dot{r}_0^2}{g^2}} \right) \tag{3.7}$$

linking the rebound dynamics with the kinematic constraint imposed by the transition condition. Applying $\Delta r_{max} = \Delta \ell_{hor}$ and using (3.4), the natural frequency ω_0 required for the appropriate rebound dynamics can be derived to

$$\omega_0 = \sqrt{\frac{2g}{\ell_0 \left(1 - \sin \alpha_0 \right)} + \frac{\dot{r}_0^2}{\left[\ell_0 \left(1 - \sin \alpha_0 \right)\right]^2}} \, . \tag{3.8}$$

Finally, by expressing ω_0 in (3.6) with (3.8), the contact time $t_c = 2 \, t_{1/2}$ resolves to

$$t_c = \frac{2\ell_0 \left(1 - \sin \alpha_0 \right)}{\sqrt{2g\ell_0 \left(1 - \sin \alpha_0 \right) + \dot{r}_0^2}} \left[\pi + \tan^{-1} \left(\frac{\sqrt{2g\ell_0 \left(1 - \sin \alpha_0 \right) + \dot{r}_0^2}}{g\ell_0 \left(1 - \sin \alpha_0 \right)} \dot{r}_0 \right) \right]. \tag{3.9}$$

In (3.9), the initial velocity $\dot{r}_0$ is unknown. However, the contact time is maximized for zero initial velocity $\dot{r}_0 = 0$

$$t_c \leq \frac{2\ell_0 \left(1 - \sin \alpha_0 \right) \pi}{\sqrt{2g\ell_0 \left(1 - \sin \alpha_0 \right)}} \, . \tag{3.10}$$

Although (3.3) and (3.4) do not correctly describe the radial dynamics of the planar spring-mass template for running, (3.10) provides an upper limit of the actual

contact time (see appendix) allowing to estimate a lower limit for the average speed at the assumed walk-run transition.

3.2.2 Minimum transition speed prediction

With (3.2) and (3.10) the minimum transition speed can be derived from (3.1) to

$$v_{min} = \sqrt{\frac{2\left(1 + \sin\alpha_0\right)}{\pi^2} \ g\ell_0} \,. \tag{3.11}$$

Next to the gravitational acceleration g and the leg length ℓ_0, the predicted transition speed depends on the angle of attack α_0. However, for a considerable angular range the pre-factor described by the fraction in (3.11) changes only marginally (e.g. 5% for α_0 from 65° to 90°). Neglecting the angular variation by assuming $\sin\alpha_0 \approx 1$, (3.11) can be written in the more general form

$$v_{min} = \sqrt{Fr\,g\ell_0} \,, \tag{3.12}$$

which is identical to the known expression for the maximum walking speed (see introduction). But in contrast to $Fr = Fr_{max} = 1$, the model predicts that the smooth walk-run transition necessitates a minimum Froude number of $Fr_{min} = \frac{4}{\pi^2} \simeq 0.4$ surprisingly well matching the experimentally observed transition speed ($Fr \approx 0.5$). Bearing in mind that v_{min} represents a lower speed limit, this close alignment of predicted and observed smooth transition suggests that instead of being forced to leave the walking motion, bipeds opt for the running pattern as soon as it becomes accessible, which in turn indicates running to offer some locomotory advantage over walking.

Interestingly, recent experimental studies support the notion of such a locomotory advantage in terms of the control effort required to maintain a gait pattern. For instance, by investigating the first two weeks of maturation in chicks, MUIR *et al.* (1996) found that although newly hatched birds need several days to develop the ability to walk in a controlled and efficient manner, they can run as able as an adult animal within a few hours suggesting the latter to be the less demanding gait than the former. A similar control advantage has also been observed in humans. By measuring the post reaction time of a secondary auditory task during treadmill walking and running, ABERNETHY *et al.* (2002) could show that when subjects are asked to maintain a single gait pattern throughout a range of speeds covering the gait transition, running is not more attentional demanding than walking below the preferred

transition speed, but walking occupies significantly more attentional resources than running above this speed.

These experimental findings are additionally supported by theoretical investigations on gait stability. Several studies establish that both walking (e.g. GARCIA *et al.*, 1998) and running (e.g. SEYFARTH *et al.*, 2002; GHIGLIAZZA *et al.*, 2003; SEYFARTH *et al.*, 2003; GEYER *et al.*, 2005, compare also Chapter 2) can be mechanically self-stabilizing reducing the actual control effort. However, whereas the running pattern can rely on this control advantage throughout the range of all speeds (SEYFARTH *et al.*, 2003), mechanically self-stable walking is restricted to comparably slow speeds by the threat of losing contact in single support (compare Chapter 4).

3.3 Mechanical limitations in running

If running offers such a control advantage over walking, why should bipeds wait until this gait can be accessed from walking in a smooth manner? Certainly, the wealth of experimental investigations mentioned in the introduction, which demonstrate that a particular physiological quantity (e.g. metabolic costs, rate of perceived exertion or experienced force) is minimized near or at transition could also be invoked in reply to this question. However, we here return to our model, and ask whether it can reveal a mechanical limitation of the running pattern towards slower speeds.

3.3.1 The transition model revisited

The walk-run transition model developed in the last section predicts that, viewed from running, a smooth walk-run transition with a nearly horizontal COM trajectory represented by $\Delta r_{max} = \Delta\ell_{hor}$ requires a minimum speed v_{min} corresponding to $Fr_{min} \simeq 0.4$. This, on the other hand, means that, below the speed v_{min}, larger leg compressions $\Delta r_{max} > \Delta\ell_{hor}$ cannot be avoided in spring-like running. In fact, reconsidering equations (3.7) to (3.11), for an arbitrary relative leg compression $\lambda \geq 1$, with

$$\lambda = \frac{\Delta r_{max}}{\Delta\ell_{hor}} \, , \tag{3.13}$$

a minimum speed

$$v_\lambda = \sqrt{\frac{Fr_{min}}{\lambda} \, g\ell_0} \tag{3.14}$$

is required. Consequently, by rewriting (3.14), this yields a lower limit of relative leg compression

$$\lambda_{min} = \frac{Fr_{min}}{Fr} \tag{3.15}$$

present at a given Froude number $Fr \leq Fr_{min}$ (compare Fig. 3.3).

Hence, the model predicts that the relative leg compression must increase towards slower speeds in spring-like running (note, however, that an increase in relative leg amplitude does not require an increase in the absolute leg compression; see below), which may have a twofold implication for bipedal running. First, it indicates that, at slow speeds, an increasing share of the mechanical system energy must be spent for the vertical movement instead of being put into the intended forward locomotion. Assuming a similar amount of metabolic energy required to maintain a spring-like leg behavior, this would result in an unfavorable growth of the cost of transport (metabolic energy per traveled distance) towards slower speeds in running. Although it is generally found that the relationship between the cost of transport and the running speed has a neutral or weakly positive correlation when considered over the normal range of running speeds (e.g. MARGARIA *et al.*, 1963; BRISSWALTER and MOTTET, 1996; ROBERTS *et al.*, 1998), experimental investigations particularly focusing on slow running speeds indeed report a negative slope (HRELJAC, 1993; MINETTI *et al.*, 1994; HRELJAC *et al.*, 2002).

Furthermore, the emphasis on the vertical bouncing movement may also point to a loss of mechanical comfort. This, however, requires that the inevitably larger *relative* leg compression λ at slow running speeds is accompanied by an amplified *absolute* vertical excursion Δz. The latter is not obvious as the relative leg compression λ is inversely proportional to the term $1 - \sin \alpha_0$ (3.4), and a steepening of the angle of attack ($\alpha_0 \to 90°$) towards slower running speeds might cause a rapid growth of the relative leg compression λ without necessarily reflecting an increase in the vertical amplitude Δz.

3.3.2 Experimental comparison

To elucidate in how far the limitations of the running pattern suggested by the model are mirrored in biological locomotion, and to what extent the walking pattern might compensate for these limitations, we asked 9 subjects (5 male and 4 female, mean $\pm$ s.d. of age = 28 ± 9 years, body mass = 66.5 ± 9.3kg, body height = 1.75 ± 0.09m) first to run and then to walk on a treadmill (Woodway, equipped with Kistler force sensors measuring the vertical GRF F_y on each belt separately, sampling rate 2kHz[1]) at 11 different speeds ($v_{belt} = 0.6 - 3.6$m/s, speed increment 0.3m/s). The leg kinematics (left and right leg: hip, ankle, and toe marker position) were measured using a motion capturing system. The COM was estimated as the

---

[1] Although the GRF is not required within the context of this chapter, it is used in Ch. 4.

mean of left and right hip marker position (plus 10cm vertical offset). The actual leg length is described as the sagittal plane distance between the COM and the foot point. The latter was assumed to be at the treadmill level and its horizontal position was approximated by the mean of the horizontal toe and ankle marker position. Additionally, the subjects' preferred walk-run transition speeds were measured (velocity ramp from 1.5 to 2.5m/s down to 1.5m/s with a speed in-/decrement of 0.1m/s).

In Fig. 3.3A, the obtained relationship between relative leg compression λ and Froude number $Fr = \frac{v_{belt}^2}{g\ell_0}$ is shown for the 11 different speed levels. In contrast to the model assumption, the 'ideal' value of $\lambda = 1$ is not approached near the transition speed (shaded area close to $Fr = 0.4$) in running (filled circle). This, however, was expected. As mentioned in the introduction, the human gait transition displays a distinct change in the kinematics and the smooth transition model does not exactly apply. It has been discussed in literature why humans prefer a more bouncy motion to the smooth running gait, and the ability to generate spring-like leg behavior in an effective manner might here play an important role since, at best, humans can save only 40% of the stride energy using elastic components of the musculo-skeletal system (KER *et al.*, 1987). The remainder must be provided by active muscle contributions. Consequently, the reduced mechanical advantage (BIEWENER, 1989) of a more crouched and smooth running style as observed in ground-dwelling birds (GATESY and BIEWENER, 1991) would require muscle activations consuming comparably large amounts of metabolic energy. In fact, it has been shown that, in humans, the crouched running style entails an increase in metabolic energy costs of up to 50% when contrasted to normal running at the same speed (MCMAHON *et al.*, 1987).

Since the transition model does not scrutinize the generation of spring-like leg behavior but rather explores the mechanical consequences, it cannot address this potential explanation for the different running patterns used by ground-dwelling birds and humans at the transition. Nevertheless, the more general prediction of larger relative leg compressions λ towards slower speeds for spring-like leg behavior (3.15) should equally affect human running and, as can be seen in Fig. 3.3A (filled circles), indeed does. Moreover, whereas λ increases only moderately towards slower speeds above the preferred gait transition ($\lambda : 2.5 \rightarrow 5$ for $Fr : 1.3 \rightarrow 0.4$), it rapidly grows below the transition ($\lambda : 5 \rightarrow 50$ for $Fr : 0.4 \rightarrow 0.04$, note the logarithmic scale). Considering that within the investigated range of running speeds, the absolute leg compression remains almost constant at about 10% of leg length
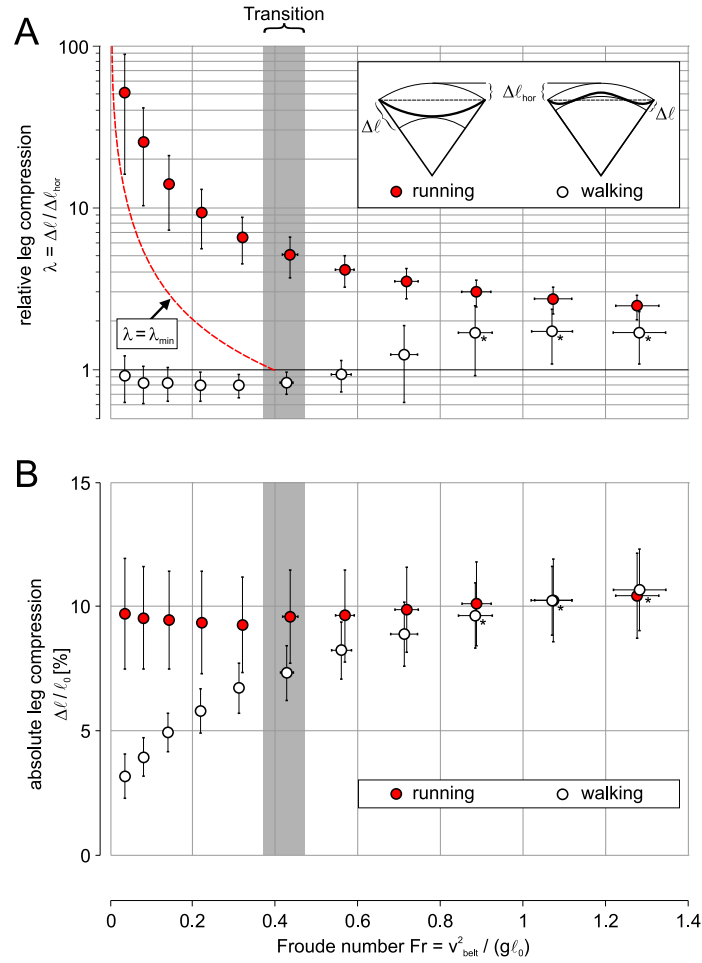
Figure 3.3. Relative and absolute leg compression (mean ± s.d.) during running and walking at different Froude numbers $Fr = \frac{v_{belt}^2}{g\ell_0}$ (mean ± s.d.; due to the individual leg lengths, the subjects' Froude numbers are different at the same speed level v_{belt} with v_{belt} ranging from 0.6 to 3.6m/s; contacts for each level: $n > 130$). (**A**) The relative leg compression λ is determined as the ratio between the maximum leg compression $\Delta\ell$ and the leg compression $\Delta\ell_{hor}$ required for virtual straight COM kinematics. In running, this ratio cannot be smaller than 1. The dashed line $\lambda = \lambda_{min}$ indicates the minimum relative leg compression derived from the model (eq. 3.15). (**B**) The absolute leg compression $\Delta\ell$ equals the maximum leg compression in (A) and is normalized to the leg length ℓ_0. The shaded area indicates the range (mean ± s.d.) of the preferred transition speed. For higher speed levels ($Fr > 0.7$, indicated by the asterisks), the 'walking' pattern approached a running style known as 'Groucho-running' (MCMAHON *et al.*, 1987, see text).

(filled circles, Fig. 3.3B), the experimental finding of a rapidly growing relative leg compression supports the hypothesis that below the transition speed most of the mechanical system energy is spent for the vertical bouncing movement and not for forward locomotion.

Compared to running, in walking, the relative leg compression shows a different dependency on locomotion speed. Below the preferred gait transition, λ remains close to the 'ideal' value of 1 (between 0.8 and 1, open circles in Fig. 3.3A) indicating that the COM is balanced at about the landing height level throughout stance. As this is accompanied by a clear reduction in the absolute leg compression (from 7% of leg length at transition down to 3% at the lowest speed level, Fig. 3.3B), walking seems to more efficiently direct the system energy into forward progression at this speed range. By contrast, above the preferred transition speed, both the relative and absolute leg compressions increase and approach similar values as in running at higher Froude numbers (λ: $0.8 \rightarrow 2$ and $\Delta\ell/\ell_0$: $7\% \rightarrow 10\%$ for Fr: $0.4 \rightarrow 1.3$) indicating no mechanical advantage over the running gait at higher speeds. In fact, based on the characteristic COM motion, the 'walking' pattern changed to a running pattern similar to 'Groucho running' (McMahon *et al.*, 1987) at higher speed levels ($Fr > 0.7$, indicated by the asterisks), although the subjects were asked to maintain walking and no flight phases were observed.

The results suggest that walking may be preferred to running at slow speeds because it can guarantee sufficient locomotion comfort. This becomes even more apparent when comparing the vertical stance phase amplitudes Δz of the COM (Fig. 3.4): they reach similar magnitudes for walking (about 5% of leg length, open circles) and running (about 7%, filled circles) at higher speed levels ($Fr > 0.4$). However, below the walk-run transition ($Fr < 0.4$), the amplitudes clearly diverge in both gaits. Whereas in running Δz increases towards slower speeds ($7\% \rightarrow 9.5\%$) reducing the mechanical comfort, in walking a considerable decrease is observed ($5\% \rightarrow 2\%$).

3.4 Conclusion

In this chapter, we resumed the dynamics based perspective on the walk-run transition, however, instead of focusing on speed limitations of walking, investigated to what extent the gait transition may be induced by a speed limitation of running. In particular, we followed the assumption that a smooth walk-run transition as observed in ground-dwelling birds (Gatesy and Biewener, 1991; Verstappen and Aerts, 2000; Rubenson *et al.*, 2004) is governed by the necessity to minimize the difference in the COM kinematics at transition (Fig. 3.1). The analysis of a simplified spring-mass model revealed that, idealized by a virtually straight COM motion during contact, this kinematic constraint imposes a minimum running speed
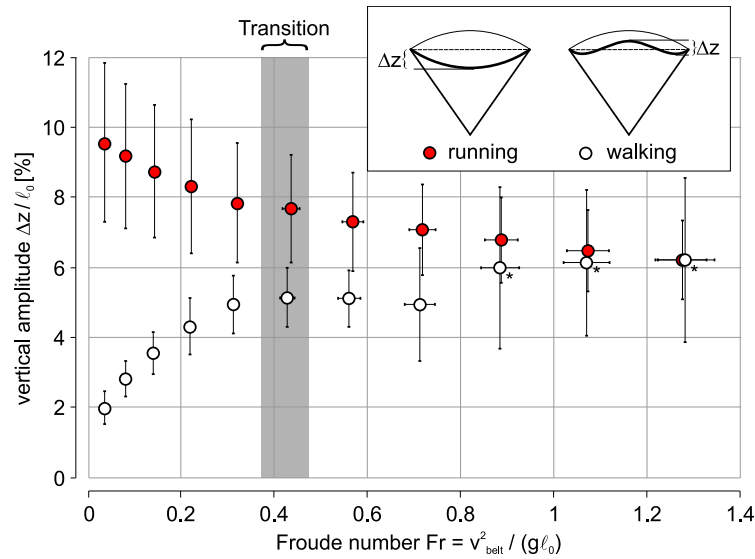
Figure 3.4. Vertical amplitude (mean ± s.d.) during walking and running at different Froude numbers (mean ± s.d). The vertical amplitude is calculated as difference between the highest and lowest point of the COM during contact, and is normalized to the leg length ℓ_0. The shaded area indicates the range (mean ± s.d.) of the preferred transition speed. For the asterisks compare Fig. 3.3

$v_{min} = \sqrt{Fr_{min}\, g\ell_0}$ leading to the same fundamental relationship as known for the maximum walking speed v_{max} derived from the inverted pendulum model for walking. But in contrast to $Fr_{max} = 1$, the minimum transition speed is characterized by the dimensionless Froude number $Fr_{min} = \frac{4}{\pi^2} \simeq 0.4$ surprisingly well matching the experimental results ($Fr \approx 0.5$: HAYES and ALEXANDER, 1983; THORSTENSSON and ROBERTHSON, 1987; GATESY and BIEWENER, 1991; HRELJAC, 1995a; KRAM et al., 1997). It should, however, be noted that as the model was derived assuming a smooth transition, it does not exactly apply to the human gait change. Future research is needed at this point to clarify to what extent the distinct change of humans may be coupled to the smooth transition. Furthermore and more generally, the model predicts that, below the minimum transition speed ($Fr \leq Fr_{min}$), spring-like running inevitably leads to increased relative leg compressions with $\lambda_{min} = \frac{Fr_{min}}{Fr}$.

The similarity between predicted minimum and experimentally observed transition speed suggests that bipeds prefer running to walking as soon as the first becomes accessible in a sufficiently smooth manner. Such a preference would indicate a locomotory advantage of running over walking, which, in terms of the control effort required to maintain a single gait pattern throughout the range of locomotion speeds, is supported by recent experimental (MUIR et al., 1996; ABERNETHY et al., 2002) and theoretical investigations (SEYFARTH et al., 2003, Chapter 4). Below the

minimum transition speed, however, the increase in relative leg compression may prevent bipedal animals and humans from switching to running as the emphasis on the vertical bouncing movement suggests an unfavorable growth of the cost of transport as well as a reduced mechanical comfort. Although the increase in the cost of transport (HRELJAC, 1993; MINETTI *et al.*, 1994; HRELJAC *et al.*, 2002) and a perception of discomfort (NOBLE *et al.*, 1973; HRELJAC, 1993) are known for slow running speeds from literature already (with the latter itself being suggested as a possible trigger for the gait transition), the derived model allows to interpret both effects as a consequence of the underlying dynamics of the mechanical system.

In the presence of these mechanical limitations, the experimental comparison between human running and walking revealed that the walking gait may be preferred at slow locomotion speeds since it can guarantee sufficient mechanical comfort, possibly, even at the expense of an increased control effort. From that perspective, the gait transition of biological systems seems to mediate between locomotion advantages and disadvantages based on more than a single movement criterion such as metabolic costs, comfort or control effort (gait stability), and disclosing the effective movement criterions could help improving the understanding of the gait transition in particular as well as biological legged locomotion in general.

3.5 Appendix: One-dimensional approximation of the radial stance phase dynamics

The equations of motion of the planar spring-mass model are given by (for notation see Fig. 3.2)

$$m\ddot{r} = k(\ell_0 - r) + mr\dot{\varphi}^2 - mg\sin\varphi \tag{3.16}$$

and

$$mr\ddot{\varphi} = -2m\dot{r}\dot{\varphi} - mg\cos\varphi \tag{3.17}$$

describing a non-integrable system. Although approximate solutions exist (e.g. GEYER *et al.*, 2005, compare also Chapter 2), we here seek a simple estimate of the contact time t_c providing a lower limit of the transition speed. Hence, only the radial component (3.16) is considered.

For symmetric contacts, the conservation of momentum yields

$$\int_0^{t_c} m\ddot{r}\, dt = -2m\dot{r}_0 \tag{3.18}$$

where $\dot{r}_0$ is the initial radial velocity. This general expression must be fulfilled for all rebounding systems. But dependent on the developed force, the contact time may vary. Thus, each simplification (*) of (3.16) that retains the rebounding characteristic and produces smaller forces $m\ddot{r}^* \leq m\ddot{r}$ guarantees that the contact time can only be increased. Approximating the radial dynamics with

$$m\ddot{r} = k(\ell_0 - r) - mg \qquad (3.19)$$

meets both requirements ($\varphi \in [0, \pi]$). Here, the centrifugal force accelerating the compression-decompression cycle of the planer spring-mass system is ignored $mr\dot{\varphi}^2 \to 0$ and the counteracting gravitational force is considered to be fully present throughout stance $-mg\sin\varphi \to -mg$.

The radial dynamics (3.19) describe a more compliant system resulting in larger spring compressions for identical initial velocities $\dot{r}_0$. Consequently, smaller values $\dot{r}_0$ have to be assumed to restrict the maximum spring compression to $\Delta r_{max} = \Delta \ell_{hor}$ given by the kinematic constraint (Fig. 3.2A). However, reducing the initial velocity can only further increase the contact time t_c (as can be seen in (3.6)).

Chapter 4

The spring-mass walking model

In Chapter 3, we could demonstrate that the predictability of the walk-run transition is not constrained to a speed limitation of the walking motion as described by the inverted pendulum model, but can equally be obtained from a running perspective using the spring-mass model as gait template. In addition, with $Fr \simeq 0.4$, the derived transition speed more accurately predicts the Froude number at which the gait transition actually occurs, supporting the notion that a compliant leg behavior could contribute to general biological legged locomotion more substantially than traditionally expected. In pursue of a gait template for walking, in this chapter we address whether such a compliant leg response may indeed suffice to obtain whole body dynamics similar to those observed in walking.

4.1 Introduction

On the mechanical level, the inverted pendulum (Fig. 1.2, p. 3) is employed as simple paradigm of the walking gait. Yet although this model represents the simplest walking model conceivable, it produces GRF patterns inconsistent with experimental observations (FULL and KODITSCHEK, 1999; PANDY, 2003). Correlated to this difference in the GRF, experimental studies also demonstrate that the COM displays much less vertical excursion than expected by the vaulting motion of the model and the stance-limbs experience significant compression-decompression cycles (LEE and FARLEY, 1998; GARD et al., 2004, compare section 1.2).

Hence, introducing leg compliance when addressing walking seems a natural consequence and, in fact, earlier simulation studies already suggest that such a leg behavior may indeed contribute to a functional walking gait. By employing higher-dimensional models incorporating segment masses and/or spring and damper

terms in the legs (Siegler *et al.*, 1982; Pandy and Berme, 1988), it could be demonstrated that the characteristic double-peak pattern of the vertical GRF in walking can be enforced if adequate initial conditions and model parameters are selected.

However, besides the increased model complexity hampering the desired parametric insights, these simulation studies focus on incomplete step cycles (either single-support from opposite toe-off to opposite heel-strike, Pandy and Berme (1988), or a sequence of single- and double-support from heel-strike assuming the opposite leg to be swinging to opposite heel-strike to toe-off, Siegler *et al.* (1982)), and hereby neglect the full contribution of the opposite leg in stance on the actual COM dynamics. In consequence, the periodicity and stability of the identified force patterns in a sequence of steps (as investigated for the inverted pendulum walking model, e.g. Garcia *et al.*, 1998) cannot be addressed.

In contrast to these studies involving more complex models, in the present chapter we restrict ourselves in two ways when addressing leg compliance in walking. First, we employ the simple spring-mass model (Blickhan, 1989; Seyfarth *et al.*, 2002) merely extended by a second idealized leg spring. Secondly, rather than enforcing certain GRF patterns, we first seek stable periodic locomotion and then scrutinize the inherent steady-state dynamics.

4.2 Methods

4.2.1 Walking model

Walking is modeled as a sagittal plane movement (Fig. 4.1). The body is reduced to a point mass m at the COM. During the gait cycle, the gravitational force $F_g = mg$ (g: gravitational acceleration) is acting on the COM. Additionally, the COM trajectory is influenced by forces originating from the alternatively contacting legs, which are idealized by two independent, massless springs attached to but freely pivoting around the COM (left and right leg: black and white spring, respectively). For symmetry, the springs are characterized by equal values of stiffness k and rest length ℓ_0.

A single leg remains in stance as long as the corresponding spring is compressed (spring length ℓ is smaller than rest length ℓ_0) exerting the force $F_s = k(\ell_0 - \ell)$ on the COM. If the spring exceeds its rest length ℓ_0 during decompression, the leg switches into the swing phase where a purely kinematic constraint is assumed. Initiated at the apex, the highest point ($\dot{y} = 0$) of the COM during the single support phase of the stance leg, the swing leg is set to a virtual length ℓ_0 and orientation α_0 with
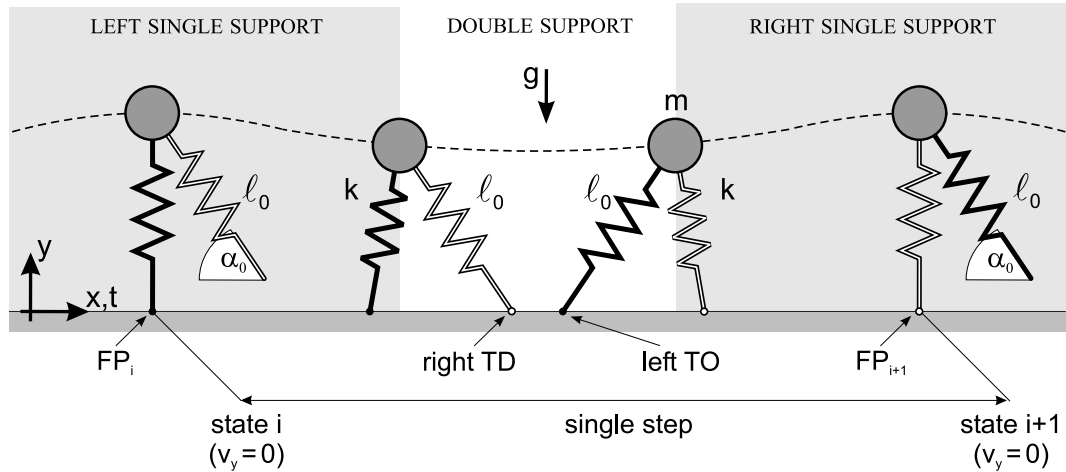
Figure 4.1. Spring-mass model for walking (for abbreviations see text).

respect to gravity, predefining a distinct landing height $y_{TD} = \ell_0 \sin \alpha_0$. When the leg strikes the ground ($y_{COM} = y_{TD}$), it returns to the freely rotating spring representation of the stance phase. Again, to attain symmetry, α_0 is equal for both legs.

For instance, in Fig. 4.1, the model starts at the apex of the left leg single support phase. Although largely decompressed (ℓ close to ℓ_0), the left leg spring (black) remains in contact (please note that the instant of apex is not necessarily characterized by an upright position of the contacting spring as depicted in the figure, it merely requires $\dot{y} = 0$). In contrast, the right leg spring (white) resembles the kinematic constraint of the fixed leg orientation during the swing phase. Since the gravitational force exceeds the counteracting force developed by the left leg spring, the COM height reduces (dotted line) while compressing the spring. When the right leg touches the ground ('right TD', Fig. 4.1), the system enters the double support phase. The vertical COM movement soon reverses as a consequence of the additional vertical push of the right leg. If the COM had sufficient horizontal speed beforehand, the forward motion continuous and eventually reaches a position where the left leg spring reaches its rest length ℓ_0 again. Consequently, the left leg takes off ('left TO', Fig. 4.1) and the system switches into the right leg single support phase.

4.2.2 Stability analysis

The previous example presumes a well distributed force generation among the leg springs balancing the COM in the vertical direction when counteracting gravity while maintaining the forward motion. But the walking pattern may also fail if (i)

the horizontal movement is reversed (backward falling), (ii) the landing height of the swing leg is larger than the actual apex height (foot below ground level), or (iii) the vertical leg forces are too large and the stance leg takes off before the swing leg lands, i.e. the system gets airborne.

To investigate whether such a model can exhibit stable walking patterns for a given set of parameters, a return map analysis of the COM system state $(x, \dot{x}, y, \dot{y})$ is performed. Due to the symmetry of the model, it suffices to analyze the state of two subsequent single support apices $(x, \dot{x}, y, \dot{y})_i$ and $(x, \dot{x}, y, \dot{y})_{i+1}$ defining a single step (Fig. 4.1). Since the vertical velocity vanishes at each apex $(\dot{y} = 0)$, the state vector can here be reduced to $(x, \dot{x}, y)_i$. Furthermore, as a consequence of the leg swing policy, the absolute x-position of the COM has no direct influence on the periodicity of the walking pattern. Only the relative position $x_{rel,i} = x_i - x_{FP,i}$ contributing to the actual spring length $\ell_i = \sqrt{x_{rel,i}^2 + y_i^2}$ is of relevance where x_{FP} represents the absolute x-position of the foot point (FP) of the contacting leg spring. Still further, as the model is conservative, i.e. the system energy E_s is constant, the horizontal velocity at apex $\dot{x}_i$ is given by $\dot{x}_i = \sqrt{\frac{2E_s}{m} - \frac{k}{m}(\ell_0 - \ell_i)^2 - 2gy_i}$. In consequence, the systems periodic behavior is uniquely determined by the reduced apex state vector $(x_{rel}, y)_i$ defining the apex return map

$$R : (x_{rel}, y)_i \rightarrow (x_{rel}, y)_{i+1} . \tag{4.1}$$

For stability, it suffices that two conditions are fulfilled. First, that a steady-state solution exists with

$$\begin{aligned} x_{rel,i+1} &= x_{rel,i} \\ y_{i+1} &= y_i \end{aligned} \tag{4.2}$$

and, secondly, that within a small neighborhood of this solution, the eigenvalues

$$\lambda_{1,2} = \frac{DR_{11} + DR_{22}}{2} \pm \sqrt{\frac{(DR_{11} + DR_{22})^2}{4} + DR_{12}DR_{21} - DR_{11}DR_{22}} \tag{4.3}$$

of the Jacobian matrix

$$DR_{ab} = \begin{pmatrix} \frac{\partial x_{rel,i+1}}{\partial x_{rel,i}} & \frac{\partial x_{rel,i+1}}{\partial y_i} \\ \frac{\partial y_{i+1}}{\partial x_{rel,i}} & \frac{\partial y_{i+1}}{\partial y_i} \end{pmatrix} \tag{4.4}$$

lie within the unit circle, i.e. $|\lambda_{1,2}| < 1$.

4.2.3 Systematic parameter scan

The dynamics of a single step are influenced by eight individual constants, the model parameters m, g, k, ℓ_0, α_0, and E_s, and the initial apex position $x_{rel,i}$ and y_i, which can, however, be reduced to only five independent parameters: angle of attack α_0, dimensionless stiffness $\tilde{k} = \frac{k\ell_0}{mg}$, dimensionless system energy $\tilde{E}_s = \frac{E_s}{mg\ell_0}$, and dimensionless initial apex position $\tilde{x}_{rel,i} = \frac{x_{rel,i}}{\ell_0}$ and $\tilde{y}_i = \frac{y_i}{\ell_0}$ (see appendix 4.5). To ensure dynamic similarity in general, all five of these parameters would have to be considered. However, we do not seek general similarity, but confine our investigation to stable periodic locomotion. Here, the initial apex position is already taken into account by analyzing whether the return map admits stable fixed point trajectories (see section 4.2.2). Hence, the systematic parameter scan characterizing the model's ability for stable locomotion reduces to the remaining parameters α_0, $\tilde{k}$, and $\tilde{E}$.

4.2.4 Simulation environment

The model is implemented in Matlab 6 using the Simulink 4 toolbox (Mathworks Inc., Natick MA, USA). The forward dynamics simulation is performed with the embedded variable step integrator ode113 with a maximum step size of 10^{-2} and an absolute and relative error tolerance of 10^{-6}. The results of the numerical integration are checked using a tenfold higher accuracy.

4.2.5 Experimental comparison

In order to evaluate to what extent the model's stability prediction compares to the strategies used in biology, the parameter combinations (α_0, $\tilde{k}$, and $\tilde{E}_s$) characterizing human walking were estimated from the data obtained in the experimental study described in Ch. 3.3.2.

The leg rest length ℓ_0 and angle of attack α_0 are calculated from the leg kinematics at touch-down detected by the rise of the corresponding vertical GRF F_y (force threshold: 20N, compare Ch. 3.3.2) . The leg stiffness is estimated by the mean stiffness k of the leg force-length trace $F_{leg}(\ell)$ during contact, where F_{leg} is approximated by $F_{leg} \approx \frac{F_y}{\sin \alpha}$ using the measured vertical force F_y and the leg angle α. The system energy E_s is estimated at the stance leg apex position ($\dot{y}_{COM} = 0$) by assuming that the leg compression at this position applies to a spring with the calculated stiffness k: $E_s = \frac{m}{2}\dot{x}_{COM}^2 + mgy_{COM} + \frac{k}{2}(\ell_0 - \ell)^2$.

4.3 Results

To avoid the restriction to certain parameter combinations, the results are presented in dimensionless form.

4.3.1 Stable walking

First, it is addressed whether the walking model can display stable periodic movements by analyzing the apex return map of a single step. As representative examples, the results for three different parameter combinations are depicted in Fig. 4.2. Starting with the parameter set $\alpha_0 = 69°$, $\tilde{k} = 17.8$, and $\tilde{E}_s = 1.04$ (Fig. 4.2A), the return map $R : (\tilde{x}_{rel}, \tilde{y})_i \rightarrow (\tilde{x}_{rel}, \tilde{y})_{i+1}$ shows a vortex curling around a fixed point (close to $\tilde{x}_{rel} = 0$ and $\tilde{y} = 0.975$). The calculation of the eigenvalues $\lambda_{1,2}$ of the Jacobian matrix DR_{ab} reveals that it is a stable fixed point ($|\lambda_{1,2}| < 1$, shaded areas). Consequently, within a sufficiently small neighborhood of this point, disturbed initial conditions are attracted in subsequent steps leading to stable periodic locomotion of the model (example tracing, Fig. 4.2A). The steady-state apex condition is characterized by a vertical stance leg position ($\tilde{x}_{rel} = 0$), which is referred to as 'symmetric solution'.

By steepening the angle of attack to $\alpha_0 = 73°$, two changes are observed in the return map (Fig. 4.2B). First, the position of the identified stable fixed point shifts towards a forward leaned leg orientation at apex ($\tilde{x}_{rel} > 0$) characterizing an 'asymmetric solution'. Moreover, a second, lower fixed point emerges (around $\tilde{x}_{rel} = 0$ and $\tilde{y} = 0.96$). However, with $|\lambda_{1,2}| > 1$ it proves to be unstable. The two selected example tracings in Fig. 4.2B demonstrate the model behavior near the two critical points. Starting close to the unstable one, the apex states of subsequent steps (small circles) steadily drift away from the initial state. Although the system achieves several steps, it finally collapses. In contrast, starting in the neighborhood of the stable fixed point, the following apex states approach this point. It requires a considerable number of steps until the steady-state is assumed.

Further steepening the angle of attack finally leads to the disappearance of stable solutions ($\alpha_0 = 76°$, $\tilde{k} = 17.8$, not shown in Fig. 4.2). However, by additionally increasing the spring stiffness ($\tilde{k} = 25.5$), stable locomotion is again obtained (Fig. 4.2C). But, instead of the upper fixed point, which does no longer exist, the lower fixed point has now turned into a stable one yielding another symmetric solution.
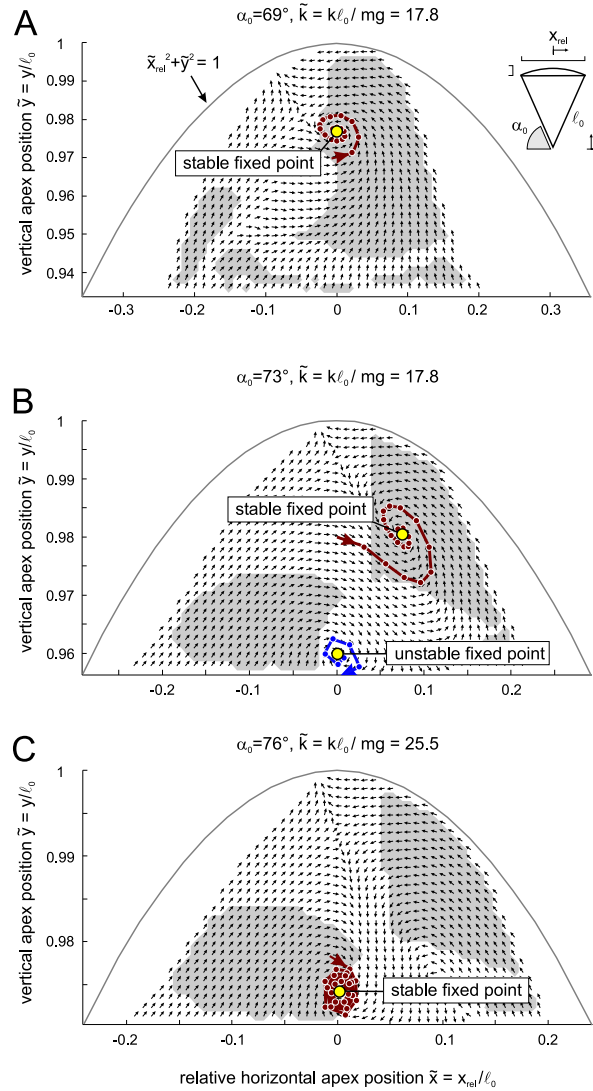
Figure 4.2. Apex return map. The single support apex state is limited by the stumbling condition ($\tilde{y} > \sin \alpha_0$) and the contact constraint ($\tilde{x}^2 + \tilde{y}^2 < 1$). The arrows point into the direction of the state vector flow $R\colon (\tilde{x}_{rel}, \tilde{y})_i \to (\tilde{x}_{rel}, \tilde{y})_{i+1}$. No direction is given for initial states i not resulting in subsequent states i+1. The shaded areas indicate regions of potential local stability ($|\lambda_{1,2}| < 1$). The traces start in the neighborhood of fixed points and follow subsequent apex states (small circles). (**A**) One stable fixed point can be identified with $\tilde{x}_{rel} = 0$. (**B**) At increased angle of attack, the stable fixed point shifts into a forward apex position $\tilde{x}_{rel} > 0$ and a lower, unstable fixed point with $\tilde{x}_{rel} = 0$ appears. (**C**) At further increased angle of attack and increased spring stiffness, the upper fixed point disappears and the lower fixed point becomes stable. *Additional parameter:* $\tilde{E}_s = 1.04$. *Scan resolution:* 60×30.

4.3.2 Characteristic steady-state patterns

The results of the apex return map analysis show that the walking model can exhibit stable periodic locomotion. But how do the corresponding COM dynamics and
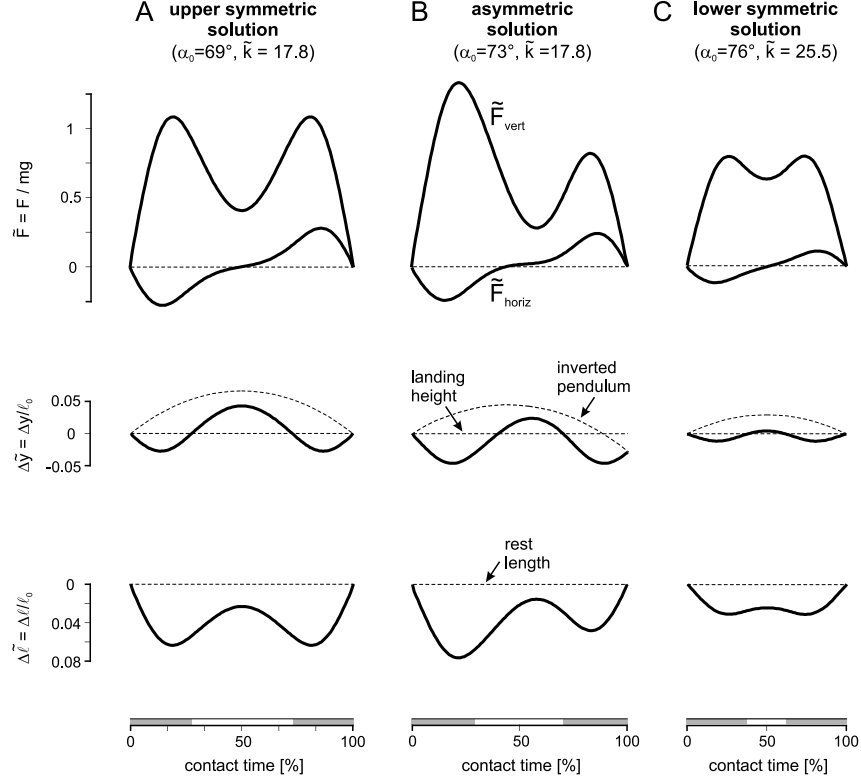
Figure 4.3. Steady state movement patterns for the investigated examples in Fig. 4.2 (**A-C**). The vertical ($\tilde{F}_{vert}$) and horizontal component ($\tilde{F}_{horiz}$) of the ground reaction force, the vertical displacement $\Delta\tilde{y} = \tilde{y} - \sin\alpha_0$, and the spring compression $\Delta\tilde{\ell} = 1 - \tilde{\ell}$ are shown for the left spring stance. The vertical displacement $\Delta\tilde{y}$ is compared to the displacement of an inverted pendulum ($\Delta\tilde{\ell} = 0$) and to a COM movement at landing height level. Double support phases are indicated by the shaded bars at the time axes. The lengths of the time scales reflect the different absolute contact times. *Additional parameter: $\tilde{E}_s = 1.04$.*

kinematics of the system look like? In Fig. 4.3, for the three examples introduced in the last section (A, B, and C, respectively), the steady-state patterns of the ground reaction force $\tilde{F} = \tilde{k}(1 - \tilde{\ell})$ with $\tilde{F} = \frac{F}{mg}$ and $\tilde{\ell} = \frac{\ell}{\ell_0}$, the vertical displacement $\Delta\tilde{y} = \Delta y/\ell_0 = \tilde{y} - \sin\alpha_0$, and the spring compression $\Delta\tilde{\ell} = \Delta\ell/\ell_0 = 1 - \tilde{\ell}$ are shown for the left leg spring (due to parametric symmetry, the patterns are identical between left and right spring).

For the solutions A and C, the dynamics and kinematics are symmetric with respect to midstance. The vertical component $\tilde{F}_{vert}$ of the ground reaction force is characterized by two equal force peaks indicating two compression cycles of the spring during the stance phase (compare $\Delta\tilde{y}$ and $\Delta\tilde{\ell}$). The horizontal component $\tilde{F}_{horiz}$ has an odd symmetry with respect to midstance (50% of stance time) representing a deceleration-acceleration cycle in the forward direction. Whereas, for

the upper symmetric solution (A), the vertical displacement $\Delta\tilde{y}$ almost reaches the spring rest length at midstance (depicted by the 'inverted pendulum' trajectory), it remains close to zero ('landing height' line) for the lower symmetric solution (C). Correspondingly, the stance spring undergoes a significant oscillation in the first case ($\Delta\tilde{\ell}$, A), and nearly remains in a resting position during the contact in the last case (C).

In contrast to the symmetric examples, the asymmetric solution (B) has a larger first peak of the vertical ground reaction force $\tilde{F}_{vert}$ (accordingly, an increased initial spring compression $\Delta\tilde{\ell}$) and a reduced take-off height ($\Delta\tilde{y}$ negative), the latter representing an asymmetry of the leg angle between touch-down and take-off.
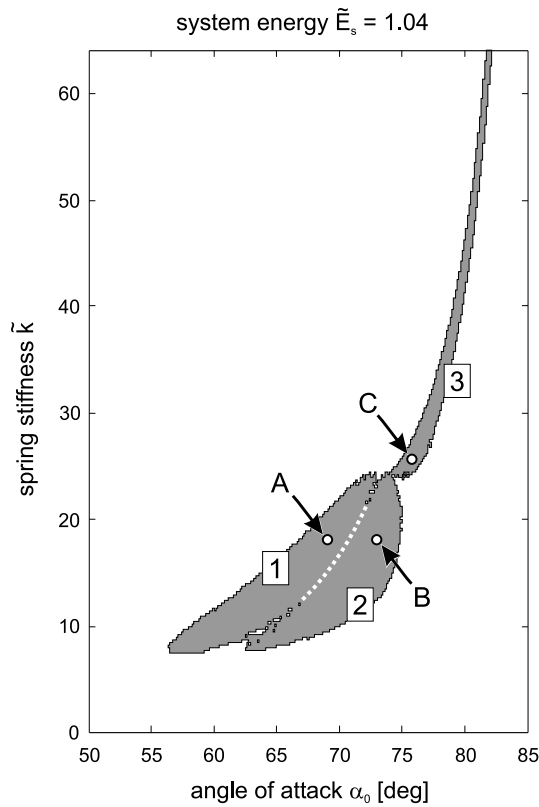
Figure 4.4. Robustness in leg parameter adjustment. The shaded areas depict regions in the $(\tilde{k}, \alpha_0)$-plane for stable walking ($\tilde{E}_s = 1.04$) indicating that, to a certain extent, the system can tolerate parameter disturbances maintaining the locomotor goal of periodic movements. The arrows point to the parameter combinations A, B, and C investigated in section 4.3.1 and 4.3.2. These examples are representative for the model behavior within the three separate parameter regions (1-3, region 1 and 2 separated by the white dotted line). *Scan resolution:* 256×256.

4.3.3 Robustness in parameter adjustment

So far, the model behavior has been scrutinized for three distinct parameter examples. To investigate how the stabilizing behavior relates to the model parameters in more detail, the apex return map analysis is applied throughout the $(\tilde{k}, \alpha_0)$-space (system energy still fixed at $\tilde{E}_s = 1.04$). The result is shown in Fig. 4.4. Three regions can be identified (1-3, region 1 and 2 separated by the white dotted line), within which adjacent parameter combinations equally lead to stable periodic movements, although different steady-state solutions are assumed (not shown in Fig. 4.4). Consequently, to a certain extent, the system is robust with respect to parameter disturbances.

The regions differ from each other by the characteristic location of the corresponding fixed point at apex. Whereas parameter combinations from the first region (1) yield upper symmetric solutions, in the second region (2) the system has asymmetric fixed points, and in the third region (3) lower symmetric solutions are assumed as shown by the three representative examples of the last two sections (A, B, and C, respectively). Other fixed point locations could not be identified.

4.3.4 'Exotic' walking patterns

In the last section, the system energy has been fixed while investigating the influence of the parameters spring stiffness $\tilde{k}$ and angle of attack α_0 on the model's stabilizing behavior. To complete the parameter scan, the analysis is now extended by systematically exploring all three parameters α_0, $\tilde{k}$, and $\tilde{E}_s$ (Fig. 4.5).[1] For a spring stiffness $\tilde{k}$ within a range of about 6.4 to 64, stable locomotion is obtained for angles of attack α_0 approximately ranging from 55° to 80°. However, the required $\tilde{k}$-α_0-adjustment is strongly modulated by the actual system energy $\tilde{E}_s$ (ranging from 0.9 to 1.11).

Moreover, instead of a single connected parameter domain, there exist multiple, separate domains in the $(\alpha_0, \tilde{k}, \tilde{E}_s)$-space enabling different parameter adjustment policies to ensure stability with increasing locomotion speed (system energy). How-

---

[1]To reduce the computational effort, instead of the apex return map analysis, a faster algorithm is employed to identify stable steady-state solutions. For each parameter combination, the system behavior is tested by counting the number of successful steps the model walks for 50 equally distributed initial apex heights $\tilde{y}_i \in (\sin \alpha_0, 1)$ while $\tilde{x}_{rel,i}$ is fixed at $x_{rel,i} = 0$, i.e. the model starts in an upright spring position at the initial apex. If the system converges to a steady-state solution, an infinite number of steps would result. Hence, the simulation is stopped as soon as 99 steps are reached. The algorithm is based on the assumption that the upright position lies within the basin of attraction for stable solutions. Whereas this assumption may not be justified for asymmetric fixed points, preliminary parameter scans showed no differences when comparing this faster algorithm with the return map analysis.
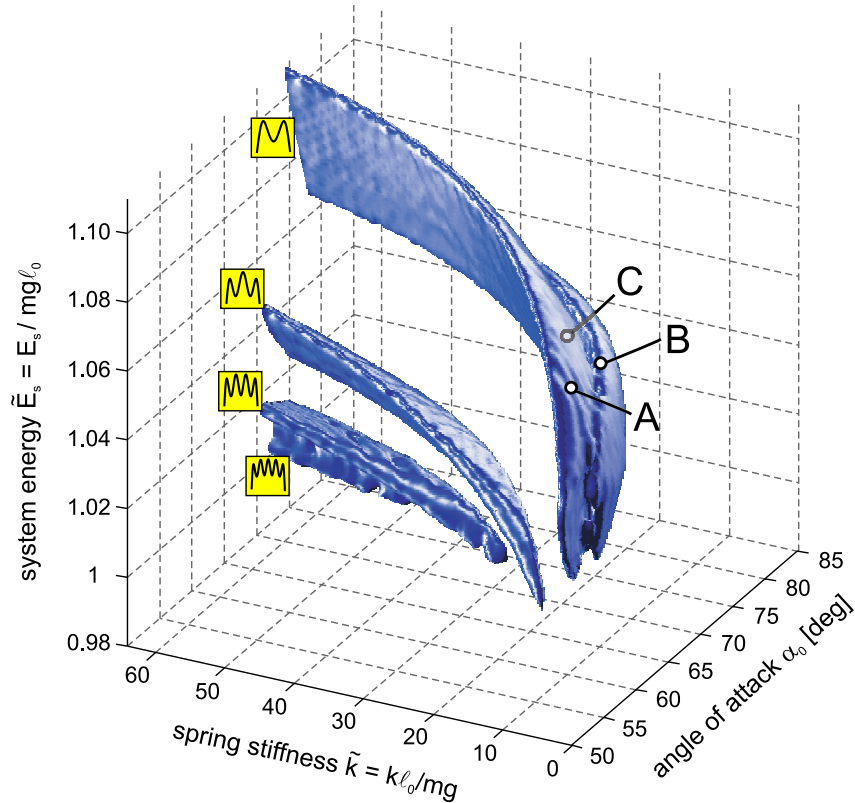
Figure 4.5. Exotic walking. The parameter combinations $(\tilde{k}, \alpha_0, \tilde{E}_s)$ leading to self-stable walking patterns are depicted. Next to the domain characterized by force patterns with two peaks in the vertical component, further domains with multiple peak patterns are observed (indicated by the small icons). Due to the limited scan resolution, only regions with up to five force peaks are resolved, and the last two domains misleadingly seem to overlap. To facilitate the orientation, again the three example parameter sets of the last sections (A, B, and C) are indicated by the open circles. *Scan resolution:* $129 \times 129 \times 129$ (data smoothed for visualization).

ever, as indicated by the adjoining icons in Fig. 4.5, only the largest domain corresponds to steady-state walking patterns with two force peaks (compare examples in Fig. 4.3, corresponding parameter combinations shown as A, B, and C in Fig. 4.5, respectively). The other domains belong to steady-state solutions having more than two force peaks. As the distance between the individual domains shortens with increasing number of force peaks, only regions with up to five peaks are resolved in Fig. 4.5 (the scan resolution is restricted to $129 \times 129 \times 129$; furthermore, the data is smoothed for visualization).

4.3.5 Experimental results

The estimates for α_0, $\tilde{k}$, and $\tilde{E}_s$ in human walking are shown in Tab. 4.1. Starting in an upright position at zero treadmill speed, in the initial six speed levels ($v_{belt} = 0.6 - 2.1 m/s$, $\tilde{E}_s = 1.00 - 1.15$) the subjects converged from a steep angle of attack ($\alpha_0 = 75.3 \pm 2.4°$) and a high leg stiffness ($\tilde{k} = 34.8 \pm 11.1$) to a flatter angle of attack ($\alpha_0 = 67.1 \pm 1.4°$) with smaller leg stiffness ($\tilde{k} = 22.7 \pm 4.8$). For the subsequent speed levels ($v_{belt} = 2.1 - 3.6 m/s$, $\tilde{E}_s = 1.15 - 1.25$), the angle of attack stabilizes and even shows a tendency to re-steepen for the highest speeds. In contrast, although to a smaller amount, the decrease in leg stiffness continuous (from $\tilde{k} = 22.7$ to $\tilde{k} = 17.3$).

$v_{belt}[m/s]$	n	α_0 [deg]	$\tilde{k}$	$\tilde{E}_s$
0.6	165	75.3 ± 2.4	34.8 ± 11.1	1.00 ± 0.01
0.9	206	73.0 ± 2.2	31.2 ± 6.3	1.01 ± 0.01
1.2	201	70.9 ± 2.1	27.8 ± 5.1	1.03 ± 0.01
1.5	152	69.1 ± 2.0	25.5 ± 4.4	1.06 ± 0.01
1.8	182	67.8 ± 1.5	24.5 ± 4.1	1.10 ± 0.01
2.1	176	67.1 ± 1.4	22.7 ± 4.8	1.15 ± 0.02
2.4	182	67.1 ± 1.5	18.9 ± 4.7	1.19 ± 0.02
2.7	164	68.5 ± 2.7	16.7 ± 4.1	1.22 ± 0.05
3.0	247	70.3 ± 4.0	16.9 ± 3.7	1.22 ± 0.07
3.3	321	70.3 ± 3.4	16.8 ± 3.3	1.22 ± 0.08
3.6	359	69.9 ± 3.4	17.3 ± 3.4	1.25 ± 0.08

Table 4.1. Experimental results. For each treadmill speed v_{belt}, the mean $\pm$ s.d. of angle of attack α_0, dimensionless stiffness $\tilde{k}$, and dimensionless system energy $\tilde{E}_s$ are shown where n indicates the number of collected left and right leg stance phases across all 9 subjects.

4.4 Discussion

In this chapter, we addressed to what degree purely elastic leg behavior may contribute to the whole body dynamics observed during walking. Therefore, we extended the planar spring-mass model for running and hopping by introducing a second idealized leg spring. The analysis reveals that walking on elastic legs can lead to stable and robust periodic locomotion if the parameters leg stiffness, angle of attack, and system energy are properly chosen. Moreover, the resulting steady-state dynamics yield GRF patterns including the characteristic double-peak structure observed in animal and human walking. The model suggests limb compliance to play a functional role not only in bouncing gaits but also in walking and, hence, for legged locomotion in general.

4.4.1 Double support is key to force pattern

Modeling the stance leg dynamics by a simple spring-mass system has already been attempted in 1987. Based on the observation that, in walking horses (where the characteristic double-peak force pattern is also present, MERKENS *et al.* (1986)), the hindlimb revealed only small changes in the knee, tarsal and proximal digital joint angles during stance (WENTINK, 1978), GURP *et al.* (1987) suggested that, within this phase, the total limb behavior can be described by a rigid element, which is slightly compressed. Consequently, the authors modeled the stance leg by a single spring-mass system, but, to account for the load bearing contributions of the other legs, the mass acting upon the spring was time dependent with the time course $m(t)$ following a trapezoid function. From heel strike ($t = 0$) to a time instant t_1 marking the end of an assumed double support phase, $m(t)$ increased linearly with time $m(t) = \frac{t}{t_1} m_0$, then remained constant at $m(t) = m_0$ until, from t_2 on, the mass decreased linearly to zero $m(t) = \left(1 - \frac{t-t_2}{t_1}\right) m_0$ in the assumed next double support. Here, the length t_1 of the double support contribution and the mass m_0 loading the stance leg in single support were taken from experimental data. Although this model is not a feedforward dynamic model (next to the explicit time dependence $m(t)$ the angular motion was assumed to be a linear function $\alpha(t) = ct + \alpha_0$), GURP *et al.* (1987) demonstrated that the characteristic double-peak pattern of the vertical GRF can be enforced.

Whereas it seems that this work has not drawn large attention subsequently, it already indicates that the COM dynamics during walking may well be described by purely elastic leg operation with the double support phase having an essential contribution. In fact, considering a complete stance phase of one spring leg of the spring-mass walking model, the effective load (mass) on this spring only gradually increases after touch-down as the opposite spring still is partially supporting the COM. Due to sufficient stiffness, the spring quickly reaches its peak compression leading to a corresponding initial force peak in the vertical GRF. In contrast to running, the spring does not relax completely afterwards since, following take-off of the opposite spring, the stance spring has to bear the full body weight. Consequently, the stance spring starts to oscillate and further force peaks occur until the ongoing rotational motion allows the opposite spring again to contact the ground initiating the next double support. From this instant on, the effective load on the spring under consideration gradually decreases (as the opposite spring takes over in supporting the COM) and, finally, the spring leg completely relaxes terminating the stance phase.

Without rotation of the stance spring, i.e. with zero forward speed (low system energy), the stance spring would oscillate indefinitely. However, with increasing speed (increasing system energy), less and less oscillations (force peaks) can be realized before the opposite leg again touches the ground. Finally, the highest walking speed (system energy) can only be obtained with just one additional compression-decompression cycle yielding the double-peak pattern of the vertical GRF (compare Fig. 4.5).

4.4.2 Self-stable walking: similarities and differences to spring-mass running

Spring-mass walking differs from spring-mass running (SEYFARTH et al., 2002) by introducing a second spring. Nevertheless, both springs operate independently and follow the same swing leg policy as investigated in the running model, i.e. assume the fixed orientation α_0. Hence, it might not surprise that, similar to spring-mass running, stable and robust locomotion patterns can be obtained. Moreover, as the parameter space available for adjustments in attaining stable locomotion remains identical (α_0, $\tilde{k}$, and $\tilde{E}_s$), one might even expect comparable parametric dependencies. And indeed, a similar $\tilde{k}$-α_0-adjustment within a stable domain can be observed (compare Fig. 4.4 with Fig. 2A in SEYFARTH et al. (2002)) indicating that the behavior of the single spring-mass system can at least in part be inherited by more complex locomotion models.

However, there are also substantial differences. For instance, instead of a single stability region as in spring-mass running, multiple separate domains can be identified in the parameter space (Fig. 4.5). These regions differ by the number of force peaks the according steady-state GRF patterns attain. Here, the limitation in locomotor speed (see 4.4.1) admissible for domains characterizing GRF patterns with more than two force peaks might explain why these 'exotic' multi-peak solutions are not observed during normal walking. We are not aware of experiments scrutinizing especially slow walking speeds (close to stand still). The spring-mass walking model suggests that if the leg behavior entirely relies on elasticity, for the lowest speeds (system energies) only multi-peak GRF patterns can be used.

Even within the parameter domain characterizing stable double-peak GRF patterns differences to self-stability in spring-mass running occur. Whereas for the running model only one class of fixed point solution exists, the double-peak domain is clustered into three distinct types of steady-state trajectories (Fig. 4.4). Next to upper and lower symmetric solutions with equal force peaks, asymmetric solutions

with a larger initial force peak can be found (Fig. 4.3) suggesting a greater flexibility in the available COM dynamics. Interestingly, in experiments on human walking a change in the (vertical) GRF pattern is indeed observed. Although the double-peak structure is maintained, with increasing speed the pattern changes from a pattern close to the lower symmetric solution to a pattern rather resembling asymmetric solutions with a larger initial force peak (Keller *et al.*, 1996). Whereas it is generally assumed that the amplified initial peak is caused by larger impacts at touch-down, the spring-mass walking model offers an alternative explanation when considering the experimentally obtained parameter adjustments for $\tilde{k}$ and α_0 with increasing speed (Tab. 4.1):

Starting from an upright position at stand-still, for slow walking speeds the subjects selected steep angles and a large leg stiffness. The model indicates that for such configurations only the lower symmetric solution leads to stable walking (Fig. 4.4). With increasing speed (system energy), the subjects changed their adjustments to flatter angles of attack and smaller spring stiffness following the $\tilde{k}$-α_0 dependency of the stability domain (Tab. 4.1 and Fig. 4.4). However, for these stiffness-angle adjustments, the lower symmetric solution vanishes, and only the upper symmetric and the asymmetric solution prevail (Fig. 4.5). Hence, the experimentally observed change in the force pattern might not only be caused by the impact at touch-down but could also reflect a functional necessity when aiming at the self-stability offered by the mechanical system.

A further difference in self-stability between the running and the walking model concerns the strength of attraction of the stable fixed point solutions. In spring-mass running, the system returns to the steady-state within few steps following disturbances (Seyfarth *et al.*, 2002). By contrast, for spring-mass walking, it takes considerably more steps to recover (e.g. traces in Fig. 4.2). Correspondingly, the strength of attraction of the fixed points appears to be weaker suggesting that if biological gaits are driven by mechanical stability, due to the inevitable irregularities in a real world environment, the walking pattern should possess larger variability than the running pattern when comparing a sequence of steps.

4.4.3 Accessible range of walking speed and limits of elastic walking

For physiologically plausible values of spring stiffness, the range of system energy accessible by stable walking is limited from $\tilde{E}_s = 0.99$ to $\tilde{E}_s = 1.11$ (Fig. 4.5). Applying the human-like parameters $m = 80kg$, $\ell_0 = 1m$, and $g = 9.81m/s^2$, this corresponds to a speed range of about $0.8m/s$ to $1.5m/s$. Although indicating that,

in accordance with animal and human locomotion, the walking gait is bound to slower speeds than running (for the same parameter set, in SEYFARTH *et al.* (2002) a minimum running speed of about $3.5m/s$ is observed), the covered range clearly underestimates walking speeds achieved in biology (humans walk at speeds smaller than the walk-run transition speed of about $2m/s$).

The discrepancy becomes even more obvious when comparing the predicted change in angle of attack and spring stiffness for increasing speed (system energy, Fig. 4.5) with the experimental findings (Tab. 4.1). Both coincide for system energies of $\tilde{E}_s \approx 1.06$, but the tendencies are quite contrary. Whereas the model suggests a change to steep angles and larger values of spring stiffness with increasing speed, the experimental data showed that humans start with steep angles and high leg stiffness and adapt to increasing speeds with flatter angles and lower stiffness values.

This difference in the stiffness-angle adjustment might not totally be conflicting. Lacking a template for the actual swing leg motion in biology, the assumption of a fixed leg orientation in the presented walking model provides a least parameter approach to investigating stability. However, in an earlier work on spring-mass running (SEYFARTH *et al.*, 2003) we could demonstrate that locomotion stability can largely be enhanced by introducing a proper feedforward kinematic leg program $\alpha(t)$ during swing. Backed by the observation that the walking model inherits part of the stability adjustments from the single spring-mass model (section 4.4.2), we hypothesize that similar swing leg policies will also enlarge the range of parameters accessible for stable spring-mass walking, especially at low speeds.

Nevertheless, walking on purely elastic legs will still be limited by a maximum speed. As mentioned in section 4.2.2, the walking model requires a force distribution among the leg springs balancing the COM in the vertical direction. In particular, mediated by the stance spring compression-decompression cycle following touch-down, part of the horizontal motion is redirected into the vertical, and the apex position is reached in the single leg support. With increasing (horizontal) speed, this apex position gradually shifts upwards. Up to a critical speed (system energy), the shift is tolerated (for symmetric fixed points $\tilde{y}_{apex} \in [\sin \alpha_0, 1]$). Above this speed, however, it threatens the stance spring to relax completely (i.e. the model gets airborne). To avoid such a complete rebound in the single support phase, the angle of attack must be steepened and, following the stiffness-angle relation for stable locomotion inherited from the single spring-mass model (section 4.4.2), the spring stiffness considerably increased (Fig. 4.5).

This shift in the $\tilde{k}$-α_0-adjustment demanded by the speed limitation of elastic
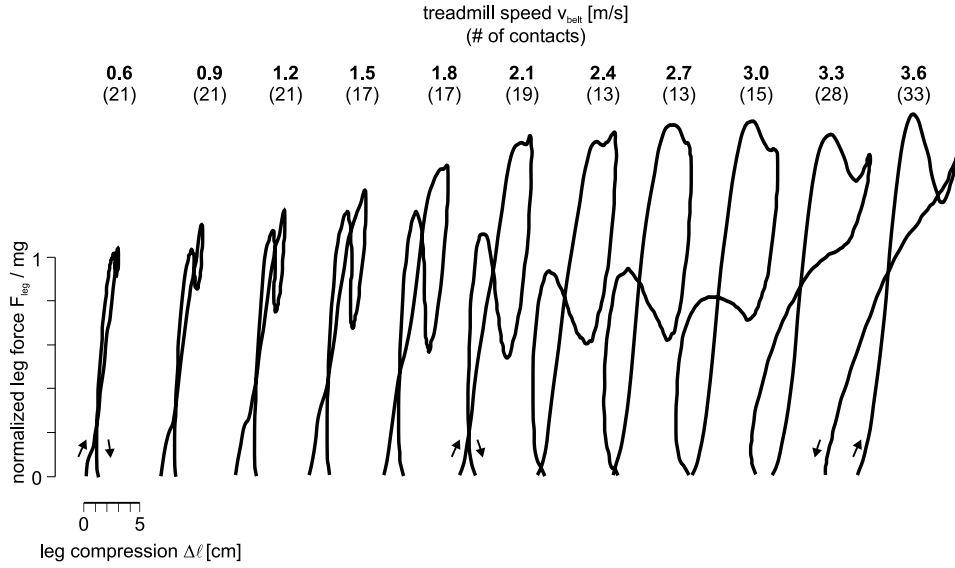
Figure 4.6. Walking speed dependent change in leg behavior of a single subject. For eleven different treadmill speeds $v_{belt} = 0.6 - 3.6 m/s$, the mean leg force-length traces $F_{leg}(\Delta \ell)$ with $\Delta \ell = \ell_0 - \ell$ are shown. The leg force and leg length are derived from GRF and kinematic data as described in section 4.2.5. The leg force is normalized to the body weight ($m = 64.6 kg$). The number of contacts collected at each speed level is indicated in parentheses.

walking is not reflected in the experimental results (Tab. 4.1). By contrast, above a treadmill speed of $v_{belt} = 1.5 m/s$ (were both model prediction and experimental results meet), no steepening in the angle of attack can be observed with increasing speed (α_0 between 67° and 70°), and the leg stiffness (estimated as mean stiffness of the force-length trace of the contacting leg) decreases (from $\tilde{k} = 23$ down to $\tilde{k} = 17$), suggesting that purely elastic leg behavior is discarded at higher speeds. As an representative example, in Fig. 4.6 the mean leg force-length trace $F_{leg}(\Delta \ell)$ of a single subject is depicted at different treadmill speeds v_{belt}. Whereas for slower speeds ($v_{belt} = 0.6 - 1.5 m/s$) the leg behavior may well be regarded as spring-like, at higher speeds ($v_{belt} = 1.5 - 3.6 m/s$) it certainly cannot. Rather it seems that an initially elastic leg behavior is interrupted at the instant of maximum leg force and replaced by a supporting leg behavior (almost constant leg compression) around midstance preventing large vertical excursions. Eventually, the leg function resumes to a behavior, which can be described by elasticity, at the end of the stance phase (the late leg shortening could be an artefact of the estimation of the actual foot point as mean of ankle and toe marker position).

4.4.4 Summary

The 'bipedal' spring-mass system put forth in this chapter is probably the simplest forward dynamic model exhibiting force patterns similar to those observed in animal and human walking. In comparison to the single inverted pendulum model, spring-mass walking establishes two new qualities. First, it emphasizes the functional importance of the double support phase. Secondly, it considers the experimentally observed motion along the leg axis as an additional degree of freedom. Moreover, as a derivative of the simple spring-mass model for running, the proposed model allows a unified description of the two fundamental gait patterns of legged locomotion within a single framework. At higher speeds, however, walking on purely elastic legs is limited by the ability to balance the COM during the support phases indicating that biological systems can no longer rely on the attractive behavior of the mechanical system. Here, an increased control effort seems necessary as supported by the more complex leg operation observed in the experiments.

In conclusion, the spring-mass walking model might serve as a simple gait template, which could encourage and guide future research directions towards a more detailed understanding of the actual leg function during walking, and in legged locomotion in general.

4.5 Appendix: Dimensional analysis

4.5.1 Initial single support

Starting at the apex ($\dot{y} = 0$) of step i, the dynamics of the single support phase are described by the governing equations of motion

$$
\begin{aligned}
m\ddot{x} &= k\left(\frac{\ell_0}{\sqrt{x^2+y^2}} - 1\right)x \\
m\ddot{y} &= k\left(\frac{\ell_0}{\sqrt{x^2+y^2}} - 1\right)y \quad - mg
\end{aligned}
\tag{4.5}
$$

and the initial conditions

$$
\begin{aligned}
x(0) &= x_{rel,i}, & \dot{x}(0) &= \dot{x}_i, \\
y(0) &= y_i, & \dot{y}(0) &= 0.
\end{aligned}
\tag{4.6}
$$

where the co-ordinate origin resides at the foot point FP_i (compare Fig. 4.1). As the system energy is conserved ($E_s = const$), not every initial condition is admissible. Conveniently, we can substitute the initial horizontal velocity by $\dot{x}_i =$

$\sqrt{\frac{2E_s}{m} - 2gy_i - \frac{k}{m}\left(\ell_0 - \sqrt{x_{rel,i}^2 + y_i^2}\right)^2}$. Hence, the system is characterized by the seven individual parameters m, g, k, ℓ_0, E_s, $x_{rel,i}$, and y_i. The dimensions of these parameters can be expressed by the three fundamental quantities length, time, and mass. Applying Buckingham's π-theorem Buckingham (1914), only $7 - 3 = 4$ independent parameter groups exist. As pertinent units we choose ℓ_0 for the length, $\sqrt{\frac{\ell_0}{g}}$ for the time, and m for the mass.[2] The independent parameter groups can be found by either forming dimensionless combinations of the pertinent units and each remaining parameter (k, E_s, $x_{rel,i}$, and y_i) or by forming the according dimensionless equations when substituting the variables x, y, and t with their non-dimensional counterparts $\tilde{x} = \frac{x}{\ell_0}$, $\tilde{y} = \frac{y}{\ell_0}$, and $\tilde{t} = t\sqrt{\frac{g}{\ell_0}}$, i.e.

$$
\begin{aligned}
\tilde{x}'' &= \frac{k\ell_0}{mg}\left(\frac{1}{\sqrt{\tilde{x}^2 + \tilde{y}^2}} - 1\right)\tilde{x} \\
\tilde{y}'' &= \frac{k\ell_0}{mg}\left(\frac{1}{\sqrt{\tilde{x}^2 + \tilde{y}^2}} - 1\right)\tilde{y} \quad - 1
\end{aligned}
\tag{4.7}
$$

and

$$
\begin{aligned}
\tilde{x}_{rel,i} &= \frac{x_{rel,i}}{\ell_0}, \quad \tilde{x}_i' = \sqrt{\frac{2E_s}{mg\ell_0} - 2\tilde{y}_i - \frac{k\ell_0}{mg}\left(1 - \sqrt{\tilde{x}_{rel,i}^2 + \tilde{y}_i^2}\right)^2}, \\
\tilde{y}_i &= \frac{y_i}{\ell_0}, \qquad\qquad\qquad\qquad \tilde{y}_i' = 0
\end{aligned}
\tag{4.8}
$$

with $\tilde{[\,]}' = \frac{d\tilde{[\,]}}{d\tilde{t}} = \frac{\dot{[\,]}}{\sqrt{g\ell_0}}$. Hence, the four independent parameter groups can be identified as dimensionless stiffness $\tilde{k} = \frac{k\ell_0}{mg}$, dimensionless system energy $\tilde{E}_s = \frac{E_s}{mg\ell_0}$, and dimensionless initial position $\tilde{x}_{rel,i} = \frac{x_{rel,i}}{\ell_0}$ and $\tilde{y}_i = \frac{y_i}{\ell_0}$.

4.5.2 Remaining step

As soon as the touch-down condition $y_{TD} = \ell_0 \sin \alpha_0$ is achieved during single support, the system enters the double support phase and the governing equations of motion (4.5) are extended by a second spring term to

$$
\begin{aligned}
m\ddot{x} &= k\left(\frac{\ell_0}{\sqrt{x^2 + y^2}} - 1\right)x \quad - \quad k\left(\frac{\ell_0}{\sqrt{(d-x)^2 + y^2}} - 1\right)(d - x) \\
m\ddot{y} &= k\left(\frac{\ell_0}{\sqrt{x^2 + y^2}} - 1\right)y \quad + \quad k\left(\frac{\ell_0}{\sqrt{(d-x)^2 + y^2}} - 1\right)y \qquad - mg
\end{aligned}
\tag{4.9}
$$

where $d = FP_{i+1} - FP_i = x_{TD} + \ell_0 \cos \alpha_0$ is the distance between the foot points of the two springs. Except for the swing leg orientation α_0, which adds an independent parameter, all other system parameters are given by the preceding single support: the touch-down state results from the single support dynamics and the

---

[2]The pertinent units ar not unique. The choice may depend on the aimed question. For instance, in Blickhan (1989) length and time are selected as $\frac{g}{\omega}^2$ and $\frac{1}{\omega}$ with $\omega = \sqrt{\frac{k}{m}}$.

spring parameters are the same for both springs.

The same applies to the subsequent single support phase. Initiated by the take off condition $x^2 + y^2 = \ell_0^2$, the dynamics are governed by

$$
\begin{aligned}
m\ddot{x} &= - k \left(\frac{\ell_0}{\sqrt{(d-x)^2+y^2}} - 1 \right) (d-x) \\
m\ddot{y} &= k \left(\frac{\ell_0}{\sqrt{(d-x)^2+y^2}} - 1 \right) y \qquad - mg
\end{aligned}
\tag{4.10}
$$

and no further system parameters have to be introduced. In consequence, the dynamics of one step are characterized by the five independent parameters α_0, $\tilde{k}$, $\tilde{E}$, $\tilde{x}_{rel,i}$, and $\tilde{y}_i$.

Chapter 5

Positive force feedback in bouncing gaits?

By employing variations of the spring-mass model, in the last three chapters, we investigated the contribution of compliant leg behavior to animal and human locomotion, and could demonstrate that this functionally simple leg response suffices to describe the different whole body dynamics observed in walking and running. On this global level of discussion, however, we omitted the question of how this remarkable unique functional leg response is realized internally when incorporating the neuromechanical properties of biological muscles and muscle actuation into the leg function. In the present chapter, we approach this question parsimoniously by modeling the neuro-musculo-skeletal locomotor apparatus with a largely simplified two-segmented leg system and by restricting the investigation to bouncing gaits.

5.1   Introduction

In bouncing gaits, animals and humans use a spring-like leg behavior during stance (CAVAGNA *et al.*, 1964, 1977). In this phase, passive compliant structures such as muscle tissue, tendons, and ligaments store and release elastic energy reducing the metabolic costs of locomotion (CAVAGNA *et al.*, 1977; ALEXANDER, 1988). For instance, in some animals tendons preserve up to 70% of the stride energy (ALEXANDER and VERNON, 1975; BIEWENER, 1998). The exploitation of passive elasticities is, however, compromised by viscous properties of the muscle-skeleton system. For example, in humans only 40–50% of the stride energy can be stored elastically (CAVAGNA *et al.*, 1964). In order to maintain a cyclic motion (e.g. running at constant speed), the energy losses due to dissipation must be 'refilled' during the

rebound, requiring positive muscles work. But how do biological systems organize the proper muscle activation? Besides the necessity of muscle force regulation to withstand the tendon strain, the energetic refill requires an adequate control mechanism. Such control schemes should be scalable, for instance, to achieve a higher running speed (increased stride energy). Although this could be realized using central motor commands (e.g. higher centers), a control based on afferent information tracking the muscle state may relax the supervisory effort.

On the muscular level, for instance, it could be demonstrated that the stretch-reflex amplifying muscle force during lengthening can control the muscle stiffness (NICHOLS and HOUK, 1976; HOFFER and ANDREASSEN, 1981). However, it is not clear whether this particular reflex modulation would suffice to generate the observed bouncing leg behavior. Here, alternative reflex schemes might even more appropriately shape the muscle activation. In a hopping simulation, GERRITSEN and NAGANO (1999) investigated vestibulospinal and long-latency stretch reflexes. They found that the afferent modulation of the extensor activity yielded slow periodic knee-bending movements. Although flight phases were not considered and the movement patterns were unstable, they demonstrated the potential contribution of reflex mechanisms to the generation of cyclic locomotion.

In this chapter, we investigate whether continuous afferent inputs based on single-loop muscle reflexes could generate an appropriate extensor muscle activity during bouncing tasks. Therefore, we employ a two-segment leg model with one extensor muscle and focus on human hopping in place. The utilized sensory information is motivated by signals from muscle spindles and Golgi tendon organs. The bouncing capacity is assessed using three movement criteria: hopping performance (maximum hopping height, i.e. stride energy), and stability and elasticity of the hopping pattern.

5.2   Model

5.2.1   Mechanical system

Running is considered a planar (Fig. 5.1A) and hopping a vertical movement (not shown in Fig. 5.1A). Both are characterized by subsequent stance and flight phases. The body is idealized to a point mass m at the COM. The COM trajectory is determined by the gravitational force $\vec{F}_G = m\vec{g}$ and, during stance, additionally by the leg force $\vec{F}_{Leg}$

$$m\ddot{\vec{r}} = \vec{F}_G + \left[\vec{F}_{Leg}\right]_{stance} .$$

(5.1)
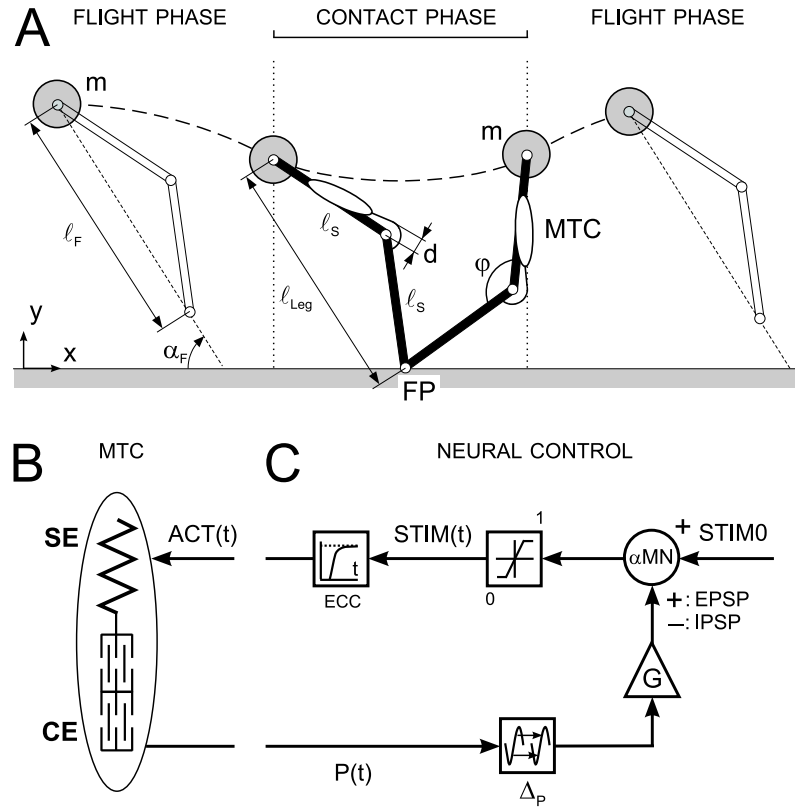
Figure 5.1. Hopping and running model. (**A**) The body is reduced to a point mass m. In stance, the leg is modeled by a two-segment system with one Hill-type extensor muscle. In flight, a fixed leg length ℓ_F and angle of attack α_F are assumed. (**B**) The muscle tendon complex (MTC) consists of a contractile (CE) and a series elastic element (SE). (**C**) The single sensory signal $P(t) \geq 0$ is time delayed (Δ_P) and gained ($G > 0$), before added to or subtracted from a constant stimulation bias $STIM0$ at the α-motoneuron (αMN) corresponding to a positive (EPSP) or negative feedback (IPSP). The resulting muscle stimulation $STIM(t)$ is restricted to be within 0 and 1. The excitation-contraction coupling (ECC) delays the muscle activation $ACT(t)$ about 30 to 40 ms. ℓ_{Leg}: leg length in stance; φ: joint angle; ℓ_S: segment length; d: moment arm of the extensor muscle; FP: foot point; EPSP/IPSP: excitatory/inhibitory postsynaptic potential

In contact the leg is modeled as a two-segment system with one Hill-type extensor muscle acting on the intersegmental joint (stance phase, Fig. 5.1A). The segments (equal length ℓ_S) and the muscle are massless. The muscle length ℓ_{MTC} is related to the joint angle φ

$$\ell_{MTC} = \ell_{ref} - d \cdot (\varphi - \varphi_{ref}) \, , \qquad (5.2)$$

where φ_{ref} is the joint angle at which the muscle reaches the reference length ℓ_{ref}, and d is the constant moment arm of the muscle. The leg force $\vec{F}_{Leg}$ acting parallel

to the leg axis (foot point FP to COM) is linked to the muscle force F_{MTC} with

$$\left|\vec{F}_{Leg}\right| = \frac{d}{\sqrt{\ell_S^2 - \left(\frac{\ell_{Leg}}{2}\right)^2}} \cdot F_{MTC} , \tag{5.3}$$

where ℓ_{Leg} is the instantaneous leg length defined as the actual distance between FP and COM.

The touch-down occurs if the COM reaches a certain landing height corresponding to an assumed, fixed leg length ℓ_F in flight. For running, additionally, a constant angle of attack α_F defines a leg orientation during flight (flight phase, Fig. 5.1A). The take-off occurs if the leg force vanishes, at latest when the initial landing length of the leg is reached during leg extension.

5.2.2 Muscle tendon complex (MTC)

The MTC consists of a contractile element CE and a series elastic element SE (Fig. 5.1B). The generated CE force depends on the muscle activation state $ACT \in [0, 1]$, the maximum isometric force F_{max}, and the force-length (f_ℓ) and force-velocity (f_v) relationships (based on AUBERT, 1956)

$$F_{CE}\left(ACT, \ell_{CE}, v_{CE}\right) = ACT \cdot F_{max} \cdot f_\ell\left(\ell_{CE}\right) \cdot f_v\left(v_{CE}\right) \tag{5.4}$$

with

$$f_\ell\left(\ell_{CE}\right) = \exp\left[c \cdot \left|\frac{\ell_{CE} - \ell_{opt}}{\ell_{opt} \cdot w}\right|^3\right] \tag{5.5}$$

and

$$f_v\left(v_{CE}\right) = \begin{cases} \frac{v_{max} - v_{CE}}{v_{max} + K \cdot v_{CE}}, & \text{if } v_{CE} < 0 \\ N + (N-1) \cdot \frac{v_{max} + v_{CE}}{7.56K \cdot v_{CE} - v_{max}}, & \text{if } v_{CE} \geq 0 \end{cases} . \tag{5.6}$$

In the *force-length relationship*, ℓ_{opt} is the optimum CE length (maximum force production), w describes the width of the bell shaped $f_\ell(\ell_{CE})$ curve, and c is $\ln(0.05)$ fulfilling $f_\ell(\ell_{opt} \cdot (1 \pm w)) = 0.05$. The *force-velocity relationship* follows the Hill-equation (HILL, 1938) for muscle shortening ($v_{CE} < 0$), where $v_{max} < 0$ is the maximum contraction velocity, and K is a curvature constant. Muscle lengthening ($v_{CE} \geq 0$) is characterized by an equation based on AUBERT (1956), where N is the dimensionless amount of force F_{MTC}/F_{max} reached at a lengthening velocity $v_{CE} = -v_{max}$.

The SE is characterized by a nonlinear, elastic force-length relationship (e.g.

$$f_{SE}(\varepsilon) = \begin{cases} (\varepsilon/\varepsilon_{ref})^2, & \text{if } \varepsilon > 0 \\ 0, & \text{if } \varepsilon \leq 0 \end{cases} \tag{5.7}$$

using the tendon strain $\varepsilon = (\ell_{SE} - \ell_{rest})/\ell_{rest}$, where ℓ_{rest} describes the tendon rest length and ε_{ref} is the reference strain with $f_{SE}(\varepsilon_{ref}) = 1$.

Since CE and SE are arranged in series, they have equal forces matching the MTC force F_{MTC}. Using this equilibrium, $F_{MTC}(t)$ is uniquely determined for a given MTC length $\ell_{MTC}(t)$ and an activation state $ACT(t)$ (e.g. van Soest and Bobbert, 1993).

5.2.3 Neural reflex pathway

The activation state $ACT(t)$ relates to a neural input $STIM(t)$ with a first order differential equation describing the excitation-contraction coupling

$$\tau\, dACT(t)/dt = STIM(t) - ACT(t), \tag{5.8}$$

where τ is a time constant. The neural input $STIM(t)$ consists of a constant stimulation bias $STIM0$ and a feedback component $\pm G \cdot P(t - \Delta_P)$

$$STIM(t) = \begin{cases} STIM0 & t < \Delta_P \\ STIM0 \pm G \cdot P(t - \Delta_P) & t \geq \Delta_P \end{cases}, STIM(t) \in [0, 1], \tag{5.9}$$

where P is the sensory information, $G > 0$ the gain factor, and Δ_P the signal-propagation time delay (Fig. 5.1C). Three possible sensory signals P are investigated separately: CE length ℓ_{CE} and velocity v_{CE}, and MTC force F_{MTC}. Signal combinations are not considered.

The signals are physiologically motivated by afferent information from muscle spindles and Golgi tendon organs (GTO). To account for a γ-adjustment of muscle spindle activity, the length and velocity signals are biased with a constant offset value ($P = \ell_{CE} - \ell_{off}$ and $P = v_{CE} - v_{off}$, respectively). The '$\pm$' sign defines a positive or negative feedback with an excitatory or inhibitory postsynaptic potential at the α-motoneuron. Although this definition may deviate from other approaches in literature, it provides a uniform assignment among the investigated feedbacks. Corresponding to the mechanism of signal transduction in neurons, the sensory signal is restricted to positive values $P(t) \geq 0$: Varying spike rates can alter the magnitude of postsynaptic potentials. However, the quality (excitatory or inhibitory) remains

constant.

5.2.4   Model parameter identification

parameter	value
body weight m	80 kg
gravitational constant g	9.81 m/s^2
assumed flight leg length ℓ_F	0.99 m
segment length ℓ_S	0.5 m
moment arm d	0.04 m
MTC reference length ℓ_{ref}	0.5 m
corresponding reference joint angle φ_{ref}	110°
maximum isometric force F_{max}	22 kN
optimum length ℓ_{opt}	0.1 m
width w	0.4 ℓ_{opt}
maximum shortening velocity v_{max}	-12 ℓ_{opt}/s
eccentric force enhancement N	1.5
curvature constant K	5
rest length ℓ_{rest}	0.4 m
reference strain ε_{ref}	0.04 ℓ_{rest}
excitation-contraction coupling constant τ	0.01 s
feedback time delay Δ_P	0.015 s

Table 5.1. Model parameters

The model parameter values used in the simulation are summarized in table 5.1. They reflect data from literature (WINTERS, 1990; VAN SOEST, 1992; HERR, 1998; VAN LEEUWEN, 1992), yet partially are compromised by the simplified leg representation: (i) The maximum isometric force $F_{max} = 22kN$ accounts for both knee and ankle extensor muscles to provide proper thrusting. (ii) The constant moment arm d of the extensor muscle would lead to exaggerated leg forces at erect leg positions (eq. 5.3) for muscle activations $ACT > 0$ (eq. 5.4). This is compensated for by the reduced width $w = 0.4$ of the force-length relationship (values from literature: e.g. $w = 0.56$ WINTERS, 1990). (iii) The signal propagation delay $\Delta_P = 15\ ms$ can be approximated by the time shift between M- and H-wave in H-reflex experiments. For the triceps surae this difference is about $20\ldots25\ ms$ (e.g. KNIKOU and RYMER, 2002; STEIN and CAPADAY, 1988). For the quadriceps femoris, a smaller delay occurs due to shorter afferent pathways (estimated to $5\ldots10\ ms$ from signal transduction difference to spinal cord between deep peroneal and femoral nerve, MEUNIER *et al.*, 1990). Taking these deviations and uncertainties into account, the robustness of the model results is checked for changes in MTC parameters (w, N, v_{max}, and ε_{ref}) and feedback time delay (Δ_P).

5.2.5 Simulation environment

The model is implemented in Matlab 6 using the Simulink 4 toolbox (Mathworks Inc., Natick, MA, USA). The forward dynamic simulation is performed with the embedded ode45 integrator with a maximum step size of 1e-3 (absolute and relative error tolerance 1e-8). The results of the numerical integration are checked using a 10 times higher accuracy.

5.2.6 Movement criteria

Three movement criteria are addressed to evaluate the model's bouncing behavior. (i) The hopping *performance* defined as maximum hopping height h_{max} is investigated with genetic algorithm optimization exploring the feedback parameter space (population of 500 individuals, 150 generations, recombination probability of 'fitter' individuals 75%, mutation rate 0.5%, single-point cross-over rate 75%; results checked by 3 times repetition, GOLDBERG, 1989).

(ii) For given feedback setups, the *stability* of the hopping pattern is investigated with the apex return map $y_{i+1}(y_i)$. At apex, the system state is uniquely determined by the apex height y_{apex} since $\dot{y}_{apex} = 0$ and the neuro-muscle-skeleton dynamics are re-initiated at each touch-down. The systems periodic behavior can therefore be addressed by analyzing the relationship $y_{i+1}(y_i)$ of two subsequent apices i and i+1 (index 'apex' omitted here). Fixed points $y_{i+1}(y_i) = y_i$ represent periodic solutions. Stable periodic solutions require a slope $dy_{i+1}/dy_i \, \epsilon \, (-1, 1)$ in the neighborhood of fixed points.

(iii) For stable hopping patterns, the *elasticity* of the leg force-length relationship is evaluated by introducing the elasticity coefficient C_{EL}

$$C_{EL} = \left(1 - \frac{A}{A_{max}}\right)^2, \tag{5.10}$$

which describes the ratio between the area A enclosed by the force-length trace of the leg and the area $A_{max} = F_{max} \cdot \Delta\ell_{max}$ given by the maximum leg force $F_{max} = \max(F_{Leg})$ and leg displacement $\Delta\ell_{max} = \max(\ell_F - y)$ in stance. In contrast to the total work done during contact (work loop equals zero in steady-state movements), for the calculation of A the absolute values of the difference of positive and negative work are added. The coefficient C_{EL} provides a measure of how close the leg resembles a perfectly elastic behavior ($C_{EL} = 1$), independent of nonlinearities in the actual spring law. The corresponding spring stiffness is approximated by $k = F_{max}/\Delta\ell_{max}$.

To elucidate what elasticity coefficient is required for spring-like human hopping, an experimental study was conducted with 12 healthy subjects (mean $\pm$ S.D.: body mass 72kg$\pm$10kg, age 32yrs$\pm$6yrs). C_{EL} was measured for each contact during hopping on a force-plate over a total time period of 60 seconds at a frequency of 2Hz. The leg displacement was calculated by twice integrating the vertical acceleration. The study will be published elsewhere. The preliminary results yielded $C_{EL} = 0.92 \pm 0.03$. The mean value is defined as reference value.

5.3 Results

5.3.1 Hopping performance – optimal stimulation vs. reflexes

At first, the maximum hopping performance of the model is assessed by optimizing the muscle stimulation $STIM(t)$. Hereto, the population of the genetic algorithm comprises individuals with 36 values determining the interpolated stimulation pattern $STIM(t)$ at every 20 ms following touch-down (total duration 700 ms). These patterns are applied to single step simulations (Fig. 5.2A). Starting at an initial apex height y_0, the simulation stops at the subsequent apex y_1. To ensure an optimization towards periodic hopping patterns, the individuals are judged by (i) the achieved hopping height $h = y_1 - \ell_F$ and (ii) the increase in height $\Delta y = y_1 - y_0$ (optimization function $f = 0.9h + 0.1\Delta y$). Hereto, y_1 is reused as initial apex height y_0 in the subsequent generation. The leg force $F_{Leg}(t)$ and muscle activation $ACT(t)$ corresponding to the optimized stimulation pattern $STIM(t)$ are shown in Fig. 5.2B ('OPT') yielding a maximum hopping performance of $h_{max} = 19.6 \ cm$.

Secondly, the influence of the different reflex pathways on the hopping performance is investigated using the same single-step simulation and optimization goals. Instead of stimulation patterns, the population now consists of different feedback parameter combinations (stimulation bias $STIM0$, gain G, and – for length and velocity feedback – offset value ℓ_{off} or v_{off}). The stimulation pattern $STIM(t)$ is generated by the acting reflex pathway. All three afferent signals can stabilize the model in the stance phase, but only positive length (L+) and force feedback (F+) generate appropriate muscle activation pattern $ACT(t)$ resulting in aerial phases ('L+' and 'F+' in Fig. 5.2B). For the maximum hopping height, positive force feedback ($h_{max} = 16.3 \ cm$) clearly outperforms positive length feedback ($h_{max} = 9.3 \ cm$) reaching almost 85% of the model's maximum hopping performance.
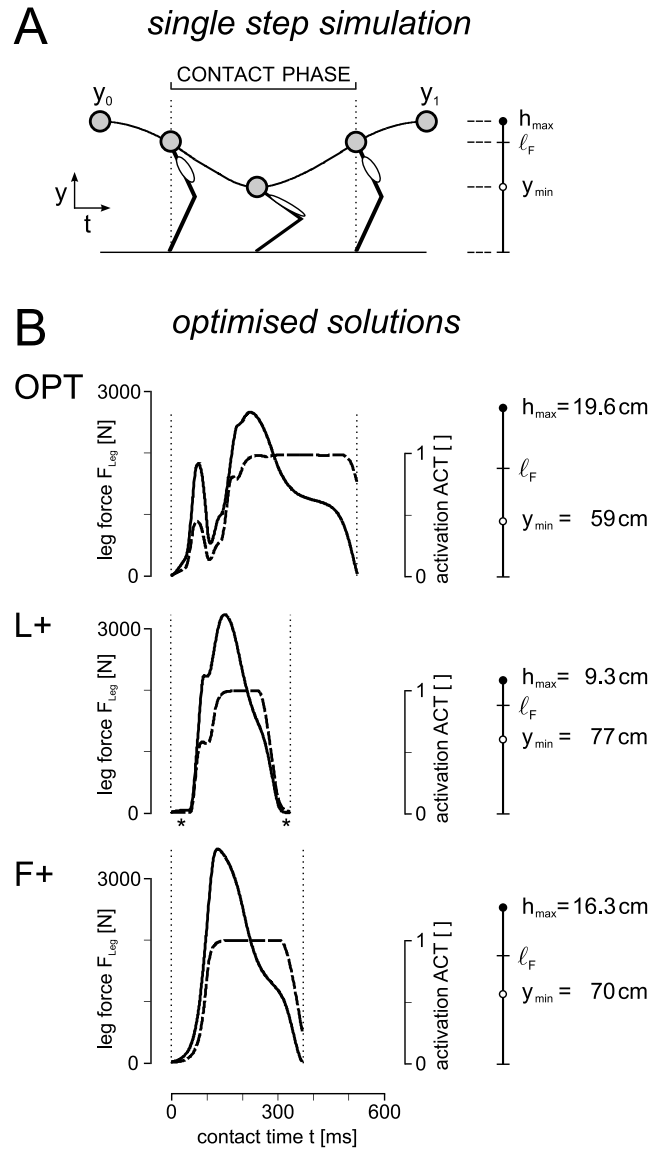
Figure 5.2. Maximum hopping performance. (**A**) Single step simulation applied to each individual of the genetic algorithm optimization (see text). (**B**) Leg force F_{Leg} (solid line) and muscle activation ACT (dashed line) during contact for maximum hopping performance h_{max} employing the optimized stimulation pattern ('OPT'), positive length ('L+', $STIM0 = 0.01$, $G = 125$, $\ell_{off} = 0.08$) and positive force feedback ('F+', $STIM0 = 0.01$, $G = 2.64/F_{max}$). The asterisks indicate suppressed signal output due to the offset value (see discussion).

5.3.2 Stabilization of the movement pattern

The performance results suggest positive force feedback as the most appropriate reflex scheme for extensor muscles in bouncing tasks. However, a functional relevance of this feedback during cyclic locomotion further requires the stabilization of the
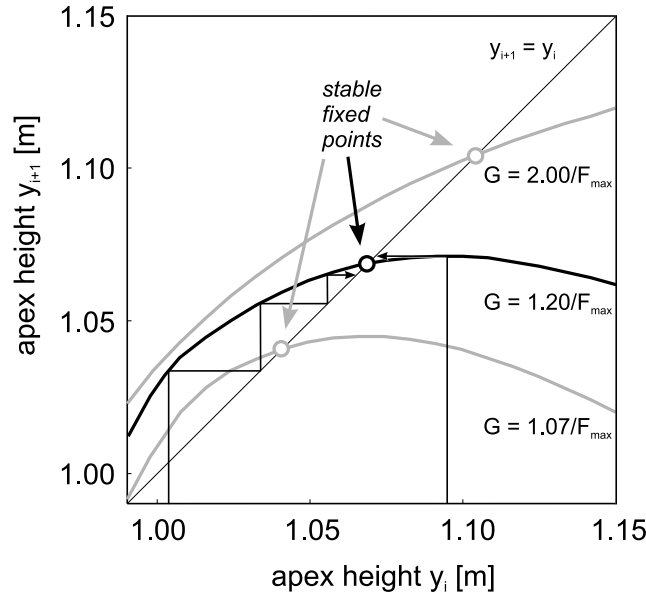
76

Figure 5.3. Stabilization of periodic hopping. The apex height return maps $y_{i+1}(y_i)$ for three different force feedback gains G are shown (stimulation bias $STIM0 = 0.05$). The intersections of the return maps with the diagonal $y_{i+1} = y_i$ represent periodic solutions (fixed points, denoted by small circles). The slope $dy_{i+1}/dy_i \in (-1, 1)$ within the neighborhood of the fixed points guarantees stable hopping. Starting from disturbed initial apex heights y_i the system converges to the steady state height after a few steps (indicated by the arrow tracings for the return map with feedback gain $G = 1.20/F_{max}$).

movement pattern. Therefore, the return map $y_{i+1}(y_i)$ of the apex height is analyzed. For a given stimulation bias ($STIM0 = 0.05$), the apex return maps for three feedback gains (G = $1.07/F_{max}$, $1.2/F_{max}$, and $2/F_{max}$ are depicted in Fig. 5.3. In all three cases stable solutions exist (denoted by the small circles in Fig. 5.3). With increasing gain the movement pattern stabilizes at increasing hopping heights (h = 5, 7.9, and 11.4 cm, respectively). After a disturbance the system returns to the steady-state condition within a few steps (arrow tracings in Fig. 5.3).

5.3.3 Elastic leg operation

In experiments on human hopping, spring-like leg operation with varying leg stiffness k is observed. To investigate the elasticity of stable hopping patterns achieved with positive force feedback, the model behavior is mapped throughout the feedback parameter space ($STIM0$, G; Fig. 5.4). For feedback adjustments leading to stable hopping (shaded area in Fig. 5.4A), the elasticity coefficient C_{EL} is calculated (eq. 5.10). Different parameter combinations result in stable hopping
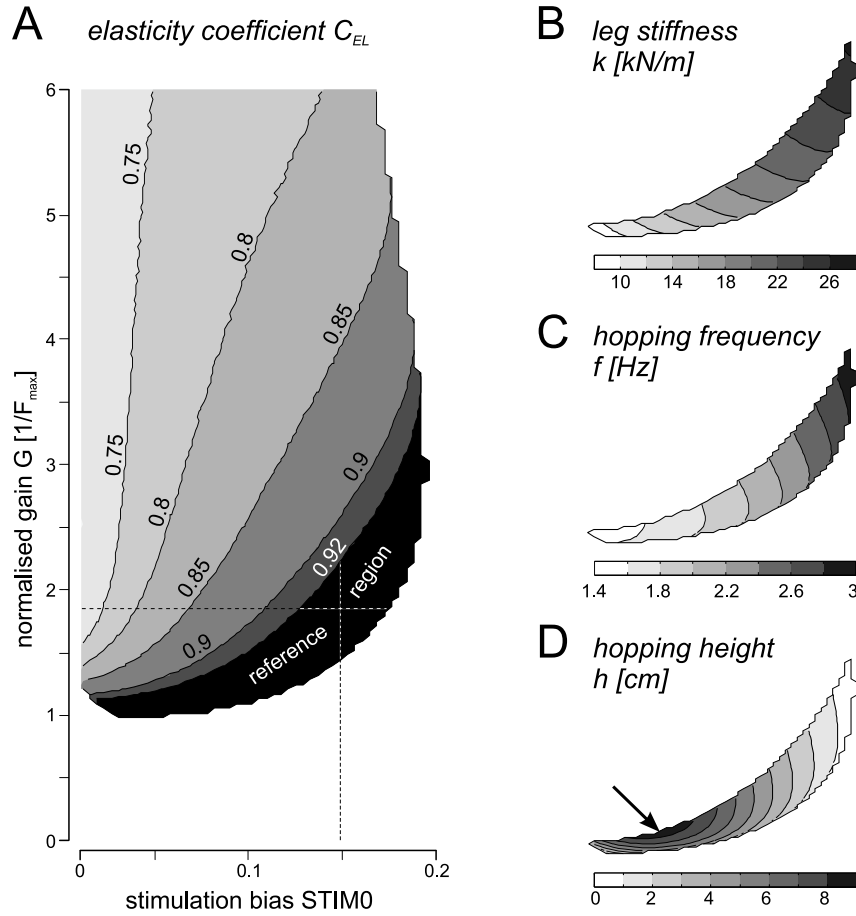
77

Figure 5.4. Elastic leg behavior. The model behavior using positive force feedback is mapped throughout the feedback parameter space ($STIM0$, G). (**A**) The elasticity coefficient C_{EL} for stable hopping patterns (shaded area) is shown. The intersection of the dashed lines refers to the parameters used for sensitivity analysis ($STIM0 = 0.145$, $G = 1.84/F_{max}$; see Fig. 5.5). (**B, C and D**) In the reference region the elasticity coefficient exceeds the reference value of $C_{EL} = 0.92$ (see A). Here, the corresponding leg stiffness (**B**), hopping frequency (**C**), and hopping height (**C**) are shown. The arrow indicates the maximum hopping height within the reference region ($STIM0 = 0.065$, $G = 1.32/F_{max}$).

($STIM0 < 0.2$, $G > 1/F_{max}$) with largely varying elasticities ($0.7 < C_{EL} < 0.97$). Only within a smaller region ($STIM0 < 0.2$, $1/F_{max} < G < 3.5/F_{max}$) the elasticity coefficient exceeds the reference value of $C_{EL} = 0.92$ ('reference region' in Fig. 5.4A).

In the reference region, with increasing stimulation bias and feedback gain the leg stiffness k and the hopping frequency f shift from 9 to 27 kN (Fig. 5.4B) and from 1.4 to 3 Hz (Fig. 5.4C), respectively. The range of hopping height from 0 to 8.8 cm (Fig. 5.4D) allows of different control strategies. For instance, starting with the parameter set of the largest height ($STIM0 = 0.065$, $G = 1.32/F_{max}$, indicated

by the arrow in Fig. 5.4D), the hopping height decreases while the leg stiffens if bias and gain are increased. Alternatively, the hopping height decreases with hardly affecting the leg stiffness if merely the gain is decreased.

To test the reliability of the elastic leg regime ($C_{EL} \geq 0.92$), a sensitivity analysis is performed for the setup $STIM0 = 0.145$ and $G = 1.84/F_{max}$ guaranteeing the largest feedback parameter tolerance within the reference region (intersection of dashed lines in Fig. 5.4A, leg force and muscle activation during contact as well as leg force-length relation shown in Fig. 5.5). The tolerance range fulfilling $C_{EL} \geq 0.92$ covers a considerable range of physiologically motivated values for the investigated muscle parameters reference strain ε ($1 \ldots 6.5$ %), eccentric force enhancement N ($1.4 \ldots 1.6$), maximum shortening velocity v_{max} ($-10.6 \ldots -13.4\ l_{opt}/s$), and width of the force-length relationship w ($0.33 \ldots 0.45\ l_{opt}$). Similarly, the model behavior is robust with respect to changes in the signal propagation delay Δ_P (tolerance range: $13 \ldots 18\ ms$).
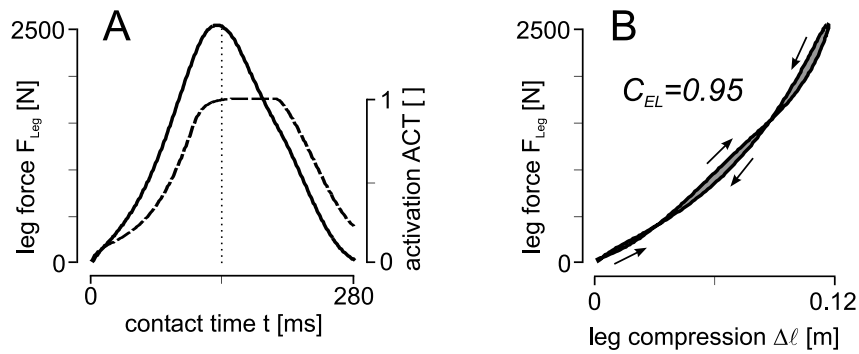
Figure 5.5. Example of the hopping pattern using positive force feedback. The leg force (solid line) and muscle activation (dashed line) (**A**), and the leg force-length curve (**B**, $\Delta \ell = \ell_F - y$) of the steady-state hopping pattern used for the sensitivity analysis are shown ($STIM0 = 0.145$, $G = 1.84/F_{max}$). The shaded area enclosed by the force-length curve depicts the area A used for the calculation of the elasticity coefficient C_{EL} (eq. 5.10).

5.4 Discussion

In this chapter, we investigated the potential role of single-loop muscle reflexes in periodic bouncing tasks. Although a rather simple approach addressing human reflex pathways is applied, a surprisingly successful strategy could be identified: positive muscle force feedback can generate and stabilize hopping patterns within a large range of hopping heights ($h_{max} = 16.3\ cm$, up to 85% of the model's maximum

hopping height). Moreover, for moderate hopping heights (up to 8.8 cm) spring-like leg behavior is achieved with a leg stiffness ranging from 9kN/m to 27kN/m.

The identified feedback is probably the simplest decentralized control strategy for bouncing tasks. Replacing a predefined ('voluntary') stimulation pattern with an adaptive control based on the actual muscle-skeleton dynamics, it could serve as an efficient and reliable alternative to a central motor control. Among the investigated reflex pathways, positive length feedback could also generate periodic hopping, but its hopping performance was clearly limited ($h_{max} = 9.3\ cm$). However, due to our simplified approach, we can not exclude that other feedback signals (e.g. joint position) or signal combinations (e.g. fibre length and velocity), or reflex structures may also succeed in bouncing tasks.

5.4.1 Comparison of optimal stimulation and reflexes

If subjects are asked to jump as high as possible, a countermovement jump is observed. Starting in stance, the subjects bent their legs prior to an extension with largely activated extensor muscles providing proper thrusting (e.g. BOBBERT and VAN INGEN SCHENAU, 1988). This implies that the achieved minimum leg position y_{min} strongly influences the maximum hopping performance h_{max}, which indeed is observed among the applied control schemes (see Fig. 5.2B). However, a complete leg flexion would exceed the ascending limb of the extensor force-length relationship (eq. 5.5), and the system would fall down due to insufficient force generation. Since large hopping heights result in high impact velocities, proper braking forces have to be applied in the early stance phase. Here, the eccentric operation of the extensor force-velocity relationship (eq. 5.6) provides adequate force to solve this issue. For instance, the *optimized stimulation pattern* (OPT) is characterized by an initial activation (force) peak sufficient to redirect the movement at the minimum position $y_{min} = 59$ cm. Similar force peaks are known from drop jump experiments (e.g. VOIGT *et al.*, 1995). Hereafter, full muscle activation is required to reach the maximum steady-state hopping height $h_{max} = 19.6$ cm.

But how closely can the considered feedbacks imitate this control strategy? The shape of the feedback based activation patterns is largely constraint by the available sensory information. For instance, the stretch-shortening cycle of the extensor muscle during the rebound leads to a negative slope of the CE-velocity time series. To achieve an increasing muscle activation during leg flexion ($P = v_{CE} - v_{off}$), *velocity feedback* requires a *negative* feedback scheme (V-). Although applicable at a first glance, this feedback inherently destabilizes periodic hopping patterns. For

instance, an increased hopping height leads to larger eccentric velocities v_{CE} (increased impact). Instead of damping, the negative feedback delays the development of increasing muscle activation. Initially, this results in a larger hopping height (as muscle activity is shifted towards the concentric phase). However, a self-amplifying cascade is induced further increasing the impact velocity as well as delaying the muscle activation growth. Inevitably, exceeding a critical impact velocity, the leg collapses during stance.

Both the length ($P = l_{CE} - l_{off}$) and force signal ($P = F_{MTC}$) increase during leg bending. Here, positive feedback schemes with small initial stimulation bias result in an increasing muscle activation during stance. *Positive length feedback* (L+) is characterized by a rapid increase of $P(t)$, which still produces considerable breaking forces. To delay this fast build-up and, therefore, to reach a lower position y_{min} during stance, the offset value ℓ_{off} is used. The length of the contractile element CE at touch-down is $\ell_{CE,TD}$. During leg compression the muscle lengthens and an offset value $\ell_{off} > \ell_{CE,TD}$ suppresses any signal output until $\ell_{CE} = \ell_{off}$ is reached (left '$*$' in Fig. 5.2B). However, as the ℓ_{CE}-signal is almost symmetric with respect to midstance, the suppression is equally present during late stance (right '$*$' in Fig. 5.2B). Consequently, the amount of positive work is limited and only moderate maximum hopping heights are achieved ($h_{max} = 9.3$ cm).

Positive force feedback (F+) has no sensory offset. Here, a different mechanism prolongs the activation build-up. The proprioceptive signal $P = F_{MTC}(t)$ depends on the instantaneous muscle activation $ACT(t)$, the normalized force-length $f_l(t)$ and force-velocity relationships $f_v(t)$, and the maximum isometric force F_{max} (eq. 5.4). The activation itself depends on the stimulation history according to the excitation-contraction coupling (eq. 5.8), which has a characteristic delay Δ_{ECC}. Thus, the contribution of the gained and time delayed feedback signal $P(t - \Delta_P)$ to the muscle stimulation $STIM(t)$ is proportional to the preceding stimulation signal $STIM(t - \Delta_P - \Delta_{ECC})$ and to the muscle state $M(t - \Delta_P) = f_l(t - \Delta_P) \cdot f_v(t - \Delta_P)$. Assuming $M = const$ the activation development is characterized by an exponential growth (see appendix). Although modulated by the muscle dynamics $M(t)$, the adjustment of the feedback gain G allows variable initial slopes of the activation build-up, and the maximum activation can be delayed until leg extension. As a result, positive force feedback yields an almost twofold better hopping performance than positive length feedback. The exponential growth of muscle activation is an appropriate response to the breaking in the eccentric phase of periodic bouncing.

An initial suppression of the sensory signal, to a certain extent, improves the

hopping performance for positive feedbacks. For each reflex, the suppression can be tuned with the signal propagation delay Δ_P. For both positive length and force feedback this allows to almost reach the model's maximum hopping height. The required 'optimal' delay is larger for length ($\Delta_P \sim 60~ms$) than for force feedback ($\Delta_P \sim 25~ms$). This suggests that length feedback could manage hopping tasks using longer latency reflex loops. However, the longer the signal delay is, the more sensitive the system gets with respect to external disturbances. Here, additional control effort would be required. In contrast, positive force feedback represents an autonomous, rapidly adapting control scheme well-suited for the short contact periods in bouncing gaits.

5.4.2 Task variability of positive force feedback

Positive force feedback has been investigated previously in an experimental study. By converting the measured ground reaction force into extensor muscle stimulation, PROCHAZKA *et al.* (1997b) showed that this reflex successfully operates in load compensation tasks. In a simulation study they further demonstrated that the muscle's force-length relationship provides an inherent feedback gain adaptation (PROCHAZKA *et al.*, 1997a), which – if opposing forces are present (e.g. antagonist muscle forces, gravity) – prevents the traditionally observed destabilizing effect of positive force feedback (VAN HELM and ROZENDAAL, 2000).

In our study we observe a similar behavior. For sufficient gains ($0 < G < 1/F_{max}$) hopping does not occur (Fig. 5.4A), but the system stabilizes in stance at leg positions characterized by the equilibrium of muscle and gravitational force (not shown in Fig. 5.4A). Any further leg extension reduces the muscle force (due to the force-length relationship of the shortening extensor muscle) and the resulting net force restores the equilibrium position. The opposite holds for leg bending.

With increasing gain ($G > 1/F_{max}$), positive force feedback leads to periodic hopping at different steady-state apex heights (examples shown in Fig. 5.3). Although the same reflex is applied, the stabilization here bases on a different mechanism. Instead of the muscle's force-length relationship, the force-velocity relationship becomes crucial. For instance, an increased apex height results in a larger landing velocity. Due to the amplified muscle response (force-velocity relationship), the force build-up is accelerated without affecting its decrease (feedback gain remains constant), which shifts the muscle operation towards the eccentric phase. The system compensates the disturbance through damping until the steady-state apex height is restored within the next ground contacts (the opposite holds for decreased apex

heights). Consequently, the stability of hopping is unaffected even if no force-length dependency $f_\ell(\ell_{CE}) = 1$ is assumed.

This suggests that the proposed muscle-reflex system represents an adjustable, biological actuator suited to more than a single movement task. The flexibility ranges from load compensation over elastic leg operation to maximum performance hopping, and clearly benefits from the muscle properties – elucidating these properties from an integrative perspective, which may help to design technical actuators adapted to legged locomotion.

5.4.3 Leg stiffness as emergent property

Since the observation that, during bouncing gaits, the legs of animals and humans behave in a spring-like manner, 'leg stiffness' has become a key parameter in investigating these gaits. For instance, it could be demonstrated that leg stiffness is hardly affected by running speed (He *et al.*, 1991; Farley *et al.*, 1993), indicating passive elastic elements (e.g. tendons, ligaments) as the likely origin of spring-like leg operation. However, humans adapt their leg stiffness if subjected to constraints (e.g. hopping frequencies or height, Farley *et al.* (1991); Seyfarth *et al.* (2001); running stride frequencies, Farley and Gonzalez (1996)) or environmental changes (e.g. surface stiffness, Kerdoc *et al.*, 2002; Ferris and Farley, 1997; Ferris *et al.*, 1998). Consequently, this posed the question on how leg stiffness is controlled at the muscle-skeleton level? Here, experimental and simulation studies suggested ankle joint moment generation to play an important role (Farley and Morgenroth, 1999). Although this indicated the participation of neural control in the adjustment of leg stiffness, evidences of what the appropriate control resulting in bouncing gaits could actually be remained elusive.

In the present chapter, positive force feedback of the extensor muscle(s) is suggested as an appropriate control scheme. For certain feedback parameters ('reference region', Fig. 5.4A), it enables elastic leg operation within a considerable range of leg stiffness (between 9 and 27 kN/m, Fig. 5.4B), hopping frequency (from 1.4 to 3 Hz, Fig. 5.4C), and hopping height (up to 8.8 *cm*, Fig. 5.4D). Experimental studies on human hopping at different frequencies ($1.5 \ldots 3$ Hz) report a similar correspondence to the leg stiffness ($10 \ldots 30$ kN/m; Farley *et al.*, 1991; Seyfarth *et al.*, 2001).

The change of hopping height within the reference region reveals a simple control strategy for the stride energy. If the feedback stimulation bias is fixed to $STIM0 = 0.065$, an increased gain leads to an increased steady-state stride energy (hopping height) while the leg stiffness almost remains constant. Reconsidering the

experimental results showing that leg stiffness is hardly affected by speed (i.e. system energies) (HE *et al.*, 1991; FARLEY *et al.*, 1993), this might indicate that the stride energy is the parameter to be controlled in animal and human locomotion. Here, leg stiffness itself rather emerges from the muscle-reflex dynamics managing external constraints.

5.4.4 From hopping to running

In a previous work (SEYFARTH *et al.*, 2002, compare also Ch. 2), we could identify a movement criterion for running with elastically operating legs: a proper adjustment of the landing angle of attack to the leg stiffness results in self-stabilized and robust running. Using this criterion, only two conditions have to be fulfilled for running based on a muscle-skeleton system: (i) elastic leg operation and (ii) stabilization of the stride energy. Positive muscle force feedback meets both requirements. Hence, the movement criterion can be successfully applied by selecting an angle of attack appropriate to the emergent leg stiffness (Fig. 5.6). This suggests that the identified muscle-reflex mechanism might also be an efficient and powerful concept for running. To our knowledge it is the first model describing running within such a framework.
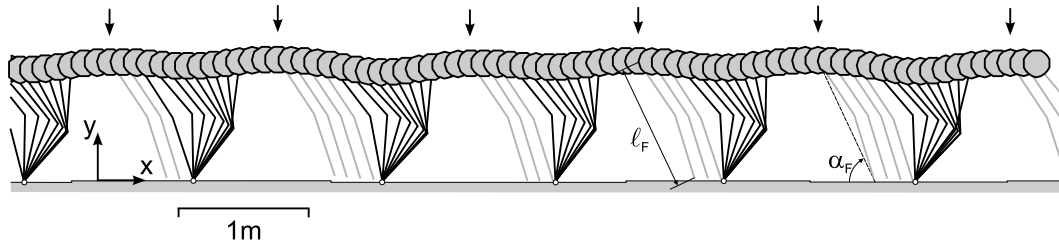

Figure 5.6. Robust running (ground irregularities ± 0.5 *cm*) using positive force feedback ($STIM0 = 0.185$, $G = 1.4/F_{max}$). The stick figures correspond to time intervals of 20 ms. The arrows denote the apices, at which the virtual leg with the length $\ell_F = 0.99$ *m* and an angle of attack $\alpha_F = 65°$ (mean leg stiffness $16.5 kN/m$) is introduced during flight.

5.4.5 Reflex generated motor control

The control of locomotion can be distinguished between (central) feedforward commands and (decentralized) feedback responses. It is assumed that the feedforward component generates a time-varying, cyclic muscle activation pattern (referred to as 'background activity') resulting in basic locomotor functions (e.g. as found in partially deafferented cats, GOLDBERGER, 1977). The identification of central pattern generators (CPG) in animals as diverse as invertebrates and mammals supports this

hypothesis (for review: ORLOVSKY *et al.*, 1999). Reflex responses can modulate this feedforward activation pattern. However, the functional relevance of this modulation in undisturbed locomotion remains largely unclear (ZEHR and STEIN, 1999).

For instance, experimental studies addressing extensor muscle activities in human hopping and running could identify a short-latency (35...45 ms) stretch-reflex response following touch-down (MELVILL JONES and WATT, 1971; DIETZ *et al.*, 1979; VOIGT *et al.*, 1998). This reflex is mainly attributed to proprioceptive information from muscle spindles (Ia-afferents), although contributions from Golgi tendon organs (GTO, Ib-afferents) can not be ruled out. Such rapid responses are likely to reduce extensor lengthening ('muscle yield') after landing and, consequently, could enhance the loading of the corresponding tendons. Hence, it is suggested that the observed stretch-reflex is of functional importance for the generation of leg stiffness during bouncing gaits. However, further contributions of this reflex (e.g. at longer latencies) to the stance phase ($\sim 200...400$ ms) are not observed. It is supposed that here the overlap with the (centrally initiated) background activity may conceal the direct observation (VOIGT *et al.*, 1998; FUNASE *et al.*, 2001).

Further information about potential reflex contributions can be obtained by evoking the H-reflex (the electrically elicited analogue to the stretch-reflex). Comparing standing with the stance phase of walking and running, such experiments indicate a progressive inhibition of the stretch-reflex activity from standing to walking to running (CAPADAY and STEIN, 1987; FERRIS *et al.*, 2001). SINKJAER *et al.* (2000) suggested that this reflex could have little or no contribution to the muscle activity during normal walking, although compensatory reflex responses to large disturbances may still occur (MORITA *et al.*, 1998). For hopping and running, this could explain the extensor stretch-reflex response following touch-down (a large disturbance) without the observation of later contributions, suggesting that, for the remaining stance phase, the centrally thought background activity would be essential. Experiments, where extensor muscles fatigue, further motivate this hypothesis. For instance, during marathon running the stretch-reflex response significantly decreases (AVELA and KOMI, 1998). However, the subjects still can run.

The findings obtained in this chapter suggest that the muscle activity usually associated with the background activity is not just a central contribution, but is largely shaped by positive force feedback. In contrast to the understanding of feedbacks as mechanisms reacting to disturbances, here the reflex organizes the muscle activation pattern. The result is a task specific, uniform leg force pattern as observed across species and individual morphologies. This reflex based force generation is, however,

restricted to the stance phase and may require other structures such as CPG triggering the phases of the gait cycle. In fact, load receptor reflexes themselves may be involved in the initiation of phase transitions (Pearson, 1995). Although we did not address a possible influence of reflex schemes on the flight phase, it seems that the self-organizing dynamics of the neuromechanical system may significantly contribute to the coordination of legged locomotion. Synchronized and supervised by central commands including CPG, this could largely simplify the required control effort.

But in how far can positive force feedback be motivated by experimental observations? Although traditionally associated with negative feedback schemes, experimental studies on leg extensor muscles could show a reflex reversal to positive force feedback in quadruped standing and during the stance phase of quadruped walking (Pearson and Collins, 1993; Gossard et al., 1994; Pratt, 1995). Subsequent investigations suggested a similar reflex reversal during the stance phase of human walking (Stephens and Yang, 1996). Although there is an increasing experimental evidence for positive force feedback as homonymous sensory pathway, its functional contribution to the stance phase of the locomotor cycle remains controversial. Some studies suggest that this reflex might appropriately modify the extensor muscle force during stance depending on the carried load (Pearson and Collins, 1993; Pratt, 1995; Prochazka et al., 1997a). However, it is still unclear, whether afferent information from GTO serves this function (Fouad and Pearson, 1997; Sinkjaer et al., 2000). Experimental investigations addressing this reflex pathway in bouncing gaits are unknown and remain for future research.

5.4.6 Summary

In our understanding, biological locomotor systems are highly redundant systems, which likely have various control strategies at their disposal to manage a distinct movement objective. In the final instance, central motor commands will solve the issue. However, the more a movement task becomes routine, the more the evolution of decentralized, largely autonomous solutions embodied in morphology seems plausible. Positive force feedback represents such a local control strategy. Whether it will be verified in experiments or not, we feel the consideration of muscle reflexes, not only as disturbance responses but also as integrated part of biological actuation, an important view on the control of locomotion of animals and humans.

5.5   Appendix: Time course of muscle activity using F$^+$

The comparison of the proprioceptive signals $P = \ell_{CE} - \ell_{off}, v_{CE} - v_{off}, F_{MTC}$ (see 5.2.3) indicates that they all are influenced by the muscle dynamics (time series of force-length- and/or force-velocity-relationship, due to eq. 5.4, 5.5 and 5.6). In contrast to the muscle fiber length or velocity feedback, the muscle force signal is further influenced by the dynamics of the muscle activation A, which itself is related to the history of the stimulation signal $STIM$ (eq. 5.8).

Assuming that (i) the stimulation does not exceed the saturation level ($STIM(t) \leq$ 1), and (ii) the muscle activation instantaneously follows the stimulation ($A \equiv STIM$), for positive muscle force feedback the time series of the stimulation signal (5.9) simplifies to

$$STIM(t) = \begin{cases} STIM0 & t < \Delta_P \\ STIM0 + G_F \cdot M(t - \Delta_P) \cdot STIM(t - \Delta_P) & t \geq \Delta_P \end{cases}, \quad (5.11)$$

with $M(t - \Delta_P) = f_l(l_{CE}(t - \Delta_P)) \cdot f_v(v_{CE}(t - \Delta_P))$ describing the muscle dynamics and $G_F = G \cdot F_{max}$ representing the normalized gain factor.

Using (5.11), the stimulation $STIM(t)$ at time t can be constructed by dividing the time scale into equal intervals of the feedback delay Δ_P. Beginning at the last interval which includes t, the actual stimulation is iteratively substituted with the corresponding stimulation of the preceding interval. This procedure yields the expression

$$STIM(t) = STIM0 \left[1 + \sum_{k=1}^{n} \left\{ G_F^k \prod_{l=1}^{k} M(t - l \, \Delta_P) \right\} \right], n \geq 0$$
$$n\Delta_P \leq t < (n+1)\Delta_P \quad (5.12)$$

for the time series $STIM(t)$. From this equation, the change in muscle stimulation between two subsequent intervals derives to

$$\Delta STIM = STIM(t) - STIM(t - \Delta_P)$$
$$= STIM0 + [G_F \, M(t - \Delta_P) - 1] \, STIM(t - \Delta_P). \quad (5.13)$$

As shown in (5.13), the development of the muscle stimulation $STIM(t)$ compares to a modulated natural growth or decay function. Provided that $G_F \, M(t - \Delta_P)$ is larger than one, the stimulation rises exponentially with each interval Δ_P. But, as soon as the muscle dynamics enforces a negative value on the right side of (5.13),

the stimulation decreases.

Chapter 6

General Conclusion

Is it possible to understand legged locomotion to a degree that we can device dexterous legged robots or offer patients artificial limbs replacing lost appendages in a truly functional manner? Perhaps in future, but at present it seems that we hardly grasp the principles underlying legged locomotion – principles that biological systems master with such a compelling ease. Nevertheless, there has been significant progress in identifying some essentials over the past decade. And, on the mechanical level, this progress primarily stems from the exploitation of simple models addressing animal and human walking and running.

Among those models, the inverted pendulum and the spring-mass model certainly rank as the most prominent. Both advanced the understanding of legged locomotion in two principal ways. First, they have inspired scientists to build legged robots that profit from the natural dynamics of the underlying mechanical system either to minimize the required actuation power (e.g. passive dynamic walkers based on the inverted pendulum motion pioneered by T. McGeer), or to largely simplify the control effort (e.g. the spring-like acting dynamically stable hopping robots introduced by M. Raibert, see also Ch. 1).

Secondly, extending on this concept of exploiting the natural system dynamics eventually led to a transition from merely utilizing these basic models for *describing* biological gaits (e.g. by virtual model control in robotics), to investigating analytically their intrinsic behavior and *predicting* explicit parametric dependencies that not only can be verified in experiments on animals and humans, but have a strong potential to advance technical realizations in robotics as well as applications in rehabilitation and prosthetics.

6.1   Change of walking gait paradigm

Although both the inverted pendulum and the spring-mass model have largely shaped our principal understanding of legged locomotion in the past, they rank differently when assessing their value as basic *gait templates* encoding parsimoniously the characteristic whole body dynamics as identified by the corresponding GRF patterns. In this respect, only the spring-mass model for running prevails and the inverted pendulum must be refuted as template for walking. Consequently, the identification of a walking template represents one of the major challenges in biomechanics.

The thesis addresses this issue by hypothesizing that in contrast to the traditional assumption of a stiff gait, walking is largely dominated by a leg behavior which, like in running, is functionally based on limb compliance. Following this hypothesis, in *Chapter 3* it is demonstrated that the predictability of the walk-run transition can not only be motivated from limits of the vaulting motion as described by the inverted pendulum, but can equally be derived from the compliant spring-mass model when imposing the kinematic constraint of a virtually horizontal motion of the COM at transition (Fig. 3.1). Moreover, with $Fr \simeq 0.4$ the predicted transition speed reproduces the speed at which animals and humans indeed prefer to switch from walking to running ($Fr \approx 0.5$) with surprising accuracy, clearly improving on the result of $Fr = 1$ obtained from the traditionally taken inverted pendulum approach.

This outcome not only supports the hypothesis of the more general importance of compliant leg behavior in legged locomotion pursued in this thesis. It likewise suggests a solution to the fundamental question of whether it is the underlying mechanics that triggers the gait transition and the physiological properties (e.g. metabolics, attentional demands) that have adapted to this change over the evolutionary process, or it is the other way around, i.e. that physiological constraints trigger the transition enforcing the mechanics to respond by modified system dynamics to maintain the physiological parameters within acceptable ranges. Although the inverted pendulum model correctly predicts the transition speed to be solely a function of gravitational acceleration and leg length, which suggested the underlying mechanics as driving mechanism early on, its quantitative discrepancy by a factor of two soon led to favoring physiological constraints as the more likely candidates triggering the transition. However, no conclusive physiological factor could be identified over the past and the origin of the gait transition still remains elusive. Here, the transition speed (eq. 3.11) derived in Chapter 3 resolves this controversial subject in favor of the underlying mechanics.

In a second step, in *Chapter 4* a bipedal spring-mass model (Fig. 4.1) is introduced to investigate in how far compliant limb behavior can indeed describe the characteristic whole body dynamics in walking. It is demonstrated that the bipedal spring-mass model produces stable periodic locomotion with the M-shaped GRF patterns typical for biological walking (Fig. 4.3). Here, the double support phase is identified as key determiner in obtaining this M-shaped GRF patterns, without the necessity of a functional separation of the leg behavior into early braking and late push-off in the single-leg stance phase, which is frequently fostered in more complex models of biological walking. Moreover, it turns out that in contrast to the general belief that legs should be stiff in walking, the actual spring stiffness required to obtain the walking motion is rather low, i.e. comparable to that in running or even smaller.

Hence, the results of Chapter 3 and 4 together suggest a shift of the gait paradigm for walking: rather than the inverted pendulum, the bipedal spring-mass model should be employed as basic mechanical model for this gait, since it more closely resembles the natural whole body dynamics observed in biological legged systems and, due to its parametric simplicity, even has the capability to serve as gait template.

6.2 Uniting two fundamental gaits – generality of limb compliance in biology

But the results obtained in Chapter 4 suggest more. In Fig. 4.5 the parameter domains leading to stable periodic locomotion of the walking model are shown. Next to the domain resulting in the M-shaped GRF pattern, there exist a multitude of domains representing steady-state locomotion with more peaks in the GRF than the characteristic double peak known from experiments on animal and human walking.

In fact, as discussed in section 4.4.1, without rotation of the stance spring (zero forward speed equivalent to low system energy), this spring would oscillate indefinitely producing an infinite number of force peaks in the GRF. However, with increasing speed (system energy) the spring rotation sets in, and less and less oscillation cycles can be completed before the opposite leg touches the ground ending the single leg stance phase. Due to the coupling of both legs via the COM, this cancelation of the single support phase requires a precise timing leading to the observation of parameter domains with discreet numbers of force peaks only. And the highest walking speed can only be obtained with just two compression-decompression cycles yielding the known double-peak pattern of the GRF (Fig. 4.5).

But what would happen if the locomotion speed (system energy) is further increased? As has been discussed in section 4.4.3, the stance spring would produce too large a rebound after the initial compression in single-support and relax completely, and the system would get airborne. Hence, this single rebound in stance would result in a GRF pattern equivalent to the contact phase in running, i.e. the bipedal spring-mass model can likewise describe running. To demonstrate this, in Fig. 6.1, the model's parameter domains for stable walking are expanded by the domain leading to stable running (single force peak).

Interestingly, the large speed gap between 2 and $3m/s$ separating the parameter domain for stable running and the double-peak walking domain (Fig. 6.1), reflects the experimental observation that although humans display a preferred transition speed at about $2.2m/s$ if instructed to walk or run on a treadmill at different speeds, they immediately switch from walking at about $1.85m/s$ to running at about $2.3m/s$ during spontaneous overground progression (Saibene and Minetti, 2003), which more closely resembles the natural situation.

In contrast to the general belief that walking and running represent two distinct phenomena of legged locomotion, the bipedal spring-mass model identified in this thesis suggests that they rather represent two out of an indefinite number of discreet oscillatory modes of the same fundamental, compliant leg behavior as identified by the number of force peaks in the characteristic GRF patterns. Here, the locomotion speed (system energy) operates as the key determiner of the actual mode, which in turn enforces the observation of 'different' gait patterns in animal and human locomotion with increasing velocity.

6.3 From templates to theory

Another major challenge for the science of legged locomotion is to put this field on a sound mathematical basis. Ideally, there would be axiomatic rules at the top from which a detailed understanding could be derived in successive steps that allows to predict the properties and functionalities of legged systems at increasing level of integration. Although we are far from such an understanding at present, it seems that gait templates could serve as suitable starting points, as they can describe the characteristic whole body dynamics observed in legged locomotion without getting lost in the overwhelming complexity that often denies an analytical access in more detailed model representations.

Here, research on the spring-mass model has already proven the value of such an
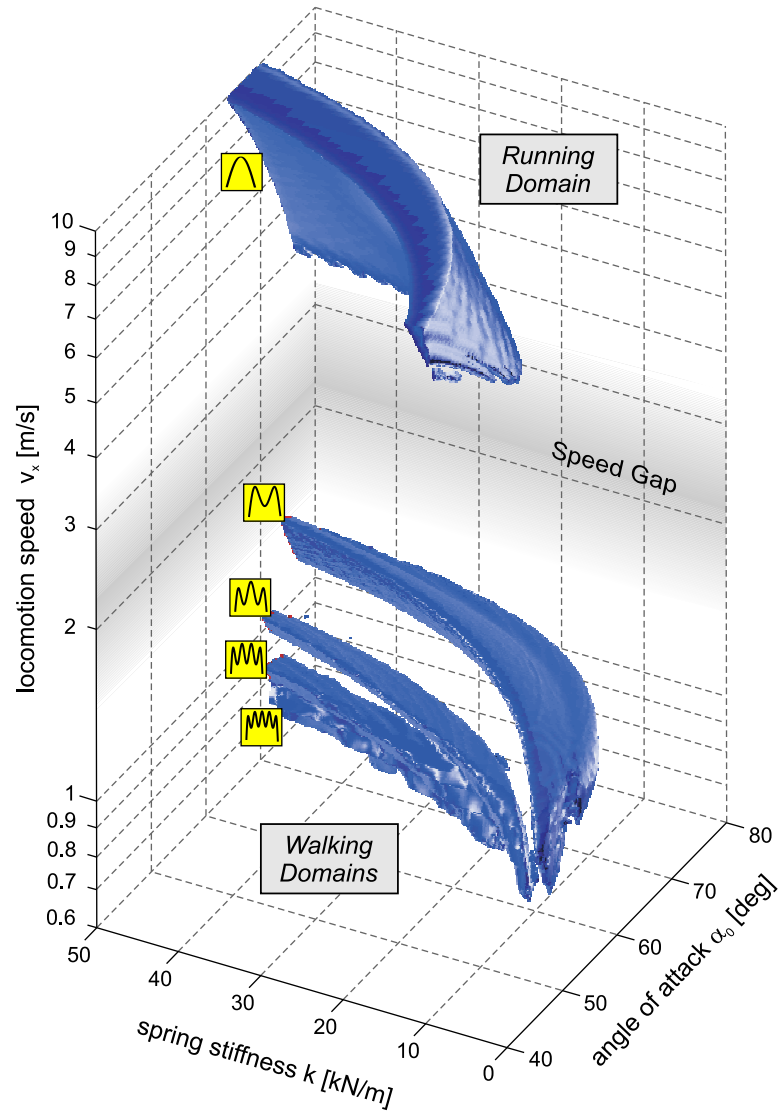
Figure 6.1. Parameter domains for stable locomotion of the bipedal spring-mass model. The figure is modified from Fig. 4.5 by including the stable parameter domain for running. Moreover, to facilitate the comparison with human locomotion, the parameters are presented in absolut values for a human-like model with $m = 80kg$, $\ell_0 = 1m$, and $g = 9.81m/s^2$ and the average forward speed v_x at apex is depicted instead of the system energy (note the logarithmic scale).

approach. For instance, by the numerical identification of parametric dependencies, a control scheme for legged systems could be derived that allows to freely distribute the available system energy into forward progression (efficiency) or vertical bouncing (safety), without requiring explicit knowledge about the ground irregularities. However, even for the simple spring-mass model an analytical access is hampered by the non-integrability of the system (compare section 1.3).

93

The work presented in *Chapter 2* of this thesis provides an analytical approximation of the spring-mass model's stance-phase dynamics, which combines *simplicity* with surprising *accuracy*. By comparison with numerical calculations it could be shown that this approximation leads to accurate predictions of the system's stability behavior for parameter combinations highly relevant to animal and human locomotion. Moreover, based on the simplicity of the solution, an explicit parametric dependency could be derived that identifies spring-mass model parameters relevant for stable locomotion hereby extending an empirically found relationship. Hence, due to both the accuracy and simplicity, the solution might well serve as analytically tractable tool that can be expanded upon in future works approaching the mathematics of legged locomotion.

Particularly, since the bipedal version of the spring-mass model is suggested as walking template in this thesis, the identified solution can immediately be applied as approximation for the single-support phase in walking. And only the double-support phase remains to be described analytically to obtain a mathematical representation of both fundamental gait patterns.

6.4 From templates to morphological embodiment

The successful interpretation of the two basic gaits using the bipedal spring-mass model indicates that the concept of limb compliance in legged locomotion reaches far wider than generally assumed. Nevertheless, mechanical spring legs cannot be found in biology. In animals and humans, muscle-tendon units comprising passive tendons in series with *active* muscle fibers span the joints of articulated legs. The active fibers are controlled by the nervous system and the question arises of how the neuromechanical interplay ensures the remarkable uniform, spring-like behavior at the global leg level.

Some researchers infer that this behavior is generated entirely by the passive tendons of the leg extensor muscles with the muscle fibers acting isometrically. But unless the muscle fibers can be locked mechanically, this assumption leads inevitably to a contradiction between cause and effect. Arranged in series, the muscle fibers could maintain a constant length only if they would generate exactly the same force as the tendon, which implies that the nervous system is always pre-informed about the extensor muscle's force development in forthcoming stance phases. Perhaps this strategy could work in a predefined environment. The irregularities and uncertainties of natural movements and terrains, however, deny such an approach. Rather, they

require the nervous system reacting continuously to unpredicted load situations to correct the muscle fiber strain. But a correction can only be applied *after* the disturbance took place. Thus, the muscle fibers cannot be forced to act isometrically and delegating the generation of the spring-like leg behavior to the passive tendons alone does not resolve the problem.

The permanent need of reacting to unforeseen load situations indicates that the nervous system monitors the muscle-tendon unit's current state using sensory feedback and employs this information in the control of the muscle fiber activation. Due to the long time delays when using central feedback loops ($\sim$ 100ms), the information about the muscle state is more likely to be processed at the spinal cord level. This, however, excludes a central command of all the control tasks in biological legged locomotion. Here, the spring-mass gait template reveals an elegant solution. As global strategies leading to self-stable locomotion could be identified, the control of legged locomotion can hierarchically be decomposed if the system can rely on compliant limb behavior in contact. Hence, the spring-mass model motivates the investigation of *local feedback control strategies* for the neuromechanical interplay generating spring-like leg behavior in biology.

By addressing single-loop muscle reflexes, in *Chapter 5*, only a small group of all the potential local control schemes is investigated. Nevertheless, with positive force feedback of the extensor muscles, a powerful strategy could be identified producing spring-like leg behavior as a subset of a more general, compliant limb response ranging from load bearing to high-performance hopping (compare Fig. 5.4). Moreover, by consequently applying the hierarchical control concept suggested by the spring-mass gait template, the first neuromechanical running model could be derived (Fig. 5.6). Hence, the identification of positive force feedback strongly suggests that although leg stiffness is treated as a key parameter in biomechanics, the spring-like behavior is not embodied directly as 'control plant' in biology, but rather emerges from the inherent muscle-reflex dynamics capable of producing a wider behavioral spectrum than merely emulating springs.[1]

The work presented in Chapter 5 exemplifies how gait templates can advance a deeper understanding of the neuromechanical organization in animal and human locomotion. Although positive force feedback has not yet been scrutinized experimentally for running or hopping, evidence is mounting for this reflex scheme to play an important role for leg extensor muscles in the stance phase of walking (compare

---

[1]When exploring the global system dynamics in models, however, implementing spring-legs represents a convenient way to express such a more general, compliant response parsimoniously as only one parameter, the spring stiffness, has to be introduced.

section 5.4.5). Considering the results of this thesis suggesting the spring-like leg behavior to be of similar importance in walking as in running, the identification of positive force feedback could point to a basic neuromechanical principle of generating this leg behavior not only in bouncing gaits but in legged locomotion in general.

Admittedly, the model employed in Chapter 5 (Fig. 5.1) is itself a largely simplified representation of the morphological complexity found in animals and humans. And it remains to investigate in detail in how far this principle based on positive force feedback can be realized, for instance, in a multi-articulated and multi-actuated leg. However, in the same way as gait templates can help to reveal basic neuromechanical principles, these basic principles may in turn guide the identification of their detailed realization in morphologically more plausible representations.

Thus, the obscurity of the organization of legged locomotion in biology that is induced by shear morphological complexity, might be resolved following such a step-by-step embodiment approach.

6.5 Application to robotics

In the previous sections, compliant limb behavior has been suggested as principle of legged locomotion in biology. This suggestion is based on the observation that although a large variety of legged systems evolved in the animal kingdom, when considering the whole body dynamics, only two fundamental gait patterns prevailed that can well be described by the compliant bipedal spring-mass model. Naturally, the question arises whether the observed functional uniformity among animals and humans reflects a solution to legged locomotion that is constrained by the material and drivers available to biological systems, or it represents an even more general principle that concerns *technical* legged systems as well.

Frequently, the importance of the compliant leg response is credited to the fact that passive elastic components store and restore a considerable amount of the stride energy in the stance phase of running. During walking, however, it is thought to be of no significance in this respect. By contrast, the 'passive dynamic walking' robots established that the energetic requirements can be minimized by adopting the inverted pendulum motion. Hence, energetics seems not to distinguish the compliant leg behavior as a general principle in legged locomotion.

But there might be a different reason for favoring compliant legs. An inherent characteristic of legged locomotion is the occurrence of impact forces at touch-down. This characteristic is well known to many scientists working in the field of robotics,

not least since impacts jeopardize that very control concept which still dominates in legged machines; namely, following prescribed kinematic trajectories for all the degrees-of-freedom in the system. As this concept requires to measure precisely the positions of all those degrees-of-freedom, rigid structural elements and tightly connected actuators and sensors are implemented avoiding unpredictable play. However, for legged locomotion, such a construction is especially impact-prone, which in turn produces erroneous sensory information compromising the whole concept of kinematic control. Holding on to this concept, legged robots are often pre-programmed to touch the ground with virtually zero foot-point velocity reducing the impacts as much as possible. Although this strategy might work in a known environment at slow speeds, it proves fatal in natural terrain or at higher speeds.

Adding to this control matter, and perhaps more importantly, the impacts threaten to inflict damage on the rigid bearing structures and the stiffly connected actuators. Hence, impact avoidance certainly ranks as one of the most prominent concerns in legged systems. In fact, this issue is very familiar to us from wheeled systems already. Cars and bikes have inflated tyres and are suspended by shock absorbers. Exactly due to their compliant properties, these elements are able to diminish impacts to a considerable extent. This not only comforts our ride. It also prevents structural damages from driving into holes in the road. However, as roads are generally flat to fit wheeled locomotion, shock absorption may be deemed *supplementary* in this case. But for legged systems that are intended to move swiftly across natural, and thus rough terrain, the compliant behavior could prove an *indispensable* strategy for averting damage.

Although this general advantage of compliant limbs is well known in principle, it is seldom exploited in legged robots, since it requires to abandon the traditional concept of kinematic control in favor of a control that is based on the inherent system dynamics. Yet, at present, it is unclear how the latter should be achieved. The hierarchical decomposition of control as suggested by the spring-mass gait template, could indicate a solution to this problem. Taking advantage of the self-stabilizing behavior of the global system dynamics, the legs have merely to produce a spring-like leg response.

Some hopping robots that have been developed over the past two decades, point towards such a decomposition of control. Implementing hardware springs, they rely on the spring-leg behavior and successfully balance the motion of the center of mass by proper leg placement during flight (compare section 1.3). This placement, however, is based on feedback control. In consequence, the hopping robots' inherent

self-stability, and hence the strength of the control decomposition, is not exploited to its full potential.

For walking robots, as for walking itself, the concept of compliant leg behavior is quite new. In our laboratory, we are currently pursuing this idea by building a nearly passive walker that is actuated at the hip joints only, and has springs spanning the knee and ankle joints of its two legs (Fig. 6.2). Thus far, it shows that a walking-like gait can indeed be obtained without the traditional control approach of prescribed kinematic joint trajectories. Additionally, and in stark contrast to the passive walkers that are based on the inverted pendulum motion, the whole body dynamics as measured by the GRF, more closely resembles that observed in biology.
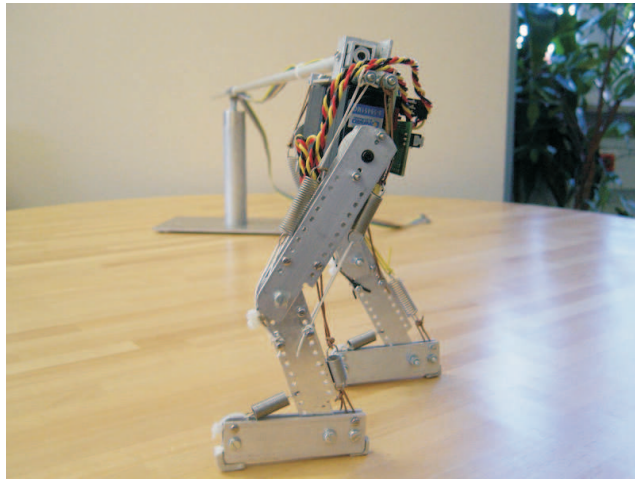

Figure 6.2. Walking robot based on the concept of compliant limbs developed at the Locomotion Laboratory of the Jena University by Y. Minekawa under supervision of F. Iida and A. Seyfarth. The robot is actuated at the hip joints only. Mostly biarticular springs span the passive joints of the segmented legs.

The robots just discussed strongly suggest the feasibility of this hierarchical control concept. But to build legged systems that echo the versatility, and suddenness, of animal and human movements, passive mechanical springs will have to be extended, or perhaps even replaced, by active components. Hence, technical legs should be able to generate the spring-like response on demand. The identified positive force feedback might serve as an inspiration for solving this task. The muscle reflex demonstrates how an actuated leg can guarantee spring-like operation in a largely decentralized and autonomous manner, without restricting the system to this behavior. For instance, simply altering the feedback parameters forces the leg to balance a load, or to accelerate or decelerate.

Whether such a reflex loop would work in a technical leg, may depend on the

specific actuator properties. For positive force feedback, the asymmetric shape of the muscle's force-velocity relationship turns out to be essential for stabilizing periodic hopping or running. By contrast, its force-length relationship has no influence on the leg's rebounding behavior, but is required for load bearing tasks. Certainly, programming current motors to imitate muscle properties could enforce the functionality of such a reflex loop. However, it might be more important to investigate to what extent biological actuators, and their neuromechanical interplay, are particularly suited to match legged locomotion; and then to reconsider the appropriateness of their technical pendants.

6.6 Application to rehabilitation and prosthetics

While in robotics we enjoy the freedom of exploration, the situation is changed in rehabilitation and prosthetics. Since here we do not have the privilege of arguing about alternative approaches to legged locomotion using biology as a mere convenient source of inspiration, but must relate our efforts in understanding legged systems, to a single, the *human* system. In particular, two fields of application are attached to these research efforts: gait rehabilitation for patients whose ability to walk and run is impeded temporarily following, for instance, spinal cord injury or stroke; and the development of prosthetic legs that restore part of the functionality of lost appendages.

The concept pursued in *gait rehabilitation* of human locomotion is comparable to the kinematic control approach taken in robotics. The identification of central pattern generators (CPG) that are located in the spinal cord of animals and rhythmically excite their leg muscles during locomotion, soon suggested a similar decentralization of neural control in humans. Following the observation that decerebrate cats can even 're-learn' to walk when subjected to treadmill training, the latter was suggested as therapy in human gait rehabilitation. Hereto, in early attempts, the patient was stationed on a split-belt treadmill with a therapist holding him upright from behind. While the treadmill belts moved the patient's legs backward simulating the stance phases in walking, two more therapists moved his legs forward imitating the swing phases.

Although an increased re-learning rate of the patients indicated the potential of the therapy, the rapid exhaustion of the therapists limited its applicability. To release them from their strenuous activity, and to prolong the training significantly, orthotic devices have been developed that suspend the patient's body and move

his legs automatically (Fig. 6.3). In these devices, the actuated joints are pre-programmed to follow kinematic trajectories recorded from healthy subjects walking at a moderate pace. The patient's sole objective is to learn supporting his own weight as the mechanical body suspension is gradually withdrawn in consecutive training sessions.

Figure 6.3. Example of orthotic device for gait rehabilitation. The 'Lokomat' has been developed at the ParaCare Research Laboratory (Prof. V. Dietz) of the University Hospital Balgrist, University of Zurich, Switzerland, in collaboration with the Institute for Automatization (Prof. M. Morari) of the Swiss Federal Institute of Technology (ETH), Zurich, Switzerland, and is now commercialized by the HOCOMA AG (picture courtesy of the ParaCare Research Laboratory).

It is currently unclear to what extent the kinematically constrained motion hampers the therapeutical success. However, a *patient-adaptive and function-specific* control concept that not only reduces the body suspension, but also delegates part of the walking effort to the patient himself, is considered a substantial improvement on the rehabilitation training.

Towards this goal, in the actual devices, the kinematic joint trajectories are overlaid with an impedance control where, proportional to the deviation of a joint from its target trajectory, a restoring force is applied. Although this solution enables the patient to depart from the prescribed motion to some degree, it does not really adapt to the progress in functionality the patient's legs make during the course of the therapy; nor can it account for his natural locomotion pattern.

The latter may immediately become apparent when considering that body weight

suspension influences the natural dynamics of human locomotion similar to a reduced gravity environment. For example, recalling from Chapter 3 that humans prefer to switch from walking to running at a speed $v_{trans} \sim \sqrt{0.5\,g\ell_0}$, at full body suspension ($g_{effective} = 0$), the patient would naturally prefer to run at the moderate 'walking speed' applied in the training.

Hence, similar to robotics, the intended control concept may require a transition from prescribed kinematics to dynamics based solutions. Here, the identified spring-mass gait template could serve as a suitable control substitute for predefined trajectories in the stance phases. For instance, the suspension system could alter the load on the stance legs according to the whole body dynamics observed in natural walking, or perhaps even running, using the gait template as a functional, virtual control model. However, existing suspension systems are designed to apply a constant lift force only and lack the dynamic response necessary to implement such a template based control. To test the latter, we are currently developing a system that fulfils the required specifications.

In contrast to the situation in gait rehabilitation, for the development of *prosthetic legs* we cannot rely on a patient's own leg apparatus, but must devise artificial replacements that literally recover the functionality of the lost appendages, by technical means. However, present-day leg prostheses lack far behind the envisioned goal. Although advances in materials and methods have pushed their cosmetic appearance, the underlying functionality is largely restricted to mimicking specific leg kinematics. This is mainly achieved by altering the behavior of prosthetic knees using programmable variable dampers (as in Endolite Intelligent Plus, Otto Bock C-Leg, and Seattle Power Knee). Foot prostheses still remain mechanically passive elements with visco-elastic properties emulating an elastic ankle joint behavior (e.g. carbon-fiber leaf springs in Flex-Foot prostheses, Flex-Foot Inc.) and the human heel pad (e.g. solid-ankle cushioning heel feet known as SACH feet). As a result, current leg prostheses are far from displaying the versatility of natural limbs. By contrast, their motion repertoire is largely restricted, and in fact, there is no artificial leg that allows an amputee to *walk and run*.

Different reasons may account for this unsatisfactory state of development. On one hand, available hardware technologies barely meet the requirements for prosthetic legs. Here, one problem is the onboard power supply in autonomous systems, the lack of which prevented early implementations of active force generation in prosthetic legs. Another technological difficulty that has to be overcome is the insufficient

torque production of existing actuators. A number of research efforts are made to develop new devices ranging from the in-series arrangement of traditional actuator and spring elements imitating muscle-tendon units, to the conception of novel high-density linear actuators, to the utilization of modified and artificially maintained muscle tissue.

On the other hand, it is currently unclear, given the prospect of sufficient power supply and actuators in near future, what general control concept should be applied to a powered leg prosthesis; and it seems that, similar to applications in robotics and rehabilitation, a deeper understanding of the principles underlying human locomotion, as well as the identification of their morphological embodiment, could have a profound impact on the development of artificial limbs. Here, the thesis results not only suggest that it is possible to devise prosthetic legs which allow an amputee to walk and run in a natural and comfortable manner based on the same fundamental principle of compliant limb behavior. They also demonstrate how the control of this global leg response could be realized at the local joint levels using positive force feedback.

However, as discussed earlier, the model employed in Chapter 5 largely simplifies the morphology of the human leg. As such it merely exemplifies how the step-by-step embodiment approach can complement physiological methods elucidating the neural control of human locomotion. It remains to continue with this line of research to obtain a more detailed picture of the neuromechanical organization for morphologically more plausible leg architectures. Nonetheless, the exploitation of this approach for leg prosthetics seems to have a strong long-term potential, since developing artificial replacements using the same general principles and control structures that operate the human leg, may also lead to man-machine interfaces linking the technical controller with the nervous system. Not only would this give the command of a prosthesis over to the amputee, but it might convey him the feeling of a truly natural limb.

List of symbols

General

Symbol	Definition	First Appearance
α_0	leg/spring angle of attack at touch-down	Fig. 1.2, p. 3
COM	body center of mass	Ch. 1.2, p. 3
E_s	system energy	Ch. 2.2.2, p. 11
g	gravitational acceleration	Fig. 1.2, p. 3
GRF	ground reaction force	Ch. 1.1, p. 2
i	index denoting initial apex event	Ch. 2.2.2, p. 11
$i+1$	index denoting subsequent apex event	Ch. 2.2.2, p. 11
k	spring stiffness	Fig. 1.2, p. 3
ℓ_0	spring rest length	Fig. 1.2, p. 3
m	body mass	Fig. 1.2, p. 3
t_c	contact time	p. 16
TD	touch-down	Ch. 2.3.1, p. 12
TO	take-off	Ch. 2.3.1, p. 12

Chapter 1

Symbol	Definition	First Appearance
$\dot{x}_0$	forward speed at initial apex	Fig. 1.3, p. 6

Chapter 2

Symbol	Definition	First Appearance
$\Delta\varphi$	angular sweep during stance	Fig. 2.1, p. 11
$\tilde{E}_s$	dimensionless system energy	eq. 2.28, p. 18
φ	angular position	Fig. 2.1, p. 11
$\dot{\varphi}$	angular velocity	eq. 2.3, p. 12
$\tilde{k}$	dimensionless spring stiffness	eq. 2.28, p. 18
P	angular momentum	p. 12
r	radial distance	Fig. 2.1, p. 11
$\dot{r}$	radial velocity	eq. 2.3, p. 12
ρ	relative spring amplitude	eq. 2.6, p. 12
ω	angular touch-down velocity	eq. 2.8, p. 13
ω_0	natural spring frequency	eq. 2.8, p. 13
$\hat{\omega}_0$	planar spring-mass system oscillation frequency	eq. 2.12, p. 13

Chapter 3

Symbol	Definition	First Appearance
φ	angular position	Fig. 3.2, p. 37
$\Delta\ell$	maximum leg compression (experimentally)	Fig. 3.3, p. 43
$\Delta\ell_{hor}$	maximum leg compression imposing horizontal COM kinematics during stance	eq. 3.4, p. 38
Δr_{max}	maximum leg compression (calculated)	eq. 3.7, p. 38
Δz	vertical COM amplitude	p. 3.3.2
λ	relative leg compression	eq. 3.13, p. 40
Fr	Froude number	p. 35
r	radial distance	Fig. 3.2, p. 37
$\dot{r}$	radial velocity	Fig. 3.2, p. 37
v	forward locomotion speed	p. 35
ω_0	natural spring frequency	eq. 3.5, p. 38

Chapter 4

Symbol	Definition	First Appearance
Δy	vertical displacement	Fig. 4.3, p. 55
$\Delta \ell$	spring compression	Fig. 4.3, p. 55
DR	Jacobian matrix of the return map R	eq. 4.4, p. 51
$\tilde{E}_s$	dimensionless system energy	p. 52
$F_{horiz/vert}$	horizontal/vertical component of GRF	Fig. 4.3, p. 55
FP	foot point	Fig. 4.1, p. 50
$\tilde{k}$	dimensionless stiffness	p. 52
λ	eigenvalue of the Jacobian matrix DR	eq. 4.3, p. 51
R	return map	eq. 4.1, p. 51
v_{belt}	treadmill speed	Tab. 4.1, p. 59
x_{rel}	relative horizontal position	p. 51
$\tilde{x}_{rel}$	dimensionless horizontal position	p. 52
y	vertical position	p. 51
$\tilde{y}$	dimensionless vertical position	p. 52

Chapter 5

Symbol	Definition	First Appearance
A	area enclosed by the leg's force-length relationship	eq. 5.10, p. 74
A_{max}	maximum area	eq. 5.10, p. 74
ACT	muscle activation	Fig. 5.1, p. 70
C_{EL}	elasticity coefficient	eq. 5.10, p. 74
CE	contractile element	Fig. 5.1, p. 70
F^+	positive force feedback	Fig. 5.2, p. 76
F_{max}	maximum isometric force	
F_{MTC}	muscle force	eq. 5.3, p. 71
G	feedback gain	Fig. 5.1, p. 70
GTO	Golgi tendon organs	p. 72

h	hopping height	Fig. 5.2, p. 76
L^+	positive length feedback	Fig. 5.2, p. 76
ℓ_{CE}	CE length	eq. 5.4, p. 71
ℓ_{off}	CE offset length	p. 72
P	proprioceptive signal	Fig. 5.1, p. 70
SE	series elastic element	Fig. 5.1, p. 70
$STIM$	muscle stimulation signal	Fig. 5.1, p. 70
$STIM0$	stimulation bias	Fig. 5.1, p. 70
v_{CE}	CE velocity	eq. 5.4, p. 71
v_{off}	CE offset velocity	p. 72

Bibliography

ABERNETHY, B., A. HANNA, and A. PLOOY, 2002 The attentional demands of preferred and non-preferred gait patterns. Gait and Posture **15:** 256–265.

ALEXANDER, R., 1988 *Elastic mechanisms in animal movement.* Cambridge Univ. Press, Cambridge.

ALEXANDER, R., 1989 Optimization and gaits in the locomotion of vertebrates. Physiol. Rev **69:** 1199–1227.

ALEXANDER, R. and A. JAYES, 1983 A dynamic similarity hypothesis for the gaits of quadrupedal animals. J. Zool. **210:** 135–152.

ALEXANDER, R. and A. VERNON, 1975 Mechanics of hopping by kangaroos (Macropodidae). J. Zool. **177:** 265–303.

ALTENDORFER, R., D. E. KODITSCHEK, and P. HOLMES, 2003 Towards a factored analysis of legged locomotion models. In *Proc. Int. Conf. on Robotics and Automation*, pp. 37–44. Taipei, Taiwan.

ALTENDORFER, R., N. MOORE, H. KOMSUOGLU, M. BUEHLER, J. BROWN, D. MCMORDIE, U. SARANLI, R. FULL, and D. KODITSCHEK, 2001 RHex: A Biologically Inspired Hexapod Runner. Autonomous Robots **11:** 207–213.

ARAMPATZIS, A., G. BRÜGGEMANN, and V. METZLER, 1999 The efect of speed on leg stiffness and joint kinetics in human running. J. of Biomech. **32:** 1349–1353.

AUBERT, X., 1956 *Le couplage énergetique de la contraction musculaire. Thesis.* Brussels: Edition Arscia.

AVELA, J. and P. KOMI, 1998 Interaction between muscle stiffness and stretch reflex sensitivity after long-term stretch-shortening cycle exercise. Muscle Nerve *21* (9)**:** 1224–1227.

BIEWENER, A., 1989 Scaling body support in mammals: limb posture and muscle mechanics. Science *245* (4913)**:** 45–48.

BIEWENER, A., 1998 Muscle-tendon stresses and elastic energy storage during locomotion in the horse. J. Appl. Physiol. *120* (1)**:** 73–87.

BIEWENER, A. and C. TAYLOR, 1986 Bone strain: A determinant of gait and speed. J. Exp. Biol. **123:** 383–400.

BLICKHAN, R., 1989 The spring-mass model for running and hopping. J. Biomech. **22:** 1217–1227.

BLICKHAN, R. and R. FULL, 1993 Similarity in multilegged locomotion: bouncing like a monopode. J. Comp. Physiol. **173:** 509–517.

BLICKHAN, R., H. WAGNER, and A. SEYFARTH, 2003 *Brain or muscles?*, Volume 1 of *Recent Res. Devel. Biomechanics*, Chapter 12, pp. 215–245. Transworld Research Network, Kerala, India.

BOBBERT, M. and G. VAN INGEN SCHENAU, 1988 Coordination in vertical jumping. J. Biomech. **21:** 249–262.

BRISSWALTER, J. and D. MOTTET, 1996 Energy costs and stride duration variablity at preferred transition gait speed between walking and running. Can. J. Appl. Physiol. **21:** 471–480.

BUCKINGHAM, E., 1914 On physically similar systems: Illustration of the use of dimensional analysis. Phys. Rev. **4:** 345–376.

CAPADAY, C. and R. STEIN, 1987 Difference in the amplitude of the human soleus H reflex during walking and running. J. Physiol. **392:** 513–522.

CAVAGNA, G., N. HEGLUND, and C. TAYLOR, 1977 Mechanical work in terrestral locomotion: Two basic mechanisms for minimizing energy expenditure. Am. J. Physiol. *233*(5): 243–261.

CAVAGNA, G., F. SAIBENE, and R. MARGARIA, 1964 Mechanical work in running. J. Appl. Physiol. *19*(2): 249–256.

COLEMAN, M., A. CHATTERJEE, and A. RUINA, 1997 Motions of a rimless spoked wheel: a simple three-dimensional system with impacts. Dyn. Stab. Sys. **12:** 139–159.

COLEMAN, M. and P. HOLMES, 1999 Motions and stability of a piecewise holonomic system: the discrete Chaplygin sleigh. Regul. Chaot. Dyn. *4*(2): 1–23.

COLEMAN, M. and A. RUINA, 1998 An uncontrolled walking toy that cannot stand still. Phys. Rev. Lett. **80:** 3658–3661.

DIETZ, V., D. SCHMIDTBLEICHER, and J. NOTH, 1979 Neuronal mechanisms of human locomotion. J. Neurophysiol. *42*(5): 1212–1222.

FARLEY, C., R. BLICKHAN, J. SAITO, and C. TAYLOR, 1991 Hopping frequency in humans: A test of how springs set stride frequency in bouncing gaits. J. Appl. Physiol. *71*(6): 2127–2132.

FARLEY, C., J. GLASHEEN, and T. MCMAHON, 1993 Running springs: speed and animal size. J. Exp. Biol. **185:** 71–86.

FARLEY, C. and O. GONZALEZ, 1996 Leg stiffness and stride frequency in human running. J. Biomech. *29*(2): 181–186.

FARLEY, C. and D. MORGENROTH, 1999 Leg stiffness primarily depends on ankle sitffness during human hopping. J. Biomech. *32*(3): 267–273.

FARLEY, C. and C. TAYLOR, 1991 A mechanical trigger for the trot-gallop transition in horses. Science **253:** 306–308.

FERRIS, D., P. AAGAARD, E. SIMONSEN, C. FARLEY, and P. DYHRE-POULSEN, 2001 Soleus H-reflex gain in human walking and running under simulated reduced gravity. J. Physiol. **530:** 167–180.

FERRIS, D. and C. FARLEY, 1997 Interaction of leg stiffness and surface stiffness during human hopping. J. Appl. Physiol. *82*(1): 15–22.

FERRIS, D., M. LOUIE, and C. FARLEY, 1998 Running in the real world: adjusting leg stiffness for different surfaces. Proc. Roy. Soc. Lond. B Biol. Sci. *265*(1400): 989–994.

FOUAD, K. and K. PEARSON, 1997 Effects of extensor muscle afferents on the timing of locomotor activity during walking in adult rats. Brain Res. **749:** 320–328.

FULL, R. and D. KODITSCHEK, 1999 Templates and anchors: neuromechanical hypotheses of legged locomotion on land. J. Exp. Biol. **202:** 3325–3332.

FUNASE, K., T. HIGASHI, A. SAKAKIBARA, K. IMANAKA, Y. NISHIHIRA, and T. MILES, 2001 Patterns of muscle activation in human hopping. Eur. J. Appl. Physiol. *84*(2): 503–509.

GARCIA, M., A. CHATTERJEE, A. RUINA, and M. COLEMAN, 1998 The simplest walking model: stability, complexity, and scaling. J. Biomech. Engng. **120:** 281–288.

GARD, S., S. MIFF, and A. KUO, 2004 Comparison of kinematic and kinetic methods for computing the vertical motion of the body center of mass during walking. Hum. Mov. Sci. **22:** 597–610.

GATESY, S. and A. BIEWENER, 1991 Bipedal locomotion – effects of speed, size and limb posture in birds and humans. J. Zool. **224:** 127–147.

GERRITSEN, K. and A. NAGANO, 1999 The role of sensory feedback during cyclic locomotor activities. In *Proc. XVIIth Congr. Int. Soc. of Biomech.*, pp. 46.

GEYER, H., 2001 Movement criterion of fast locomotion: mathematical analysis and neuro-biomechanical interpretation with functional muscle reflexes. Dipl. thesis, Faculty for Physics and Astronomy, Jena University, Germany.

GEYER, H., R. BLICKHAN, and A. SEYFARTH, 2002 Natural dynamics of spring-like running – Emergence of selfstability. In *Proc. 5th Int. Conf. on Climbing and Walking Robots*, pp. 87–92. Prof. Eng. Publ. Ltd.

GEYER, H., A. SEYFARTH, and R. BLICKHAN, 2005 Spring-mass running: simple approximate solution and application to gait stability. J. Theoret. Biol. (232): 315–328.

GHIGLIAZZA, R., R. ALTENDORFER, P. HOLMES, and D. KODITSCHEK, 2003 A simply stabilized running model. SIAM J. Applied. Dyn. Sys. *2*(2): 187–218.

GOLDBERG, D., 1989 *Genetic algorithms in search, optimization and machine learning.* Addison-Wesley Publications.

GOLDBERGER, M., 1977 Locomotor recovery after unilateral hindlimb deafferentiation in cats. Brain Res. *123*(1): 59–74.

GOSSARD, J., R. BROWNSTONE, I. BARAJON, and H. HULTBORN, 1994 Transmission in a locomotor-related group Ib pathway from hindlimb extensor muscle in the cat. Exp. Brain Res. **98:** 213–228.

GRAY, J., 1968 *Animal locomotion.* London, Great Britain: Weidenfeld and Nicholson.

GURP, M. V., H. SCHAMHARDT, and A. CROWE, 1987 The ground reaction force pattern from the hindlimb of the horse simulated by a spring model. Acta Anat. **129:** 31–33.

HAYES, G. and R. M. ALEXANDER, 1983 The hopping gaits of crows (Corvidae) and other bipeds. J. Zool. **200:** 205–213.

HE, J., R. KRAM, and T. MCMAHON, 1991 Mechanics of running under simulated low gravity. J. Appl. Physiol. *71*(3): 863–870.

HERR, H., 1998 A model of mammalian quadrupedal running. Ph. D. thesis, Department of Biophysics, Harvard University, USA.

HERR, H. and T. MCMAHON, 2000 A trotting horse model. Int. J. Robotics Res. **19:** 566–581.

HERR, H. and T. MCMAHON, 2001 A galloping horse model. Int. J. Robotics Res. **20:** 26–37.

HILL, A., 1938 The heat of shortening and the dynamic constants of muscle. Proc. Roy. Soc. *126*(B): 136–195.

HOFFER, J. A. and S. ANDREASSEN, 1981 Regulation of soleus muscle stiffness in pre-mammillary cats: intrinsic and reflex components. J. Neurophysiol. **45:** 267–285.

HRELJAC, A., 1993 Preferred and energetically optimal gait transition speeds in human locomotion. Med. Sci. Sports Exerc. **25:** 1158–1162.

HRELJAC, A., 1995a Determinants of the gait transition speed during human locomotion: kinematic factors. J. Biomech. **28:** 669–677.

HRELJAC, A., 1995b Effects of physical characteristics on the gait transition speed during human locomotion. Human Mov. Sci. **14:** 205–216.

HRELJAC, A., D. PARKER, R. QUINTANA, E. ABDALA, K. PATTERSON, and M. SISON, 2002 Energetics and perceived exertion of low speed running and high speed walking. Facta Universitatis, Physical education and Sport *1*(9): 27–35.

INGEN SCHENAU, G. V., 1984 An alternative view to the concept of utilisation of elastic energy. Hum. Mov. Sci. **3:** 301–336.

KELLER, T., A. WEISBERGER, J. RAY, S. HASAN, R. SHIAVI, and D. SPENGLER, 1996 Relationship between vertical ground reaction force and speed during walking, slow jogging, and running. Clin. Biomech. *11*(5): 253–259.

KER, R., M. BENNETT, S. BIBBY, R. KESTER, and R. ALEXANDER, 1987 The spring in the arch of the human foot. Nature *325*(7000): 147–149.

KERDOC, A., A. BIEWENER, T. MCMAHON, and H. HERR, 2002 Energetics and mechanics

of human running on surfaces of different stiffnesses. J. Exp. Biol. *92*(2): 469–478.

KIM, S., J. CLARK, and M. CUTKOSKY, 2004 iSprawl: Autonomy, and the effects of power transmission. In *Proc. 7th Int. Conf. on Climbing and Walking Robots (CLAWAR)*, Madrid, Spain.

KNIKOU, M. and W. RYMER, 2002 Effects of changes in hip joint angle on H-reflex excitability in humans. Exp. Brain Res. **143:** 149–159.

KRAM, R., A. DOMINGO, and P. FERRIS, 1997 Effect of reduced gravity on the preferred walk-run transition speed. J. Exp. Biol. **200:** 821–826.

LEE, C. and C. FARLEY, 1998 Determinants of the center of mass trajectory in human walking and running. J. Exp. Biol. **201:** 2935–2944.

MARGARIA, R., 1938 Sulla fisiologia e specialmente sul consumo energetico della marcia e della corsa a varie velocita ed inclinazioni del terreno. Atti Accad. Naz. Lincei Memorie: 69–75.

MARGARIA, R., P. CERRETELLI, P. AGHEMO, and G. SASSI, 1963 Energy cost of running. J. Appl. Physiol. **18:** 367–370.

MCGEER, T., 1990 Passive dynamic walking. Int. J. Rob. Res. *9*(2): 62–82.

MCMAHON, T., 1985 The role of compliance in mammalian running gaits. J. Exp. Biol. **115:** 263–282.

MCMAHON, T. and G. CHENG, 1990 The mechanism of running: how does stiffness couple with speed? J. Biomech. **23:** 65–78.

MCMAHON, T., G. VALIANT, and E. FREDERIK, 1987 Groucho running. J. Appl. Physiol. *62*(6): 2326–2337.

MELVILL JONES, G. and D. WATT, 1971 Observations on the control of stepping and hopping movements in man. J. Physiol. *219*(3): 709–727.

MERKENS, H., H. SCHAMHARDT, W. HARTMAN, and A. KERSJES, 1986 The ground reaction force pattern of the Dutch warmblood horse at normal walk. Equine Vet. Jour. **18:** 207–214.

MEUNIER, S., A. PENICAUD, E. PIERROT-DESEILLIGNY, and A. ROSSI, 1990 Monosynaptic Ia excitation and recurrent inhibition from quadriceps to ankle flexors and extensors in man. J. Physiol. **423:** 661–675.

MINETTI, A. and R. ALEXANDER, 1997 A theory of metabolic costs for bipedal gaits. J. Theoret. Biol. **186:** 467–476.

MINETTI, A., L. ARDIGO, and F. SAIBENE, 1994 The transition between walking and running in humans: metabolic and mechanical aspects at different gradients. Acta Physiol. Scand. **150:** 315–323.

MORITA, H., N. PETERSEN, L. CHRISTENSEN, T. SINKJAER, and J. NIELSEN, 1998 Sensitivity of H-reflexes and stretch reflexes to presynaptic inhibition in humans. J. Neurophysiol. *80*(2): 610–620.

MUIR, G., J. GOSLINE, and J. STEEVES, 1996 Ontogeny of bipedal locomotion: walking and running in the chick. J. Physiol. *493*(2): 589–601.

MUYBRIDGE, E., 1955 *The human figure in motion.* Dover Publ. Inc.

NICHOLS, T. and J. HOUK, 1976 Improvement in linearity and regulation of stiffness that results from actions of stretch-reflex. J. Neurophysiol. **39:** 119–142.

NOBLE, B., K. METZ, K. PANDOLF, C. BELL, E. CAFARELLI, and W. SIME, 1973 Perceived exertion during walking and running. Med. Sci. Sports **5:** 116–120.

ORLOVSKY, G., T. DELIAGINA, and S. GRILLNER, 1999 *Neuronal control of locomotion: from mollusc to man.* Oxford University Press, New York.

PANDY, M., 2003 Simple and complex models for studying muscle function in walking. Phil. Trans. Roy. Soc. Lond. B **358:** 1501–1509.

PANDY, M. and N. BERME, 1988 Synthesis of human walking: a planar model for single support. J. Biomech. *21*(12): 1053–1060.

PEARSON, K., 1995 Proprioceptive regulation of locomotion. Curr. Opin. Neurobiol. *5*(6): 786–791.

PEARSON, K. and D. COLLINS, 1993 Reversal of the influence of group Ib afferents from plantaris on activity in medial gastrocnemius muscle during locomotor activity. J. Neurophys. **70:** 1009–1017.

PRATT, C., 1995 Evidence of positive force feedback among hindlimb extensors in the intact standing cat. J. Neurophys. **73:** 2578–2583.

PROCHAZKA, A., D. GILLARD, and D. BENNETT, 1997a Implications of positive feedback in the control of movement. J. Neurophys. **77:** 3237–3251.

PROCHAZKA, A., D. GILLARD, and D. BENNETT, 1997b Positive force feedback control of muscles. J. Neurophys. **77:** 3226–3236.

RAIBERT, M., 1986 *Legged robots that balance.* MIT press, Cambridge.

RAYNOR, A., C. YI, B. ABERNETHY, and Q. JONG, 2002 Are transitions in human gait determined by mechanica, kinetic or energetic factors? Hum. Mov. Sci. *21*(5–6): 785–805.

RINGROSE, R., 1997 Self-stabilizing running. Ph. D. thesis, Department of Elec. Eng. and Comp. Sci., Massachusetts Institute of Technology, USA.

ROBERTS, T., R. KRAM, P. WEYAND, and C. TAYLOR, 1998 Energetics of bipedal running. I. Metabolic costs of generating force. J. Exp. Biol. **201:** 2745–2751.

RUBENSON, J., D. HELIAMS, D. LLOYD, and P. FOURNIER, 2004 Gait selection in the ostrich: mechanical and metabolic characteristics of walking and running with and without an aerial phase. Proc. Roy. Soc. Lond. B Biol. Sci. *271*(1543): 1091–1099.

RUINA, A., 1998 Non-holonomic stability aspects of piecewise holonomic systems. Rep. Math. Phys. *42*(1/2): 91–100.

SAIBENE, F. and A. MINETTI, 2003 Biomechanical and physiological aspects of legged locomotion in humans. Eur. J. Appl. Physiol. **88:** 297–316.

SARANLI, U., M. BUEHLER, and D. KODITSCHEK, 2001 RHex: A simple and highly mobile hexapod robot. Int. J. Rob. Res. *20*(7): 616–631.

SARANLI, U. and D. KODITSCHEK, 2003 Template based control of hexapedal running. In *Proc. IEEE Int. Conf. on Robotics and Automation, Taipei, Taiwan*, pp. 1374–1379.

SARANLI, U., W. SCHWIND, and D. KODITSCHEK, 1998 Towards the control of a multijointed, monoped runner, Leuven, Belgium. In *Proc. IEEE Int. Conf. on robotics and automation*, pp. 2676–2682.

SAUNDERS, J., V. INMAN, and H. EBERHART, 1953 The major determinants in normal and pathological gait. J. Bone Jt. Surgery *35*(A): 543–558.

SCHMITT, J. and P. HOLMES, 2000 Mechanical models for insect locomotion: dynamics and stability in the horizontal plane I. Theory. Biol. Cybern. **83:** 501–515.

SCHWIND, W. J. and D. E. KODITSCHEK, 2000 Approximating the stance map of a 2-DOF monoped runner. J. Nonlinear Sci. **10:** 533–568.

SEYFARTH, A., T. APEL, H. GEYER, and R. BLICKHAN, 2001 Limits of elastic leg operation. In R. Blickhan (Ed.), *Motion Systems 2001*, pp. 102–107. Shaker Verlag, Aachen.

SEYFARTH, A. and H. GEYER, 2002 Natural control of spring-like running – optimized self-stabilization. In *Proceedings of the 5th international conference on climbing and walking robots*, pp. 81–85. Professional Engineering Publishing Limited.

SEYFARTH, A., H. GEYER, M. GÜNTHER, and R. BLICKHAN, 2002 A movement criterion for running. J. Biomech. **35:** 649–655.

SEYFARTH, A., H. GEYER, and H. M. HERR, 2003 Swing-leg retraction: a simple control model for stable running. J. Exp. Biol. **206:** 2547–2555.

SIEGLER, S., R. SELIKTAR, and W. HYMAN, 1982 Simulation of human gait with the aid of a simple mechanical model. J. Biomech. *15*(6): 415–425.

SINKJAER, T., J. ANDERSEN, M. LADOUCEUR, L. CHRISTENSEN, and J. NIELSEN, 2000 Major role for sensory feedback in soleus EMG activity in the stance phase of walking in

man. J. Physiol. *523*(3)**:** 817–827.

STEIN, R. and C. CAPADAY, 1988 The modulation of human reflexes during functional motor tasks. Trends Neurosci. **11:** 328–332.

STENTZ, A., 1983 Behavior during stance. In M. Raibert (Ed.), *Dynamically stable legged locomotion – third annual report*, pp. 106–110. Robotics Institute, Carnegie-Mellon University, CMU-RI-TR-83-20.

STEPHENS, M. and J. YANG, 1996 Short latency, non-reciprocal group I inhibition is reduced during the stance phase of walking in humans. Brain Res. **743:** 24–31.

THORSTENSSON, A. and H. ROBERTHSON, 1987 Adaptations to changing speed in human locomotion: speed of transition between walking and running. Acta Physiol. Scand. **131:** 211–214.

VAN HELM, F. and L. ROZENDAAL, 2000 Muskuloskeletal systems with instrinsic and proprioceptive feedback. In J. Winters and P. Crago (Eds.), *Biomechanics and neural control of movement and posture*. Springer Verlag.

VAN LEEUWEN, J. L., 1992 Muscle function in locomotion. In R. Alexander (Ed.), *Mechanics of animal locomotion*, Volume 11, pp. 191–249. Springer-Verlag, New York.

VAN SOEST, A., 1992 Jumping from structure to control – a simulation study of explosive movements. In *Thesis*. Thesis Publishers, Amsterdam.

VAN SOEST, A. and M. BOBBERT, 1993 The contribution of muscle properties in the control of explosive movements. Biol. Cybern. **69:** 195–204.

VERSTAPPEN, M. and P. AERTS, 2000 Terrestrial locomotion in the black-billed magpie. I. Spatio-temporal gait characteristics. Motor Control **4:** 150–164.

VOIGT, M., P. DYHRE-POULSEN, and E. SIMONSEN, 1998 Modulation of short latency stretch reflexes during human hopping. Acta Physiol. Scand. *163*(2)**:** 181–194.

VOIGT, M., E. SIMONSEN, P. DYHRE-POULSEN, and K. KLAUSEN, 1995 Mechanical and muscular factors influencing the performance in maximal vertical jumping after different prestretch loads. J. Biomech. *28*(3)**:** 293–307.

WENTINK, G. H., 1978 Biokinetical analysis of the movement of the pelvic limb of the horse and the role of the muscles in the walk and the trot. Anat. Embryol. **152:** 261–272.

WHITTACKER, E. T., 1904 *A treatise on the analytical dynamics of particles and rigid bodies*. Cambridge University Press, New York, 4th edition.

WICKLER, S., D. HOYT, E. COGGER, and K. HALL, 2001 Effect of load on preferred speed and cost of transport. J. Appl. Physiol. **90:** 1548–1551.

WINTERS, J., 1990 Hill-based muscle models: a system engineering perspective. In J. Winters and S.-Y. Woo (Eds.), *Multiple muscle systems: biomechanics and movement organization*. Springer, New York.

ZEHR, E. and R. STEIN, 1999 What functions do reflexes serve during human locomotion? Prog. in Neurobiol. **58:** 185–205.

Curriculum vitae

Name:	Hartmut Geyer
Citizenship:	German
Date of birth:	16 July 1976
Place of birth:	Leipzig, Germany
Marital status:	Single

Education

- since 2003, Research assistant at the Locomotion Laboratory (Dr. A. Seyfarth) of the Friedrich-Schiller University of Jena, Germany.

- 2002–2003, Research stipend (graduate student scholarship, German Academic Exchange Service 'DAAD') at the ParaCare Research Laboratory (Prof. V. Dietz) of the Balgrist University Hospital, University of Zurich, Switzerland.

- 2001–2002, Research stipend (graduate student scholarship, German Academic Exchange Service 'DAAD') at the Leg Laboratory (Prof. H. Herr) of the Artificial Intelligence Laboratory of the Massachusetts Institute of Technology, Cambridge, USA.

- 2001, Enrolment as graduate student, Department of Social and Behavioral Sciences of the Friedrich-Schiller University of Jena, Germany.

- 2001, Diploma in Physics (Prof. R. Blickhan) 'Movement criterion of fast locomotion - mathematical analysis and neuro-biomechanical interpretation through muscle reflexes.'

- 1996–2001, Studies of Physics, Faculty for Physics and Astronomy, Friedrich-Schiller University of Jena, Germany.

- 1995–1996, Compulsory military service.

- 1995, Abitur (general qualification for university entrance), Wilhelm-Ostwald Special High School (mathematical and natural sciences), Leipzig, Germany.

Publications in peer reviewed journals

- Geyer, H., Seyfarth, A., Blickhan, R. (2005) Spring-mass running: simple approximate solution and application to gait stability. *J. Theor. Biol.*, **232**: 315–328.

- Geyer, H., Seyfarth, A., Blickhan, R. (2003) Positive force feedback in bouncing gaits? *Roy. Soc. Lond. Proc. B.*, **270**: 2173–2183.

- Seyfarth, A., Geyer, H., and Herr, H. (2003) Swing-leg retraction: a simple control model for stable running. *J. Exp. Biol.*, **205**: 2547–2555.

- Seyfarth, A., Geyer, H., Günther, M., and Blickhan, R. (2002) A movement criterion for running. *J. of Biomech.* **35**: 649–655.

Publications in selected conference proceedings

- Geyer, H., Seyfarth, A., Blickhan, R. (2003) From running to walking. *Proceedings XIXth Congress International Society of Biomechanics*, pp. 121.

- Seyfarth, A., Geyer, H., Dietz, V. (2003) The use of leg retraction in obstacle avoidance. *Proceedings XIXth Congress International Society of Biomechanics*, pp. 356.

- Geyer, H., Seyfarth, A., Blickhan, R., Herr, H. M. (2002) Local feedback mechanisms for stable bouncing. *World Congress of Biomechanics WCB 2002*, Calgary.

- Seyfarth, A., Geyer, H., Blickhan, R., Herr, H. M. (2002) Does leg retraction simplify control of running? *World Congress of Biomechanics WCB 2002*, Calgary.

- Geyer, H., Seyfarth, A., Blickhan, R. (2002) Natural dynamics of spring-like running: emergence of self-stability. In *CLAWAR Climbing and Walking Robots*, Ed. P. Bidaud and F. B. Amar, Professional Engineering Publishing Ltd., London.

- Seyfarth, A., Geyer, H. (2002) Natural control of spring-like running: optimized self-stabilization. In *CLAWAR Climbing and Walking Robots*, Ed. P. Bidaud and F. B. Amar, Professional Engineering Publishing Ltd., London.

Patents

- Seyfarth, A., Geyer, H., Herr, H., inventors; A speed-adaptive control scheme for legged running robots. US patent pending, 2003.

Ehrenwörtliche Erklärung

Hiermit erkläre ich, dass mir die geltende Promotionsordnung der Fakultät bekannt ist und dass ich die Dissertation selbst angefertigt und alle von mir benutzten Hilfsmittel, persönliche Mitteilungen und Quellen in meiner Arbeit angegeben habe. Weiterhin erkläre ich, dass mich keine Personen bei der Auswahl und Auswertung des Materials unterstützt haben.

Mit Ausnahme der allgemeinen Einleitung und Schlussfolgerung (Kap. 1 und 6) sind die Kapitel des vorliegenden Manuskripts entsprechend den Anforderungen an Veröffentlichungen in wissenschaftlichen Zeitschriften organisiert. Diese Struktur wurde gewählt, da ein Teil bereits wissenschaftlich publiziert (Kap. 2[1] und 5[2]) und der andere Teil zum Einreichen vorbereitet ist (Kap. 3 und 4). Für den publizierten Teil der Arbeit habe ich von den beiden Mitautoren Prof. R. Blickhan und Dr. A. Seyfarth konzeptionelle Unterstützung bei der Erstellung des Erstmanuskripts erhalten. Als Hauptautor jedoch oblag mir die Überarbeitung in Bezug auf die Anmerkungen und Empfehlungen der von den Zeitschrifteneditoren bestellten, anonymen Gutachten. Weitere Personen haben mich bei der Herstellung des Manuskripts nicht unterstützt.

Ferner erkläre ich, dass ich nicht die Hilfe eines Promotionsberaters in Anspruch genommen habe und dass Dritte weder unmittelbar noch mittelbar geldwerte Leistungen von mir für Arbeiten erhalten haben, die im Zusammenhang mit dem Inhalt der vorgelegten Dissertation stehen. Die Dissertation wurde noch nicht als Prüfungsarbeit für eine staatliche oder andere wissenschaftliche Prüfung eingereicht und keine gleiche, ähnliche oder andere Abhandlung bei einer anderen Hochschule als Dissertation eingereicht.

Ich versichere, nach bestem Wissen die reine Wahrheit gesagt und nichts verschwiegen zu haben.

Jena, den 11. April 2005

Hartmut Geyer

---

[1] Geyer, H., Seyfarth, A., Blickhan, R. (2005) *J. Theor. Biol.*, **232**: 315–328.
[2] Geyer, H., Seyfarth, A., Blickhan, R. (2003) *Roy. Soc. Lond. Proc. B.*, **270**: 2173–2183.